THE STRUCTURE OF CANOPY FLOW FIELD

by

Takeshi Kawatani

and

Robert N. Meroney

Prepared under

U.S. Army Materiel Command

Grant No. DA-AMC-28-043-65-G20

FLUID MECHANICS PROGRAM
ENGINEERING RESEARCH CENTER
COLLEGE OF ENGINEERING

COLORADO STATE UNIVERSITY
FORT COLLINS, COLORADO

Technical Report

THE STRUCTURE OF CANOPY FLOW FIELD

by

Takeshi Kawatani

and

Robert N. Meroney

Prepared under

U.S. Army Materiel Command

Grant No. DA-AMC-28-043-65-G20

Fluid Dynamics and Diffusion Laboratory

College of Engineering

Colorado State University

Fort Collins, Colorado

August 1968

CER67-68TK66

ACKNOWLEDGMENTS

Financial support provided by the Integrated Army Meteorological Wind-Tunnel Research Program under Grant DA-AMC-28-043-65-G20 is gratefully acknowledged.

ABSTRACT

THE STRUCTURE OF CANOPY FLOW FIELD

A model study of canopy flow over high roughness elements was carried out in the Army Meteorological Wind Tunnel at Colorado State University using roughness consisting of pegs 9 cm high and 0.48 cm in diameter arranged in four patterns. The mean velocity and the turbulence intensity were measured within and above the roughness elements. Empirical expressions derived from field measurements for mean velocity profiles, turbulent velocity, and turbulence intensity were used to examine the data obtained in this model study. The logarithmic profile was adapted to analyze the data of mean velocity above the canopy. In this analysis, the friction velocity and the roughness parameter were calculated from the mean velocity profiles and related to the density of roughness elements to show the effects of roughness density on the flow field. The growth of the internal boundary layer was estimated from the mean velocity profiles and the turbulence intensity. The results of estimation were compared with semi-empirical equations. Although the coefficient of anisotropy above the canopy in this model study is larger than that in the field, the model study gave data about the turbulent flow field similar to the field data. Hence, this model was verified to be suitable for the study of diffusion.

TABLE OF CONTENTS

TABLE OF CONTENTS - Continued

LIST OF TABLES

LIST OF FIGURES

LIST OF FIGURES - Continued

LIST OF FIGURES - Continued

LIST OF SYMBOLS

Symbol	Definition	Dimension
d	Zero plane displacement	L
E	Mean voltage	V
$\sqrt{e^2}$	Root mean square of voltage	V
h	Height of roughness element	L
Δh	Dynamic pressure	M/LT^2
U	Mean velocity	L/T
U_h	Mean velocity at the height of roughness element	L/T
U_*	Friction velocity $(\sqrt{\tau_o/\rho})$	L/T
u,w	Fluctuating velocity	L/T
$u'=\sqrt{u^2}, w'=\sqrt{w^2}$	Root mean square of velocity fluctuations	L/T
x	Horizontal coordinate positive downwind	L
Z	Height above ground	L
Z_o	Roughness length	L
δ	Height of internal boundary layer	L
μ	Absolute viscosity	M/LT
ν	Kinetic viscosity	L^2/T
ρ	Mass density	M/L^3
τ	Shear stress	M/LT^2
τ_o	Shear stress at a wall	M/LT^2

Any other symbol not listed here is explained whenever it appears.

Chapter I

INTRODUCTION

The study of the effect of roughness on the turbulent boundary layer is one of the most important problems yet to be solved in fluid mechanics. When the structure of a turbulent boundary layer is related to the characteristics of roughness, the results can be applied to various practical problems. For example, the growth of crops or trees is closely related to temperature, humidity, and the rate of exchange of carbon dioxide or moisture in and above these plants. A knowledge of the effect of roughness on the flow field may suggest what is the best manner to space crops or trees. If the direction of prevailing wind is known, it should be possible to find the best arrangement of a crop or tree planting to diminish frost damage. Moreover, the proper method of dispersion of agricultural medicines will be determined when the direction and speed of wind are known.

The canopy flow field, which is the flow field affected by a crop or forest, changes its characteristics with variations in the shape, stiffness, and configuration of the vegetative element. That is, various structures of mean velocity and turbulence will occur depending upon the characteristics of the roughness element. The flow field in the case of flexible roughness (for instance a rice plant) is quite different from that in the case of stiff roughness (trees, corns) (20, 28). Numerous experiments have been made varying the roughness parameters, for example, changing height, diameter or stiffness of the roughness, or the free stream velocity (9, 18). Many theoretical and experimental expressions have been proposed for these individual experiments (3, 4, 25, 28).

Since the canopy flow field shows different aspects depending upon the characteristics of the roughness, most of the equations proposed for a specific configuration cannot be successfully applied to a different configuration. Progress in the tall roughness problem has been curtailed because most of the data available to describe the phenomena have been obtained in field experiments. Field experiments are inherently difficult and costly due to the vagrancies and unsteadiness of the atmosphere.

In this study, the wind tunnel was used to obviate the mentioned difficulty found in field experiments for the necessary flow conditions could be maintained as long as desired. The structure of the prototype canopy flow field is so complex that only a limited number of parameters should be selected to describe the model flow field. Even if a surface has only one single type of roughness element, the flow over such a roughness will depend not only upon the form and height of the roughness elements but also upon the density, i.e., the number of elements per unit surface area. Furthermore, the manner in which the roughness elements are distributed on the surface will also influence the flow. The primary purposes of this study were to characterize the effect of roughness configuration on the mean velocity profiles and the turbulence intensity and to compare data taken in the wind tunnel with some empirical formulas derived from the field data.

The roughness utilized in this study was the result of arrays of pegs, whose individual height and diameter are 9 cm and 0.48 cm, respectively. The flow field above and within the roughness elements were studied for four different configurations of roughness.

Measurements of mean velocity and turbulence intensity were compared with existing empirical equations.

Chapter II

THEORETICAL BACKGROUND OF VEGETATIVE CANOPY RESEARCH

2.1 Review of Literature

Many experiments have been completed to study flow characteristics over a variety of large size roughness elements. Early work in this area is summarized in the book by Geiger (7). Further studies may be classified according to the character of the roughness elements. Measurements have been made over wheat, rice, corn, sugar beets, tea plants, and various forests (1, 7, 21, 25, 26, 28).

Among the various types of large size roughness elements, rice and wheat are similar in response to the wind. These roughness elements are characterized by the waving phenomena and the self sealing which depends on the wind speed. The waving phenomena cause the eddy structure to be different from that generated by the stiff roughness. Self sealing causes a change in the roughness parameter in the estimation of mean velocity profiles. The flow field above and within the rice plant has been investigated to study the exchange processes concerning the growth of rice by the staffs of the National Institute of Agricultural Sciences (Japan) (10, 11, 12, 26). The flow field over a wheat crop has been examined by Penman and Long (17). In their measurements, wind profiles are observed to have a completely different shape in calm and windy weather. For the study of vertical transport processes in the lowest portion of the earth's atmosphere, Tan and Ling proposed that separate studies must be made of the quasi-steady and transient states in the micrometeorological boundary layer of the earth (25). They also reported a set of field measurements over a wheat crop.

Roughness like corn and trees is less flexible than rice and wheat, so that the stiff roughness behaves against the wind in a different manner. Uchijima and Wright measured the mean velocity and turbulent velocity in and above a corn crop (28). The generalized wind profile in the corn crop was approximated by an empirical equation in which the wind velocity at the top of corn is used as the reference wind velocity. In a similar manner, the turbulent velocity profile was empirically approximated by using a turbulent velocity at the plant height as the reference velocity. To present momentum transfer coefficients, Lemon and Wright measured the flow field within and immediately above the corn canopy (30). The wind in pine stands was measured for the study of fire behavior and spread by Cooper (5). Mean horizontal wind speed profiles within and above a plantation of Japanese larch were obtained by Allen (1). He pointed out that a log-profile analysis of above-vegetation wind speeds yields a wide range of values for the roughness length parameter, Z_o , and the zero-plane displacement, d . His turbulence measurements showed deeper penetration of large eddies during high winds. The tree spacing is shown to be the important factor for the estimate of the variation in wind speed from power spectra. It is pointed out from the measurements of the intensity of turbulence within a deciduous forest by Huston, that wind speeds in a forested area appear to be related in a regular manner to the wind speed measured on the outside (8). In addition, he observed that measurements of the intensity of turbulence tend to be stable with height and vary regularly with the stability ratio.

According to a concept of controlled micrometeorological experimentation, as outlined by Lettau, two different wind profile

modification experiments in air flow over the ice of Lake Medota, Wisconsin, were made by employing an array of conifer saplings in the first case and bushel baskets in the second case (22). The same type of experiments on wind profiles within and above an artificial Christmas tree forest planted on the Lake Mendota ice were made by Stearns (23). These experiments stand between field experiments and model experiments in a wind tunnel.

Relatively few model studies have been carried out concerning the flow over large roughness elements in a shear layer. A study of the flow over flexible roughness has been made in the wind tunnel by Plate and Quraishi (18). This model study showed good agreement of the laboratory data with the field data of wheat and corn. To determine the necessary width of a normal windbreak, a wind tunnel experiment was performed by Iizuka (9). In his experiments, model trees were 15 cm in height and had crowns of iron net. Flat plates of iron net and board of the same height (15 cm) were also used as roughness for comparison. The results of this experiment were also found to be similar to those of the field experiments. In the study of the turbulent diffusion over a rough surface, Yano developed the concept of momentum defect superposition in the wakes of an array of roughness elements (31). Pegs 4.45 cm in height and 0.48 cm in diameter were used as roughness elements. The pegs were spaced 2.54 cm in the longitudinal and lateral directions. The roughness surface was 12.2 m long and 1.83 cm wide. The free stream velocity was set at 3.0 m/sec. Reference is made in Chapter IV to his theoretical results, relevant to the present research results. Similarity of flow patterns over barriers in the wind tunnel are discussed in detail in the report by Woodruff and Zingg (29). It

is pointed out that the problem of similarity becomes complicated if the body is placed in an already existing turbulent boundary layer, but at sufficiently high Reynolds numbers the drag coefficient is independent of Reynolds number.

To analytically understand the structure of the canopy flow field, Poppendiek considered a force balance on a differential lattice through which fluid is flowing (20). An expression for the velocity profiles is derived by postulating that the mixing length increases linearly with distance from the boundary in the turbulent layers within and above the boundary resistance region but the rates of increase in these two layers are different. In this paper, limited sets of experimental results are reported about the velocity profiles over an orange orchard and a brush field. The characteristic parameters of wind flow in an idealized vegetative canopy were examined by Cionco, Ohmstede and Appleby (3). The ideal canopy in this report is characterized by the assumption that (i) there exists a uniform vertical distribution of both the area density and the drag coefficients of the leaf-stalk configuration; (ii) the drag coefficient of the leaf-stalk configuration is independent of local Reynolds number; (iii) the mean velocity distribution within the canopy is exponential; (iv) there is a constant mixing length; and (v) a constant turbulence intensity exists within the canopy. The velocity profiles within and above the canopy which result from the idealized canopy are analogous to the logarithmic wind profiles based on the roughness and zero-plane displacement. Restricting consideration to the turbulent transfer of momentum, Cionco developed the model to predict the canopy wind profile within semi-rigid canopies (4). Making the same assumptions concerning the general characteristics

of the canopy's mixing processes, a solution was given for the wind profiles within a semi-rigid canopy. It is concluded in his study that although the model has limitations for semi-rigid vegetation, it yields reasonable results for canopies that meet the model's requirements.

2.2 Similarity

Geometrical, dynamical and thermal similarity must be achieved to complete the flow similarity in two systems of different length scales. The roughness used in our experiments is not related to any specific prototype so that geometrical similarity is not discussed here. Moreover, since the experiments have been made under the thermally neutral condition, the requirement for thermal similarity need not be considered either.

For complete dynamic similarity, the Rossby number (Ro), Reynolds number (Re) and Froude number (Fr) would have to be the same for both the model and the prototype (2). The Rossby number (Ro) can be eliminated from the requirements for similarity if the prototype length in horizontal plane is less than 150 km. The Froude number which is the ratio of a reference inertial force divided by a reference body force produced by differences in specific weight becomes important only when temperature differences exist. Iizuka based his model study in the wind tunnel on the assumption that the effects of Reynolds number on the application of the model study to actual flow field are very small (9). This is justified by the fact that the Reynolds number may have a great influence on a streamlined body but separated flow about elements like trees results in inertially dominated flow. This assumption about the effects of Reynolds number is supported in the discussion

of similarity of flow patterns in the wind tunnel by Woodruff and Zingg (29).

In addition to the similarity in the dimensionless parameters, the boundary conditions must be the same for both model and prototype. Accordingly, similarity in upstream conditions and in conditions at the upper boundary must be satisfied as well as the geometric similarity of the lower boundary. In our experiments, the upstream turbulent boundary layer was thickened artificially and the velocity profile measured upstream was observed to have the logarithmic distribution characteristic of the lower atmospheric flow field.

2.3 Mean Velocity Profile

For the case where the size of the roughness elements is such that the Reynolds number of the flow in their vicinity is large, the structure of the flow field becomes complex, and a number of parameters should be considered to describe the flow field. For instance, the roughness height and the number of roughness elements per unit area will affect the flow. Moreover, the manner in which the roughness elements are distributed on the surface will be of influence. Yet for convenience, the formulas which describe the velocity profiles in this type of flow should not be too complicated, hence, to simplify the profile description, the flow field is usually divided into two regions. One of the regions is the flow field above the roughness, the other is the flow inside the roughness elements.

In 1925, Prandtl expressed the fully developed turbulent pipe flow near the smooth surface in non-dimensional form on the assumption that the shearing stress at the wall τ_o, density of fluid ρ and

the viscosity μ have an affect on the velocity profile but that the diameter does not. Hence,

$$\frac{U}{\sqrt{\tau_o/\rho}} = f\,(ZU/\nu)$$

or

$$\frac{U}{U_*} = f\left(\frac{Z\,U_*}{\nu}\right) \qquad \text{where} \qquad U_* = \sqrt{\frac{\tau_o}{\rho}} \quad . \tag{2-1}$$

When the effect of the roughness is considered, the law of similarity, Eq. (2-1), expands to

$$\frac{U}{U_*} = f\left(\frac{Z\,U_*}{\nu} \;,\; \frac{k_r\,U_*}{\nu}\right) \tag{2-2}$$

where k_r is a representative roughness length scale. For the case of a very rough surface with high Reynolds number flow condition, Nikuradse's pipe measurements show that the mean velocity distribution is completely independent of viscosity; thus the relation becomes

$$\frac{U}{U_*} = \frac{1}{k}\,\ell n\,\frac{Z}{k_r} + C_r$$

where the experimental constant C_r depends on the type of roughness.

In order to apply this concept of the velocity profile for the rough pipe to the flow over a flat plate covered with relatively high roughness elements, the action of roughness can be interpreted as being equivalent to a shift of the flat plate upward, or a zero-plane displacement, while k_r in the pipe flow can be replaced by an effective roughness size, or a roughness length Z_o .

Thus, the steady wind velocity profiles in the atmospheric shear layer over the roughness may be expressed for an adiabatic or neutral case by

$$\frac{U}{U_*} = \frac{1}{k} \ln \frac{Z - d}{Z_o} \quad (Z > h) \tag{2-3}$$

where

$k = 0.4$, von Karman's constant

$Z =$ Height above ground

$h =$ Height of roughness element

$U_* = \sqrt{\tau_o/\rho}$ Friction velocity

$d =$ Zero-plane displacement

$Z_o =$ Roughness length

τ Shear stress

ρ Mass density.

The velocity profile given by Eq. (2-3) is called the logarithmic profile. This expression has been derived by modifying the expression for the fully developed turbulent velocity profiles in a smooth pipe to apply the flow on the rough flat plate.

Several normalized wind profiles measured within a corn field by Stoller and Lemon are in good agreement with one another (24). From this fact, Saito concluded that the gradient of wind velocity within a crop is proportional to the reference wind velocity (wind velocity at the height of the corn), so that

$$\frac{dU}{dZ} = P(Z) \cdot U_h \tag{2-4}$$

where $P(Z)$ is a proportionality factor dependent upon wind velocity only (21). Under the boundary condition given by $U = U_h$ at the crop surface $Z = h$, Eq. (2-4) becomes

$$U = U_h \, e^{-\int_z^h P dZ} \quad . \tag{2-5}$$

He also suggested that the same equation mentioned above for the corn field is valid for the wheat field data, although P in the flow over the surface covered by wheat is a function of not only Z but also U because of the presence of the self sealing.

An exponential wind profile within the wheat field is also obtained empirically by Inoue, that is,

$$U = U_h \, e^{-\alpha(h-Z)} \tag{2-6}$$

where α = const. He indicates, however, that the condition α = const. throughout the height of the roughness element is not well satisfied in the general case. The roughness in our experiments consists of pegs whose height h and diameter ϕ are 9 cm and 0.48 cm, respectively. Therefore, the behavior of flow within the roughness elements might be similar to the behavior of flow in a corn field rather than in a wheat field.

2.4 Growth of Internal Boundary Layer

The mean velocity profile depends on the roughness over which the wind has blown and is blowing. If the wind blows steadily over a homogeneous roughness of large fetch, the profile of mean velocity will

be in equilibrium with the underlying surface. It will be worth considering the case where the flow experiences an abrupt change in roughness. Two-dimensional and steady flow is assumed to flow at right angles to the line of the change in roughness. Whenever a flow passes over an area of different surface roughness, the flow does not immediately adjust at all levels to this new surface, rather the adjustments occur gradually. The depth of the new equilibrium layer increases with downstream distance from the line of discontinuity in roughness. This zone where finite time and distance are required for the flow to reach equilibrium with the new surface will be called the internal boundary layer.

By considering the net gain of momentum due to vertical flux into the region bounded by the top of the boundary layer, which is simply equal to the difference in the shearing stress between the top and bottom of the column of air, Elliot (6) arrived at the following differential equation

$$\left[\ln H - 3 - \frac{1}{H} + \frac{4}{\ln H}\left(1 - \frac{1}{H}\right)\right] \frac{dH}{d\chi} = \left(1 + \frac{\ln H}{\ln mH}\right) \frac{k^2}{Z_o}$$

where the velocity profiles were assumed to follow Prandtl's logarithmic law whose validity has been established, and

$$H = \frac{\delta}{Z_o} \quad , \quad \chi = \frac{x}{Z_o} \quad , \quad m = \frac{Z_o}{Z_o}$$

Z_o = Roughness parameter

δ = Height of boundary layer

x = Horizontal coordinate, positive downwind and primed quantity refers to values outside the boundary layer.

The solution to the above relation may be approximated by the simple expression

$$H = a\chi^n \quad \text{for} \quad \chi > 10^3 \quad .$$

Evaluation of a and n yielded the relation

$$\delta = \left(0.75 - 0.03 \ln \frac{Z_o}{Z_o'}\right) Z_o^{0.2} x^{0.8} \quad . \tag{2-7}$$

This expression implies a discontinuity in stress; however, it is very simple to apply in practice if the transition zone is narrow enough.

Panofsky and Townsend (16) removed this discontinuity on the assumption that the friction velocity ($\sqrt{\tau/\rho}$ where τ is the local shear stress) below the boundary increases with height. Using the equation of continuity and the equation of motion, they derived

$$\frac{dH}{d\chi} = \frac{k^2 \left(\frac{2}{S} - 1\right) \ln \frac{Z_o'}{Z}}{\frac{1-S}{2} (\ln H)^2 + \left(\frac{7}{3} S - \frac{5}{2}\right) \ln H - \left(\frac{7}{2} S - 4\right)}$$

where

$$S = \frac{\ln (Z_o'/Z_o)}{\ln \frac{h}{Z_o} - 1} \quad .$$

This relation was approximated after the necessary numerical integrations by

$$\delta = \left[1 + 0.28 \left(\frac{Z_o'}{Z_o}\right)^{0.30}\right] Z^{0.2} x^{0.8} \quad . \tag{2-8}$$

Except near the roughness discontinuity, the theories given above are in good agreement on the shape of the inner boundary layer growth.

A different approach to the problem of the growth of internal boundary layer has been made by Miyake (14). He assumed that the vertical rate of spread of a surface change is proportional to the standard deviation of the vertical velocity, and that it takes place locally in a framework moving with the local mean wind. Then

$$\frac{dH}{dx} = A \frac{\sigma_w}{U} \tag{2-9}$$

where σ_w is the standard deviation and A is a constant, and

$$\chi = \frac{x}{Z_o} \quad , \quad H = \frac{\delta}{Z_o} \quad .$$

For neutral conditions, U is given by the logarithmic law and σ_w is estimated as $1.05\ U_*$ according to a summary of unpublished data (15). The constant A is evaluated separately for each roughness. Assuming Gaussian distribution of vertical velocities, the internal boundary is chosen to be such that one percent of the air affected by the surface reaches above it. Then the solution to Eq. (2-9) reduces to

$$\chi = H\ (\ell n\ H-1) \tag{2-10}$$

The advantages of this theory are that it can be generalized to unstable air and that it presents a simple physical interpretation of the growth of the boundary.

2.5 Turbulence Intensity and Shear Stress

The investigation of turbulent velocity within and above the canopy is important to improve the understanding of the mass transport and heat transfer phenomena. Even if we restricted ourselves to deal with the behavior of the flow close to the ground covered by plants, the energy dissipation due to the turbulent or fluctuating quantities

in a boundary layer are treated from the statistical viewpoint so that the correlation products of the turbulent velocity components play important roles in the studies related to the fluctuating quantities. However, the main purpose of the turbulence measurements reported herein is to find a relation between the mean velocity and the turbulent velocity. Accordingly, the data taken in the wind tunnel are compared with the expressions obtained empirically. Further discussion about correlation of the turbulent components, distribution of the mixing length, etc., is not given here.

Several scientists have attempted to correlate the turbulent velocity at various heights with the mean velocity because the structure of turbulence depends not only on the conditions of roughness elements over which the flow is observed, but also on the flow's upstream history. The general expression is difficult to infer from the limited data taken in field measurements.

In 1952, Inoue (13) proposed the following expression.

$$\sqrt{\overline{u^2}}/U \propto Z^{-1/3} \, (\log Z/Z_o)^{-2/3} \quad . \tag{2-11}$$

By replacing the term $\log Z/Z_o$ by $Z^{1/4}$ as an approximation, Eq. (2-11) becomes

$$\sqrt{\overline{u^2}}/U \propto Z^{-1/2} \quad .$$

In the case where the roughness is high,

$$\sqrt{\overline{u^2}}/U \propto (Z-d)^{-1/2} \quad . \tag{2-12}$$

This relation has been used to evaluate the data taken in the wind tunnel.

For the turbulent velocity within crops, the following expression has been empirically formed by Inoue (11).

$$\sqrt{\overline{u^2}}/U_h \propto e^{-\beta(1 - Z/h)} \quad . \tag{2-13}$$

The above expression is based on the experimental results that the turbulence intensity is almost independent of height within the canopy. Meanwhile, Uchijima and Wright have claimed that the intensity of turbulence within crop canopies is not constant but decreases gradually downward from the top of crop height (28).

The structure of turbulence in the wind over a large size roughness is highly nonhomogeneous and nonisotropic. Accordingly, it is difficult to find a simple relation between the longitudinal turbulence component u' and the vertical component w'. The vertical turbulence component w' is theoretically found to be nearly equal to the friction velocity U_* (10). The experimental results of the ratio w'/U_* are reported to fall between 0.8 and 1.8 for the case of rice plants (11, 26). On the other hand, the vertical turbulence component w' over a rice plant was measured to be about one third of the longitudinal component u' when the wind speed is strong enough to cause a waving motion of the rice plants (11).

The friction velocity U_* in the nonisotropic turbulent flow field is defined by

$$U_* = \frac{\tau}{\rho} = -\sqrt{\overline{uw}} \quad . \tag{2-14}$$

The turbulent shear stress $-\rho\overline{uw}$ is a very important quantity for the study of the mean velocity distribution and the momentum transport phenomena.

In our experiments, unfortunately, the measurements of $-\overline{uw}$ are reliable only in the case of pegs spaced 2.54 x 2.54 cm (sq). Hence, only in the case of 2.54 x 2.54 cm (sq), the turbulent shear stress is compared with the vertical turbulence components (w') .

Chapter III

EXPERIMENTAL APPARATUS AND PROCEDURE

The objective of the experiments was to obtain data on mean wind velocity and turbulence intensity within and above a canopy consisting of peg elements, in order to relate the configuration of the roughness to the structure of the flow field.

The measurements described in this report were carried out in the Army Meteorological Wind Tunnel in the Fluid Dynamics and Diffusion Laboratory at Colorado State University (19).

3.1 Wind Tunnel

The recirculating meteorological wind tunnel, driven by a 250 hp d.c. motor, has a 27 meter long test section with a normal cross-sectional area 1.8 x 1.8 m. A set of fine screens reduces ambient turbulence to a level of less than 0.1 percent. A trip fence (turbulence stimulator), located just upstream from the test section, serves to stabilize the flow pattern as well as to provide a thicker turbulent boundary layer than would exist without it. The artificial roughness used was placed in the tunnel to cover an 11 meter length of the test section floor beginning 12.2 m from the upstream end (Fig. 1). In all measurements, the slope of the test section ceiling was adjusted to make the pressure gradient zero in the flow direction. An additional turbulence stimulator made from strips of flexible plastic 6.3 cm wide and 0.019 cm thick was placed on the first 3 m of the wind tunnel floor to make the turbulent boundary layer thicker at the test section. The

floor section between the rough surface of pegs over which measurements were made and the flexible roughness of plastic strips was smooth (9.2m).

3.2 Arrangement of the Roughness Elements

The rough surface was composed of 18 aluminum plates into which pegs 9 cm in diameter and 0.48 cm in height were inserted as the roughness elements.

The pegs were arranged in four patterns:

a) The pegs were spaced 2.54 cm in the longitudinal direction and in the lateral direction. This arrangement is designated as 2.54 x 2.54 cm (sq).

b) The pegs were spaced 5.08 cm in the longitudinal direction and in the lateral direction. This arrangement is designated as 5.08 x 5.08 cm (sq).

c) One peg was inserted at the center of a square formed by four pegs spaced 2.54 cm in both longitudinal and lateral directions. That is, pegs were spaced 1.80 cm on the diagonal. This arrangement is designated as 1.27 x 1.27 cm (diag).

d) One peg was inserted at the center of a square formed by four pegs spaced 5.08 cm in both longitudinal and lateral direction. That is, pegs were spaced 3.60 cm on the diagonal. This arrangement is designated as 2.54 x 2.54 cm (diag). These four arrangements of pegs are shown in Fig. 2. In the cases of 2.54 x 2.54 cm (sq) and 5.08 x 5.08 cm (sq), the measurements of the mean velocity and turbulence within or just above pegs were made at the center of a square formed by four pegs. In the cases of 1.27 x 1.27 cm (diag) and 2.54 x 2.54 cm (diag), one peg was removed and the measurements were made at this position.

3.3 Measuring Equipment

3.3.1 Mean velocity profiles - The free stream velocity was set to be 12 m/s at x = - 1 m and z = 1 m. Since the tunnel ceiling was set for a zero pressure gradient the mean velocity above the canopy boundary layer remained constant. The mean velocity profiles were measured by using not only a pitot static tube but also a hot-wire anemometer, because the turbulence level in and immediately above the canopy is very high, which introduces a large error in the pitot static tube measurement. The accuracy of a hot-wire anemometer is not expected to be as sensitive to the high turbulence intensity in the measurement of mean velocity.

The pitot static tube and the single hot wire were installed on a vertical carriage so that the vertical position of the pitot tube and the hot wire could be changed continuously by the driving action of a small d.c. motor. The hot-wire probe used for the experiments is the tungsten wire of 0.005 mm in diameter and approximately 2.54 mm in length, soldered on a Disa hot-wire probe. The resistance of the wire was kept constant by continuously correcting the amount of current required to maintain the bridge balance of a Colorado State University Solid State Anemometer System (32).

The outputs of total and static pressure from the tube were connected to the two ports of an electronic differential pressure transducer (Trans-sonic, Equibar type 120). The d.c. voltage output of this pressure transducer was recorded on an x-y plotter versus the output which indicated the vertical position of the carriage.

The wind speed can be calculated by the relation,

$$U = 2.36 \sqrt{\frac{\Delta h}{\rho}} \qquad (3\text{-}1)$$

where

Δh = dynamic pressure in mm Hg

ρ = air density in slugs/ft

U = wind speed in ft/sec.

To measure the mean velocity by the hot-wire anemometer, the output voltage from the single hot wire was recorded on an x-y plotter versus vertical position of probe. The mean velocity can be determined from a calibration curve which shows the relation between the output voltages of the hot wire and the mean velocity as measured by a pitot static tube.

3.4 Turbulence Intensity Profiles

The longitudinal and vertical turbulence profiles were measured by monitoring the a.c. signal of the hot-wire anemometer probes. The longitudinal turbulence u' was measured by a single-wire probe. The fluctuating voltage required to maintain the bridge balance was presented on an x-y recorder from an RMS meter (B & K, Electronic Voltmeter, type 2409). The vertical turbulence intensity was measured by a cross wire (x-wire, Disa 55A32). The fluctuating signals of two wires through an RMS meter were presented on an x-y recorder.

The data of turbulence intensity were interpreted according to the relations described below. For the longitudinal turbulence measurements by a single hot wire, the relation between the turbulent velocity u' and the output voltage of an RMS meter $\sqrt{\overline{e^2}}$ is given by

$$u' = \sqrt{\overline{u^2}} = \frac{\sqrt{\overline{e^2}}}{(dE/dU)} \tag{3-2}$$

where (dE/dU) is the sensitivity of a hot wire, namely the slope of the single wire calibration. In the case where a cross wire is used to measure the vertical turbulence intensity distributions (w') and the turbulent shear stress $(-\overline{u\,w})$, the following relations were used to calculate those values.

$$\sqrt{\overline{w^2}} = \left[\frac{1}{2}\left\{\frac{\overline{e_1^2}}{(dE/dU)_1^2} + \frac{\overline{e_2^2}}{(dE/dU_2^2)} - 2\overline{u^2}\right\}\right]^{\frac{1}{2}} \tag{3-3}$$

$$\overline{uw} = -\frac{1}{4}\left|\frac{\overline{e_1^2}}{(dU/dE)_1^2} - \frac{\overline{e_2^2}}{(dU/dE)_2^2}\right| \tag{3-4}$$

where $\overline{e^2}$ is the fluctuating output voltage through an RMS meter and (dE/dU) is the sensitivity of a cross wire determined from the wire calibration. The subscripts 1 and 2 refer to the values corresponding to each of two wires of a cross-wire probe.

The measurements described by Eqs. (3-2) and (3-3) were also checked by a second, somewhat less accurate method by using a sum and difference circuit which gives the instantaneous sum and difference of the output signals from a cross-wire probe. The longitudinal and vertical components $(u'$ and $w')$ are given by

$$u' = \sqrt{\overline{u^2}} = \left[\frac{\overline{e_s^2}}{2(dU/dE)^2}\right]^{\frac{1}{2}} \tag{3-5}$$

$$w' = \sqrt{\overline{w^2}} = \left[\frac{\overline{e_d^2}}{2(dU/dE)^2} \right]^{\frac{1}{2}} \tag{3-6}$$

in which $\overline{e_s^2} = \overline{(e_1 + e_2)^2}$, that is, the mean square of the instantaneous sum of the output signals from a cross-wire probe, and $\overline{e_d^2} = \overline{(e_1 - e_2)^2}$. In the above two relations, the sensitivity of the two wires of a cross-wire probe are assumed to be the same.

Chapter IV

RESEARCH RESULTS AND DISCUSSION

The purpose of the experiments was to find the characteristics of the flow field within and above the roughness elements variously arranged. Therefore, the mean velocity profiles and the turbulence intensity were of primary interest.

The experimental results are separately described in the following three sections with respect to mean velocity profiles, the growth of boundary layer and turbulence intensity.

4.1 Mean Velocity Profiles

The mean velocity profiles in the vertical direction can be divided into two parts, that is, the mean velocity profiles within the canopy and those above the canopy. The velocity profiles within and above the canopy are quite different from each other.

One criterion, possibly the most reasonable one, for the division of the mean velocity profiles into two parts is the height of the roughness elements. (In the experiments, the height of roughness elements was equal to 9 cm).

Figures 3, 4, 5 and 6 are non-dimensional isoheights of the flow above and within the canopies. These figures suggest that flow above the canopy is divided into two regions along the canopy, namely, initial and quasi-established regions. In the initial regions, the change in the mean velocity dominates. The quasi-established region is characterized by smaller, yet finite changes in the mean velocity.

This is the reason that this region is called "quasi-established" instead of "established" or "equilibrium."

It is observed from the comparison of the lengths of the initial regions in four different densities of roughness that the retardation of flow is closely related to the density of roughness. With more dense roughness, the retardation of flow becomes larger. It is also shown in these four figures that the region between x 8.0 m and $x = 10.0$ m can be regarded as the region which characterizes an equilibrium flow field and might be a model of an actual canopy flow.

Figures 7, 8, 9 and 10 are the streamlines in four cases. As shown in Fig. 11 (2.54 x 2.54 cm (sq)), the lateral distribution of the mean velocity within the canopy is not uniform. According to the measurements made by Yano (31), the velocity profiles directly behind the roughness elements are not the same as the velocity profiles between two elements, even if the profiles are taken at a very far downwind distance from the leading edge of the rough surface. But this difference in profiles becomes negligible above the rough surface. In our measurements, the velocity magnitude varies by up to 30 percent laterally within the canopy. The lateral distribution of the mean velocity immediately above the canopy may not be uniform, although the measurements in the lateral direction above the canopy were not made for our study. But for convenience, the velocity distribution was assumed to be two-dimensional in the calculation of these streamlines to obtain a qualitative picture of the flow field. These figures also show that the initial region is affected by the roughness density, and, in this region, the flow patterns differ from each other according to the density of roughness. With denser roughness elements, more flow is pushed upward. Between $x = 0.2$ m

and 3.0 m , the flow immediately above the roughness elements seems to repenetrate into the roughness.

The streamlines in the case of pegs spaced 1.27 x 1.27 cm diag reveal that the adjustment of the ceiling of the wind tunnel to make the pressure gradient along the canopy zero had not been done correctly, so that the flow was accelerated beyond $x = 7.0$ m . In the case of pegs spaced 2.54 x 2.54 cm (sq), perturbations in the streamlines near the end of the canopy may result from irregular ceiling adjustment.

Because of the small change in the gradient of streamlines, the region near the end of the canopy should again be called a "quasi-established" region.

In Figs. 12 and 13, the mean velocity profiles taken in the wind tunnel are compared with field data for a deciduous forest taken by Tourin and Shen (27). The roughness consisting of pegs is expected to simulate the deciduous forest in winter. As shown in Fig. 12, the wind-tunnel data of the velocity profile, especially the data for the cases of 1.27 x 1.27 cm (diag) and 2.54 x 2.54 cm (sq), fit the field data well. Concerning the velocity profile above the canopy, the data for the cases of 1.27 x 1.27 cm (diag) and 2.54 x 2.54 cm (sq) also fit the field data well. Tourin pointed out that the field data in summer are not accurate in measurements of the mean velocity within the canopy.

The measured values of the mean velocity described in Chapter II are given in Tables 1, 2, 3 and 4. The values of the mean velocity from the floor ($Z = 0$) to $Z = 60$ cm were taken by using a single hot wire. The values above $Z = 60$ cm were measured by a pitot static tube. Although a single hot wire was expected to give better results in the regions of the high turbulence level than a pitot static tube,

as mentioned in Chapter III, a fairly large discrepancy existed between the values given by a hot wire and by a pitot static tube, even at $Z = 60$ cm where the turbulent velocity is very small compared with the local mean velocity. Yet the values measured by a hot wire and a pitot static tube at this height should be nearly equal.

After repeating the calibrations of the hot wire to find the causes of this discrepancy, it was realized that a very small difference of the output voltage from a hot wire for a high velocity gives a large difference in the mean velocity. Moreover, the calibration curves themselves shifted with time after a hot wire was stabilized for an entire day; however, the shape of the calibration curve for the hot wire, namely, the sensitivity of a hot wire dE/dU remained the same. This shift of the calibration curve is large enough to cause the discrepancy between the measured values of the mean velocity by a hot wire and a pitot static tube. The following method was adopted as a reasonable and practical method of correction based on the above results. First, the voltage corresponding to the velocity by a pitot static tube at $Z = 60$ cm was found from the calibration curve of a hot wire, which is designated as E_1 . The output voltage of a hot wire at $Z = 60$ cm is designated as E_2 . Then the curve of the output voltage of a hot wire recorded by an x-y recorder was shifted as a whole by adding $\Delta E = E_1 - E_2$ to the values of this curve. From this modified curve of the output voltage, the mean velocity up to $Z = 60$ cm was evaluated from the calibration curve of a hot wire. Figure 14 shows the example of the corrected velocity profile.

4.1.1 Mean velocity profiles above canopy - Figures of the experimental mean velocity profiles in the region between $x = 8.0$ m

and $x = 10.3$ m were prepared as U/U_* versus $(Z-h)/Z_o$ according to Eq. (2-1), because Eq. (2-1) is the expected expression of the velocity profile in the established region. In Eq. (2-1), three parameters, U_* (friction velocity), d (zero plane displacement), and Z_o (roughness length), are unknowns. They are to be determined from the measured wind profiles. If three values of the velocity distribution are known, the three parameters U_*, d and Z_o can be found from a system of three equations with three unknowns. That is, if U_1, U_2 and U_3 are the wind speed at the heights Z_1, Z_2 and Z_3, respectively, U_*, d and Z_o are determined by the following three equations:

$$\frac{U_2 - U_1}{U_3 - U_2} = \frac{\ell n\ (Z_2 - d)/(Z_1 - d)}{\ell n\ (Z_3 - d)/(Z_2 - d)} \tag{4-1}$$

$$U_* = \frac{k\ (U_1 - U_2)}{\ell n (Z_1-d)/(Z_2-d)} \tag{4-2}$$

$$Z_o = \frac{Z_1 - d}{e^{kU_1/U_*}} \quad . \tag{4-3}$$

Since d is difficult to evaluate from the measured velocity profiles, d was assumed to equal the height of the roughness elements $h = 9$ cm in the computation. This approximation has been applied successfully previously by Plate and Quraishi (18) for flow over a canopy of flexible plastic strips. Hence,

$$U_* = \frac{k\ (U_1 - U_2)}{\ell n \left(\frac{Z_1 - h}{Z_2 - h}\right)} \tag{4-2}'$$

$$Z_o = \frac{Z_1 - h}{e^{kU_1/U_*}} \quad . \tag{4-3)'}$$

The calculated values of U_* and Z_o are shown in Figs. 15 and 16. Some values of the friction velocity are also shown with respect to the density of roughness in Figs. 17 and 18.

Next, the values of the friction velocity U_* in the region between $x = 8.0$ m and 10.3 m were recalculated by adopting the average values of Z_o in this region for each case of four different densities of roughness according to the relation

$$U_* = \frac{U_1}{\frac{1}{k} \ln \frac{Z_1 - h}{Z_o}} \tag{4-4}$$

where U_1 is referred to as the velocity at any one height Z_1 in the region where the velocity profile plotted U versus ℓn (Z-d) is a straight line. Figures 19, 20, 21 and 22 show the logarithmic velocity distributions calculated with the values of $k = 0.4$, $d = h = 9$ cm, the average values of Z_o and the corrected values of U_* in four cases of roughness density. The mean velocity profiles are roughly approximated by the logarithmic profile except near the top of the roughness. Because of this exception, it should be observed that the logarithmic profile is not good enough to represent the entire velocity profile above the canopy. In fact, the mean velocity profiles measured in the field are also approximated by the logarithmic form, but cannot be well defined in that form. Yano (31) suggested that one should separate the profile into 5 zones depending upon the flow characteristics.

In his arguments, zone 2 is defined as the horizontal two-dimensional wake zone of the pegs. The magnitudes of wind velocity in this zone and the zone's extent decay in the wind direction. Zone 4 is defined as the turbulent shear flow zone where logarithmic or power law theory satisfies the experimental data. Zone 3 is a type of transition zone which connects zone 2 and zone 4. Yano pointed out that when the logarithmic or power law is applied to the velocity profile in zone 4, then it is necessary to specify zone limits; however, the upper limit of zone 3 is not clear. If the upper limit of zone 3 is defined as the height where the velocity profiles plotted versus $\ell n(z-h)$ deviate from a straight line, this limits zone 3 for the 9 cm pegs to $2.5 \sim 3.0$ h. In zone 3, the periodic velocity profile in the lateral direction is also observed to change gradually to a uniform profile by Yano.

In the case of roughness elements spaced 2.54 x 2.54 cm (diag), the friction velocity U_* was also estimated from the measurements of the drag force by means of a shear plate. This result is shown with the results calculated from the velocity profiles along the canopy in Fig. 23. In the initial region, the differences between the values of the friction velocity U_* estimated from the velocity profiles and from the drag measurements are large. In the initial region, the velocity is in the state of transition so that the friction velocity estimated from the mean velocity profiles is not necessarily of the same order as that obtained from the drag measurement. The friction velocity calculated from the drag force suddenly increases near the leading edge of roughness because the stagnation pressure exerted on the front of roughness contributes to the increase of the drag force in this region. In the quasi-established region, the difference between the

friction velocities estimated from velocity profiles and the drag force is at most 32 percent of the values obtained from the drag balance.

4.1.2 Mean velocity profiles within canopy - Experimental wind profiles within the canopy have been expressed empirically for field data as

$$U = U_h \, e^{-\alpha(h-Z)}$$

or

$$\ell n \, \frac{U}{U_h} = - \alpha(h-Z) \quad .$$

The logarithmic values of $\frac{U}{U_h}$ are plotted against $(h-Z)$ as shown in Fig. 24. It is concluded that the above relation holds well for the data obtained in the wind tunnel as well as for field data. This relation fits quite well for the cases of 5.08 x 5.08 cm (sq) and 2.54 x 2.54 cm (diag), although the value of α is not constant along the canopy. For the case of 1.27 x 1.27 cm (diag), the roughness is so dense that the flow near the ground surface is almost zero. Therefore, it cannot be confirmed as to whether the exponential velocity profile actually exists in very dense roughness. As pointed out above, the value of α is not constant along the canopy, but it has been verified that the velocity at an arbitrary height within a canopy is readily estimated if the velocities at the top of roughness element and at any other height are measured. The values of α evaluated are given in Table 17.

4.2 Growth of Internal Boundary Layer

The growth of the internal boundary layer was estimated in two manners. One estimation was made from the data of mean velocity profiles on the assumption that the logarithmic profiles in the internal

boundary layer are different from those upstream of the discontinuity of roughness, although the logarithmic profiles hold both upstream and downstream of the change in roughness. The measured values of wind velocity were plotted against the logarithm of height minus roughness height, $Z - h$. As shown in Fig. 25, a break in the profile occurred at the intersection of two logarithmic profiles. The height of this "kink" is regarded as the height of the internal boundary layer. The other estimation was realized from the data of turbulence intensity, u'/U_{local} . The internal boundary layer height was taken as the height at which the turbulence intensity becomes equal to the intensity in front of the roughness $(x = -1m)$. The results of the estimation are shown in Figs. 26, 27, 28 and 29. In Figs. 30 and 31, the same results are plotted in logarithmic scale. From the figures in logarithmic scale, the heights of the internal boundary layer are evaluated for four different arrangements of roughness as follows.

For 1.27 x 1.27 cm (diag), $\delta - h = 0.183\ x^{0.809}$

For 2.54 x 2.54 cm (sq), $\delta - h = 0.338\ x^{0.727}$

For 2.54 x 2.54 cm (diag), $\delta - h = 0.152\ x^{0.768}$

For 5.08 x 5.08 cm (sq), $\delta - h = 0.128\ x^{0.781}$

According to the evaluation of the growth of internal boundary layer by both Elliot (6) and Panofsky and Townsend (16), the height of the internal boundary is given as

$$\delta = \text{const}\ x^{0.8} \qquad (4\text{-}5)$$

when the roughness parameters upstream and downstream of change in roughness are known. In their theoretical work, the displacement height $(d = h$ in our case$)$ is regarded as small compared with the

height of the internal boundary layer. Moreover, their equations are actually available for the large value of χ . Yano analyzed the development of the internal boundary layer by taking the width envelope of the combined wakes (31). He pointed out that the development of the internal boundary layer cannot be represented by a power function as x^{α} , but at the local zone of the far downwind distance from the leading edge of the rough surface, the height of internal boundary layer δ is approximately represented by the function of x^{α} where $\alpha \simeq 0.8$. In our experiments, the roughness height is large compared with that of the internal boundary layer, particularly when the growth of the internal boundary layer close to the change in roughness is of interest; the effect of the roughness height on the growth of boundary layer cannot be ignored. Therefore, the difference between the height of internal boundary layer and the roughness height, δ-h , will be substituted into Eq. (4-5) instead of the boundary layer height, δ . Thus

$$\delta - h = \text{const } x^{0.8} \quad . \tag{4-6}$$

As seen above, the plotting of data according to Eq. (4-6) seems to give the good results. To estimate the growth of the internal boundary layer near the change in roughness, an estimation based on turbulence intensity gives better results than one based on mean velocity profiles. In the case where the height of the internal boundary layer is estimated from turbulence intensity data, the relation (4-6) will hold, although it is in fact derived for large value of χ .

4.3 Turbulence Intensity

Profiles of the longitudinal component of turbulent velocity (u') are shown in Figs. 32 to 35c. The turbulence intensity u'/U

for four different densities of roughness are also shown in Figs. 36 to b. From these figures, turbulence is observed to reach an equilibrium state beyond $x = 8.0$ m $(x/h \simeq 89)$ in our experiments. As stated in Cahpter II, the turbulence intensity profiles are proposed to be functionally

$$u'/U = \sqrt{\overline{u^2}}/U \propto (Z-h)^{-\frac{1}{2}}$$

or

$$\log (u'/U) \propto -\frac{1}{2} \log (Z-h) \quad .$$

According to the above relation, the ratio of log (u'/U) to log $(Z-h)$ must be equal to minus one half. But, as seen in Fig. 40, a "kink" exists at $Z-h \simeq 20$ cm $(Z/h \simeq 3.3)$. The ratios log (u'/U)/log $(Z-h)$ for $(Z-h)$ larger than 20 cm lie between -0.48 and -0.70 , while the ratios below the "kinks" are far from minus one half. Apparently, in the lower region, a three-dimensional wake caused by the top of the roughness elements interacts with the upper shear layer. To describe the turbulence intensity profiles immediately above the roughness, the interaction of the three-dimensional wake should be considered in more detail. The measured values of turbulent velocity u' and turbulence intensity u'/U are given in Tables 5 to 12. The slopes of turbulence intensity profiles in the exponential form (i.e., the value of α in $\frac{u'}{U} = (z-h)^{-\alpha}$) are given in Table 18.

Figures 41a, b and c show the turbulent velocity profiles within crops plotted according to Eq. (2-13) and estimated as follows:

For 2.54 x 2.54 cm (sq), $\beta = 1.38$

For 2.54 x 2.54 cm (diag), $\beta = 1.02$

For 5.08 x 5.08 cm (sq), $\beta = 0.72$.

In the case of 1.27 x 1.27 cm diag, the density of roughness is large, and the mean velocity and turbulent velocity within the roughness could not be measured accurately.

Figures 42 to 44b show the profiles of vertical component of turbulent velocity for three cases of different arrangements of pegs. In Tables 13 to 15, the measured values of $w' = \sqrt{\overline{w^2}}$ are given. The coefficient of anisotropy is a measure of the anisotropy of turbulence. It is very important in turbulent diffusion because the square of it represents the ratio of total eddy energy for the vertical (or lateral) and longitudinal components of wind velocity (27). The vertical coefficient of anisotropy is given by w'/u' . Tourin and Shen reported that the vertical-longitudinal coefficient of anisotropy above the deciduous forest canopy under neutral and stable conditions has a value of 0.4 (27). This coefficient is also observed to increase with height in the surface layer under neutral and stable conditions due to u' decaying more rapidly with height than does w' . The field data obtained for rice plants give 0.33 as this coefficient w'/u' (26). The coefficient of anisotropy (w'/u') above the canopy for our measurements falls between 0.5 and 0.7. Within the canopy, high intensity turbulence exists so that the measurements of u' and w' are not sufficiently accurate to give a quantitative picture. To improve the accuracy in this measurement, the use of a linearizer is recommended. In Fig. 45, the wind tunnel data are compared with field data taken by Tourin (27).

Figures 46a and b show the profiles of the turbulent shear stress for the case of 2.54 x 2.54 cm (sq). The measured values of

$-\overline{uw}$ are given in Table 16. The ratio of w' to $\sqrt{|\overline{uw}|}$ is between 1.0 and 1.8 in the quasi-established region, while in the initial region this ratio is between 1.4 and 3.7. Yano also predicted the ratio $w'/\sqrt{\overline{uw}}$ should be a constant (31). From the field measurements, the ratio $w'/\sqrt{|\overline{uw}|}$ is observed to fall between 0.8 and 1.8 (26). Therefore, the roughness models in our experiments can be used for the study of the transport phenomena.

Chapter V

SUMMARY AND CONCLUSION

The structure of a canopy flow field was investigated for four different densities of roughness elements. The following results were obtained:

1. The mean velocity profiles above the canopy are roughly approximated by the logarithmic profile except for the region up to $2.5 \sim 3.0\ h$ from the floor.

2. For the mean velocity within the canopy, the exponential velocity profile holds well for the data obtained in the wind tunnel as well as for field data.

3. When the roughness height is large compared with the height of the internal boundary layer, the height of the boundary layer is approximated by

$$\delta - h = \text{const} \cdot x^{\alpha}$$

where

$$\alpha \simeq 0.8 \quad .$$

To evaluate the height of the internal boundary layer close to the change in roughness, an estimation based on turbulence intensity gives good results.

4. The turbulence intensity profiles above the canopy can be divided into two parts. One is the region above $Z/h = 3.3$ and the other region is below $Z/h = 3.3$. In both regions, the turbulence intensity profiles can be approximated by

$$\log (u'/U) \propto - \alpha \log (Z-h) \quad ,$$

but the values of α in two regions are quite different. To represent the turbulence intensity profiles below $Z/h = 3.3$, the effects of the three-dimensional peg wake should be considered.

5. The turbulence velocity within the canopy can be represented in the exponential form (Eq. 2-13) and is related to the mean velocity at the top of roughness.

6. The coefficient of anisotropy above the model canopy is $20\% \sim 80\%$ larger than that measured in the field.

7. The ratio $w'/\sqrt{\overline{uw}}$ falls between 0.8 and 1.8, and agrees quite well with the results for flexible crops obtained in the field. No data were found for similar measurements in a stiff canopy, such as a forest.

BIBLIOGRAPHY

BIBLIOGRAPHY

1. Allen, Jr., L. H., Turbulence and wind speed spectra within a Japanese larch plantation. Journal of Applied Meteorology, Vol. 7, February 1968.

2. Cermak, J. E., V. A. Sandborn, E. J. Plate, G. H. Binder, H. Chuang, R. N. Meroney and S. Ito, Simulation of atmospheric motion by wind tunnel flows. Technical Report, Colorado State University, Fort Collins, Colorado, May 1966.

3. Cionco, R. M., W. D. Ohmstede and J. F. Appleby, Model for wind flow in an idealized vegetative canopy (Meteorological Research Notes No. 5) ERDAA-MET-7-63 Research Study, June 1963, U.S. Army Electronic Research and Development Activity, Fort Huachuca, Arizona.

4. Cionco, R. M., A mathematical model for air flow in a vegetative canopy. Atmospheric Sciences Research Division, Fort Huachuca, Arizona, AD No. 634668.

5. Cooper, R. W., Wind movement in pine stands. Georgia Forest Research Council, Macon, Ga.

6. Elliott, W. P., The growth of the atmospheric internal boundary layer. Transactions, American Geophysical Union, Vol. 39, No. 6, December 1958.

7. Geiger, R., The climate near the ground. Harvard University Press, Cambridge, 1950.

8. Huston, J. S., Observations of the micrometeorology and intensity of turbulence within a deciduous forest. CRDL Technical Memorandum 5-6, August 1964.

9. Iizuka, H., On the width of windbreak. Bulletin of the Government Forest Experiment Station, No. 56, Tokyo, Japan, December 1952.

10. Inoue, E., N. Tani and I. Imai, Measurements of the wind turbulence over cultivated fields. The Bulletin of the National Institute of Agricultural Sciences (Japan), Series A, No. 4, Tokyo, Japan, September 1955.

11. Inoue, E., On the turbulent structure of airflow within crop canopies. The Journal of Meteorological Society of Japan, Series II, Vol. 41, No. 6, December 1963.

12. Inoue, E., The environment of plant surface. Environmental Control of Plant Growth, Chapter 3, Academic Press Inc., N. Y., 1963.

13. Inoue, E., The structure of wind near the ground. The Bulletin of the National Institute of Agricultural Sciences (Japan), A-2, 1-93, 1952.

14. Miyake, M., Transformation of atmospheric boundary layer induced by inhomogeneous surfaces. Unpublished M.S. Thesis, University of Washington, 1961.

15. Oliphant, J. E., Growth of the internal boundary layer following large changes in roughness. M.S. Thesis in Meteorology, Pennsylvania State University, June 1964.

16. Panofsky, H. A. and A. A. Townsend, Change of terrain roughness and the wind profile. The Quarterly Journal of the Royal Meteorological Society, Vol. 9, No. 384, April 1964.

17. Penman, H. L. and I. F. Long, Weather in wheat; An essay in micro-meteorology. Quarterly Journal of Royal Meteorological Society, Vol. 86, pp. 16-50, 1960.

18. Plate, E. J. and A. A. Quraishi, Modeling of velocity distributions inside and above tall crops. Journal of Applied Meteorology, Vol. 4, No. 3, pp. 400-408, June 1965.

19. Plate, E. J. and J. E. Cermak, Micrometeorological wind tunnel facility. Final Report on Contract No. DA-36-039-SC-80371, U.S. Army, CER63EJP-JEC9, Colorado State University, Fort Collins, Colorado.

20. Poppendiek, H. F., Investigation of velocity and temperature profiles in air layers within and above trees and brush. University of California, Department of Engineering, Los Angeles, March 1949.

21. Saito, T., On the wind profile within plant communities. The Bulletin of the National Institute of Agricultural Sciences (Japan), Series A, No. 11, February 1964.

22. Stearns, C. R. and H. H. Lettau, Report on two wind-profile modification experiments in airflow over the ice of Lake Mendota. Annual Report, November 1963.

23. Stearns, C. R., Report on wind profile modification experiments using fields of Christmas trees on the ice of Lake Mendota. Annual Report, University of Wisconsin, Department of Meteorology, Madison, December 1964.

24. Stoller, J. and E. R. Lemon, Turbulent transfer characteristics of air stream in and above the vegetative canopies at the earth's surface. U.S. Department of Agriculture Prod. Res. Report No. 72, 1963.

25. Tan, H. S. and S. C. Ling, Quasi-steady micro-meteorological atmospheric boundary layer over a wheat field. TAR-IR 602, Therm Advanced Research Division of Therm Inc., Ithaca, New York, July 1960.

26. Tani, N., The wind over the cultivated field. The Bulletin of the National Institute of Agricultural Sciences (Japan), Series A, No. 10, March 1963.

27. Tourin, M. H. and W. C. Shen, Deciduous forest diffusion study. Report 3004, Vol. 1, Applied Science Division, Litton Systems, Inc., Minneapolis, Minnesota, August 1966.

28. Uchijima, Z. and J. L. Wright, An experimental study of air flow in a corn plant-air layer. Research Report No. 367, Bailey Hall, Ithaca, New York, July 1963.

29. Woodruff, N. P. and A. W. Zingg, Wind tunnel studies of fundamental problems related to windbreaks. U.S. Department of Agriculture, Soil Conservation Service, SCS-TP-112, Washington, D. C., August 1952.

30. Wright, J. L. and E. R. Lemon, Estimation of turbulent exchange within a corn crop canopy at Ellis Hollow (Ithaca, New York), 1961. Interim Report 62-7, Bailey Hall, Ithaca, New York, July 1962.

31. Yano, M., The turbulent diffusion in a simulated vegetative cover. Ph.D. Dissertation, Colorado State University, Fort Collins, Colorado, April 1966.

32. Operating and Maintenance Manual, (CSU Hot Wire Anemometer), Fluid Dynamics and Diffusion Laboratory, College of Engineering, Colorado State University, Fort Collins, Colorado.

APPENDIX A

APPENDIX A

THE EFFECT OF TURBULENCE ON THE MEASUREMENT OF MEAN VELOCITY

There is a high turbulence level in or immediately over the canopy. This high turbulence level introduces a large error in a pitot static tube measurement because the holes on the side of a pitot static tube for the measurement of static pressure sense not only the static pressure but also the dynamic pressure due to the turbulent velocity. As mentioned in Chapter III, the mean velocity profiles were measured by using a hot-wire anemometer in addition to a pitot static tube in order to reduce or to estimate the error introduced into the mean velocity measurements by the high turbulence.

The effect of turbulence on the measurements of the mean velocity as evaluated by Hinze and Corrsin are briefly discussed with respect to a pitot static tube and a hot-wire anemometer.

A.1 Pitot Static Tube

Goldstein suggested that the total-head tube measured the total head of the total velocity vector on the assumption that the frontal part of the tube might be considered a point of stagnation. In this case,

$$\overline{P}_{tot} = \overline{P}_{stat} + \frac{1}{2}\rho\left[\overline{(\overline{U}+u)^2} + \overline{v}^2 + \overline{w}^2\right]$$

$$= \overline{P}_{stat} + \frac{1}{2}\rho\left[\overline{U} + \overline{u} + \overline{v} + \overline{w}\right] \quad . \qquad \text{(A-1)}$$

However, in fact, the diameter of the total-head-tube hole is not infinitesimally small. The finite diameter of the total-head-tube hole causes deviations from the above relation (A-1). The total pressure measured by the tube is not equal to the total pressure existing in the center of the tube hole, since a lateral velocity gradient in turbulent flow may give a difference in velocity over a distance equal to the hole diameter. Moreover, the static pressure will be measured too low, mainly because of the lateral turbulent velocities perpendicular to the tube. Unfortunately, there has been no systematic investigation concerning the effect of turbulence on the readings of the pitot static tube.

Some idea of the effect of turbulence can be obtained by making use of the sensitivity characteristic of a pitot tube to deviations of the flow direction. The empirical relation for this characteristic can be roughly approximated by

$$\left(P_{tot}\right)_{means} = P_{stat} + \frac{1}{2}\rho\, U_{eff}^2 + B\,(\cos\phi - 1)\,\frac{1}{2}\rho\, U_{eff}^2 \qquad \text{(A-2)}$$

and

$$\left(P_{stat}\right)_{means} - P_{stat} = A\,(\cos\phi - 1)\,\frac{1}{2}\rho\, U^2 \qquad \text{(A-3)}$$

where $\cos\phi = \dfrac{\overline{U} + u}{U_{eff}}$, A and B are constant.

$$U_{eff} = \sqrt{(\overline{U} + u)^2 + v^2 + w^2} \quad .$$

After the series expansions according to powers of $\dfrac{u}{\overline{U}}$, $\dfrac{v}{\overline{U}}$ and $\dfrac{w}{\overline{U}}$ Eqs. (A-2) and (A-3) read

$$\left(\overline{P}_{tot}\right)_{means} = P_{stat} + \frac{1}{2}\rho\,\overline{U}^2\left[1 + \frac{\overline{u^2} + \overline{v^2} + \overline{w^2}}{\overline{U}^2} - B\left(\frac{\overline{v^2} + \overline{w^2}}{2\overline{U}^2} + \frac{\overline{v^4} + \overline{w^4} + 2\,v^2w^2}{8\overline{U}^4} + \ldots.\right)\right] \quad \text{(A-4)}$$

$$\overline{P}_{stat\ means} - P_{stat} = -A\,\frac{1}{2}\rho\,U^2\left[\frac{\overline{v^2} + \overline{w^2}}{2\overline{U}^2} + \frac{\overline{v^4} + \overline{w^4} + 2\,\overline{v^2w^2}}{8\,\overline{U}^4} + \ldots.\right] \quad \text{(A-5)}$$

By combining the expression (A-4) and (A-5)

$$\left(\overline{P}_{tot}\right)_{means} - \left(\overline{P}_{stat}\right)_{means} = \frac{1}{2}\rho\overline{U}^2\left[1 + \frac{\overline{u^2} + \overline{v^2} + \overline{w^2}}{\overline{U}^2} - (B-A)\left(\frac{\overline{v^2} + \overline{w^2}}{2\overline{U}^2} + \ldots.\right)\right] . \quad \text{(A-6)}$$

In the case of an isotropic turbulence, or in the case of $\overline{u^2} + \overline{v^2} + \overline{w^2}$, this yields

$$\left(\overline{P}_{tot}\right)_{means} - \left(\overline{P}_{stat}\right)_{means} = \frac{1}{2}\rho\overline{U}^2\left[1 + \frac{u^2}{\overline{U}^2}\ (3-B+A)\right] .$$

From static measurements, it has been found that $A \simeq 1$ and $B \simeq 3$. Hence,

$$\left(\overline{P}_{tot}\right)_{means} - \left(P_{stat}\right)_{means} = \frac{1}{2}\rho\overline{U}^2\left[1 + \frac{u^2}{\overline{U}^2}\right] . \quad \text{(A-7)}$$

This expression is also obtained by Hinze and Van der Hegge Zijnen who neglected the effect of the total turbulence velocities and considered only the axial turbulent velocity in Eq. (A-1).

A.2 Hot-Wire Anemometer

An estimate of the effect of large turbulent fluctuations on the hot wire response was made as suggested by Corrsin. The hot wire is sensitive essentially to the velocity components perpendicular to it since the velocity component parallel to the wire has comparatively little cooling effect. Hence, to estimate the effect of large turbulent fluctuations on the cooling of the wire, only longitudinal and lateral turbulent velocity components perpendicular to the wire are considered. Then,

$$U_{eff} = \sqrt{(U + u)^2 + w^2} \quad .$$

A series expansion gives

$$U_{eff} = \overline{U} \left(1 + \frac{u}{\overline{U}} + \frac{w^2}{2\overline{U}} + \frac{uw^2}{2\overline{U}^3} + \ldots \right) .$$

According to the results of King's solution for the subsonic convection of heat from small cylinders in continuum flow, the mean heat loss is given by

$$\frac{i^2 R}{(R-R_a)} = A + B \sqrt{U}$$

where A and B are constant. Hence, the value of $\sqrt{U_{eff}}$ must be considered instead of the value of U_{eff} . Thus,

$$\sqrt{U_{eff}} = \sqrt[4]{(\overline{U} + u)^2 + w^2}$$

$$= \sqrt{\overline{U}} \left(1 + \frac{u}{2\overline{U}} - \frac{1}{8}\frac{w^2}{\overline{U}^2} + \frac{1}{4}\frac{u}{\overline{U}^2} + \frac{1}{16}\frac{u^3}{\overline{U}^3} - \frac{3}{8}\frac{uw^2}{\overline{U}^3} + \ldots \right) .$$

The time average of the above expression is

$$\overline{\sqrt{U_{eff}}} = \sqrt{\overline{U}} \left(1 - \frac{1}{8}\frac{\overline{w^2}}{\overline{U}^2} + \frac{1}{4}\frac{\overline{u^2}}{\overline{U}^2} + \frac{1}{16}\frac{\overline{u^3}}{\overline{U}^3} - \frac{3}{8}\frac{\overline{uw^2}}{\overline{U}^3} + \ldots \right) .$$

From the above expressions, it is noticed that a "mixture" of the two turbulence components u and w affects the cooling of the wire. The expressions of $\overline{\sqrt{U_{eff}}}$ may be equated with $\sqrt{\overline{U}_{mean}}$. For $\overline{U}_{mean}$

$$\overline{U}_{mean} = \overline{U} \left(1 - \frac{1}{4}\frac{\overline{u^2}}{\overline{U}^2} + \frac{1}{2}\frac{\overline{w^2}}{\overline{U}^2} + \frac{1}{8}\frac{\overline{u^3}}{\overline{U}^3} - \frac{3}{4}\frac{\overline{uw^2}}{\overline{U}^3} + \ldots \right)$$

$$\simeq \overline{U} \left(1 - \frac{1}{4}\frac{\overline{u}}{\overline{U}} + \frac{1}{2}\frac{\overline{w}}{\overline{U}} \right) .$$

Then, the correction of the measured value for large turbulence may be either negative or positive depending on the ratio $\overline{u^2}/\overline{w^2}$. In the case of local isotropy, that is, $\overline{u^2} \simeq \overline{w^2}$, the correction is negative so that the actual velocity is smaller than the measured value.

APPENDIX B

Tables

Figures

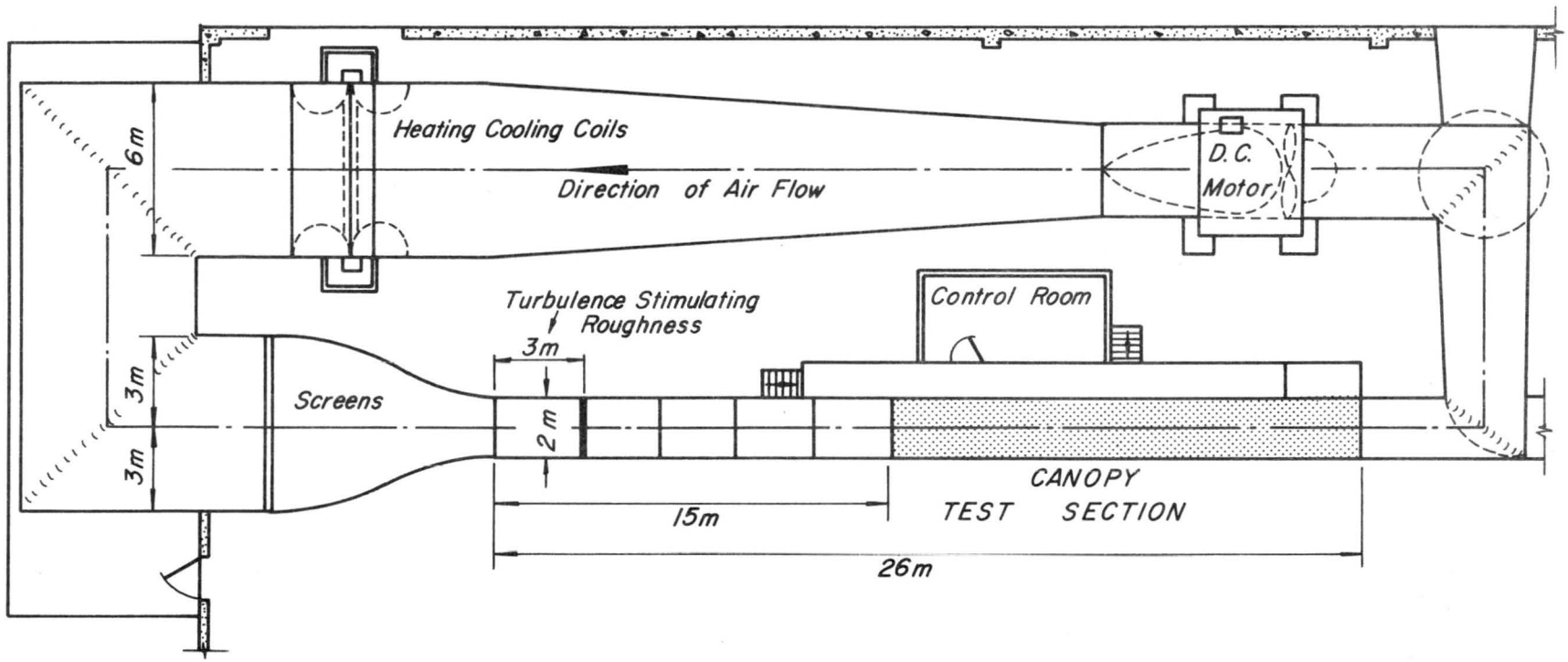

Fig. 1. Plan view of wind tunnel

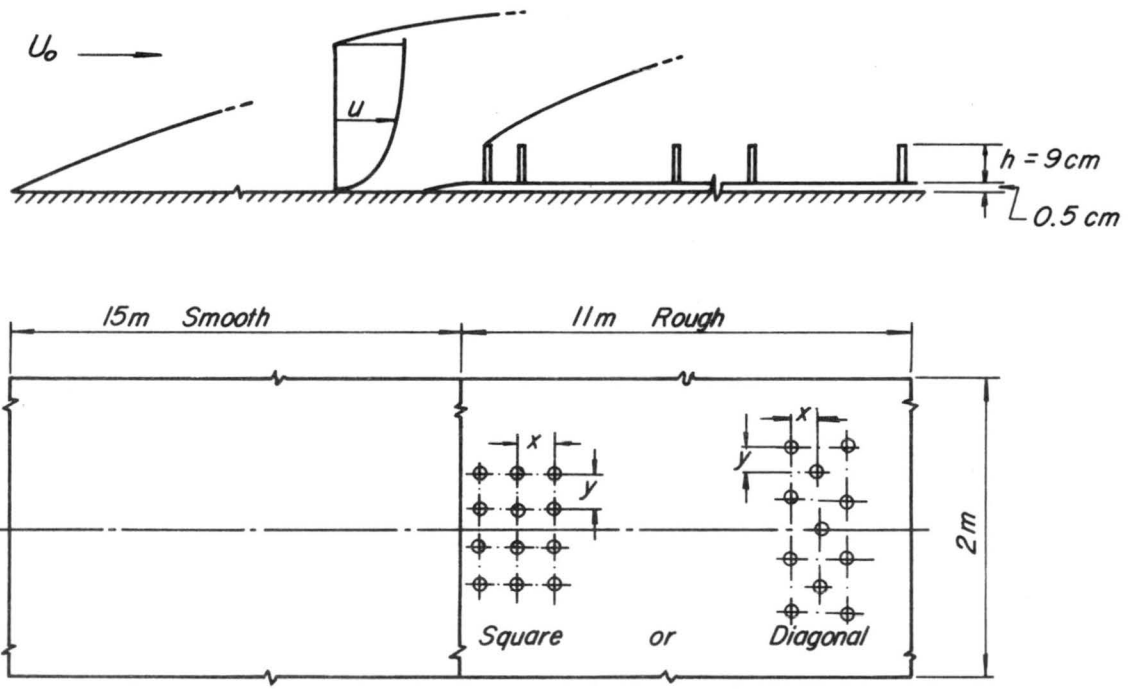

PEG ARRAYS STUDIED

x, cm	y, cm	ARRAY
1.27	1.27	DIAG.
2.54	2.54	SQ.
2.54	2.54	DIAG.
5.08	5.08	SQ.

Fig. 2. Artificial canopy configuration

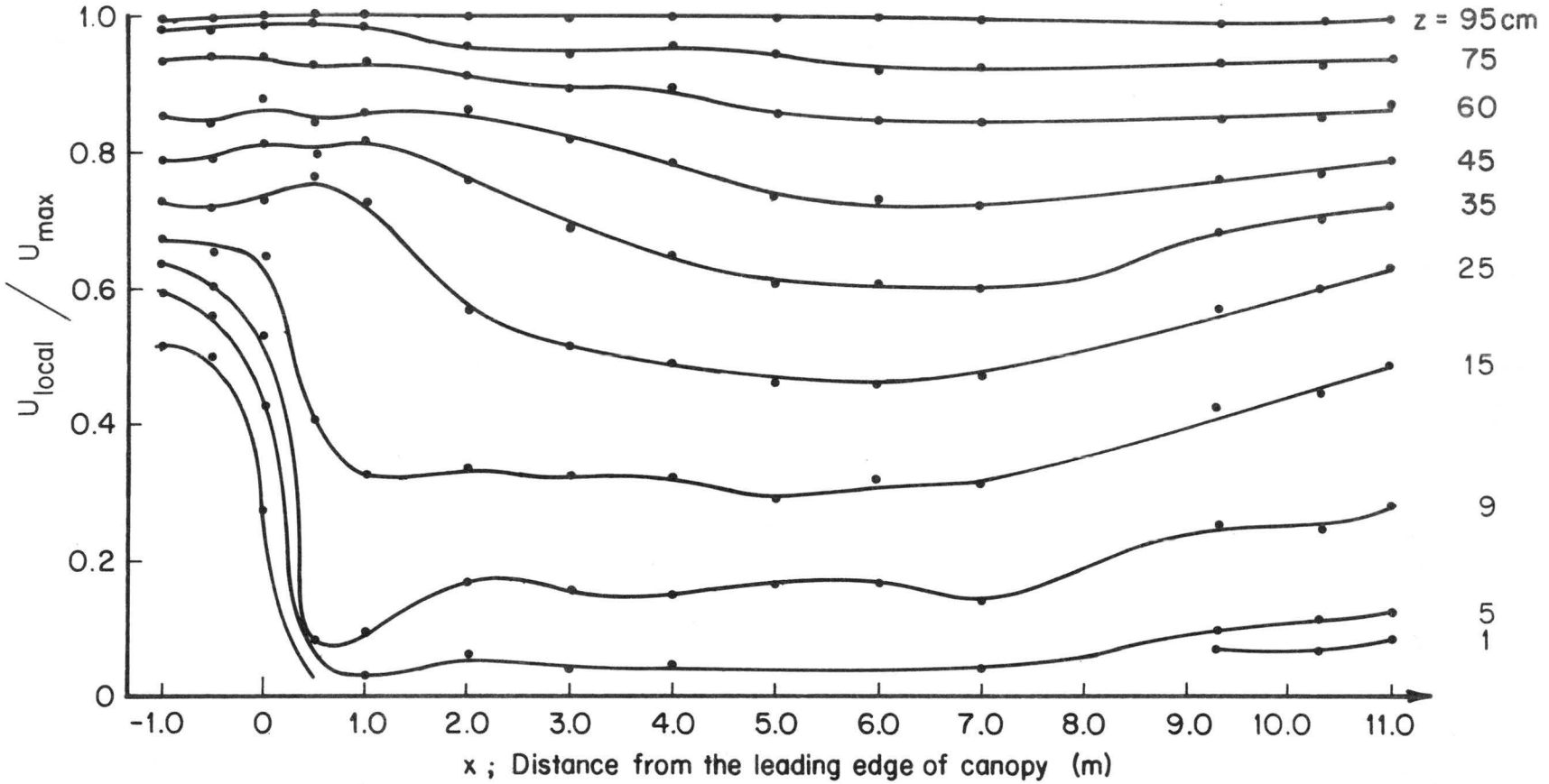

Fig. 3. Non-dimensional isoheight of the flow along the canopy (1.27 x 1.27 cm diag.)

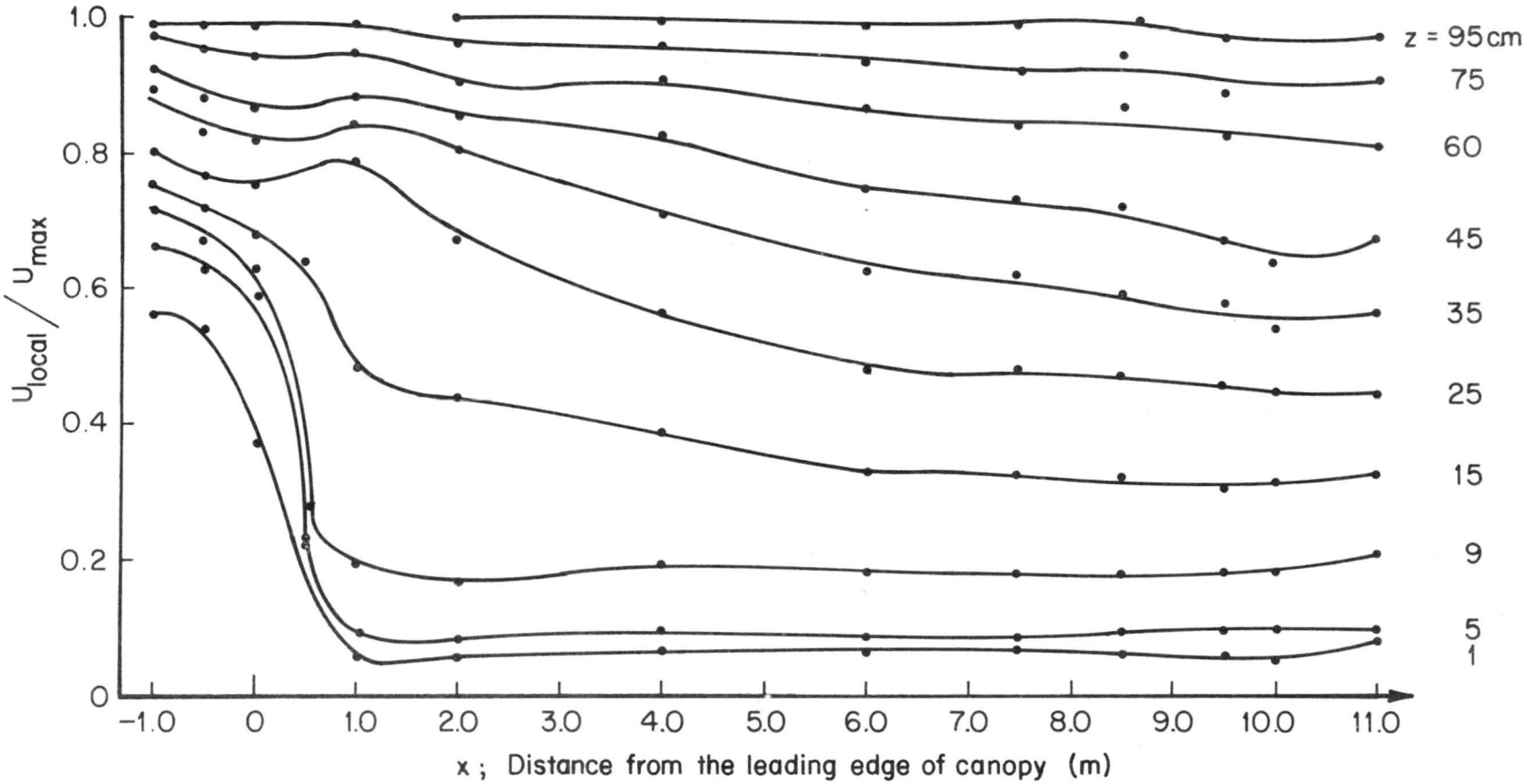

Fig. 4. Non-dimensional isoheight of the flow along the canopy (2.54 x 2.54 cm sq.)

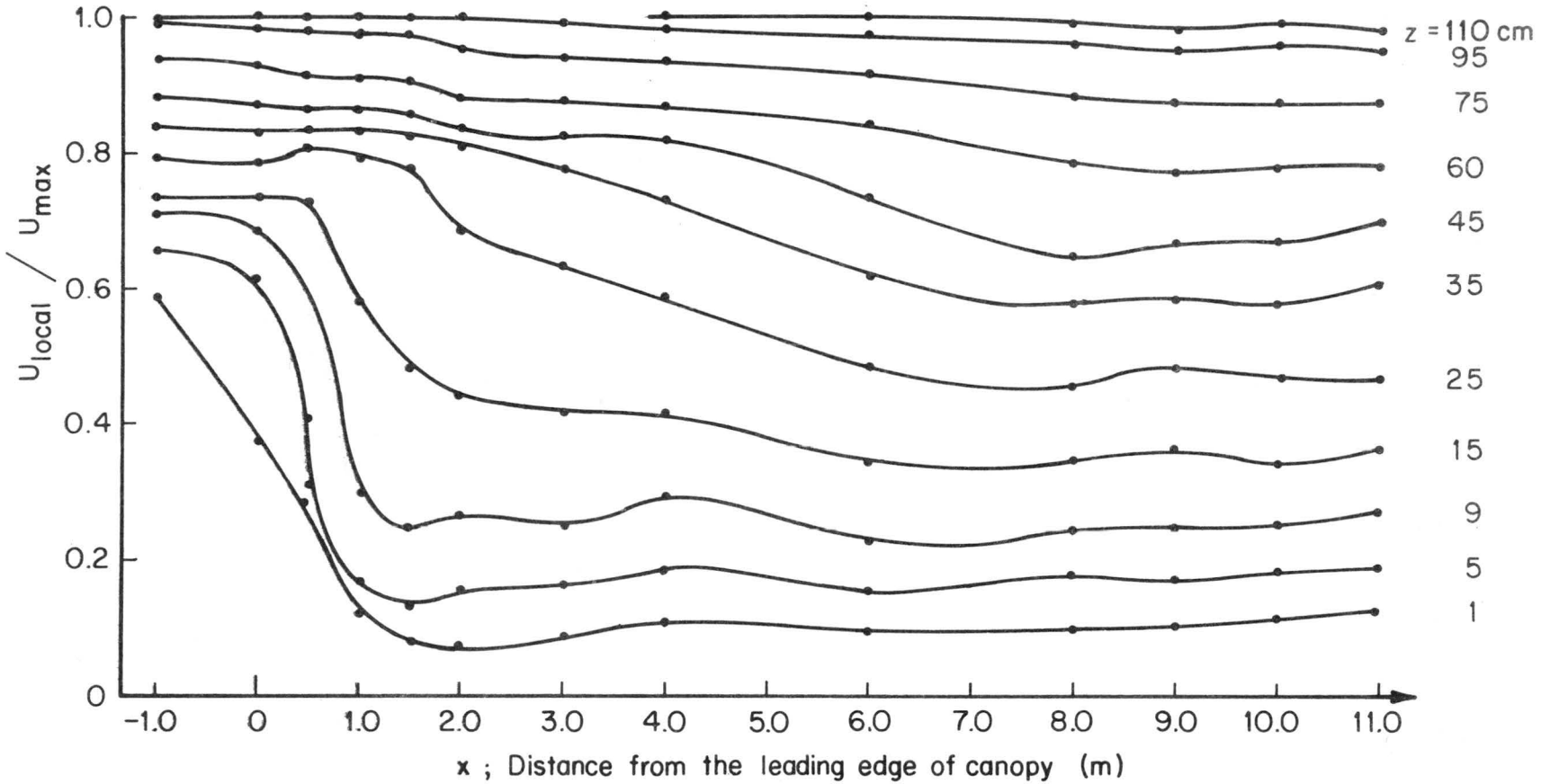

Fig. 5. Non-dimensional isoheight of the flow along the canopy (2.54 x 2.54 cm diag.)

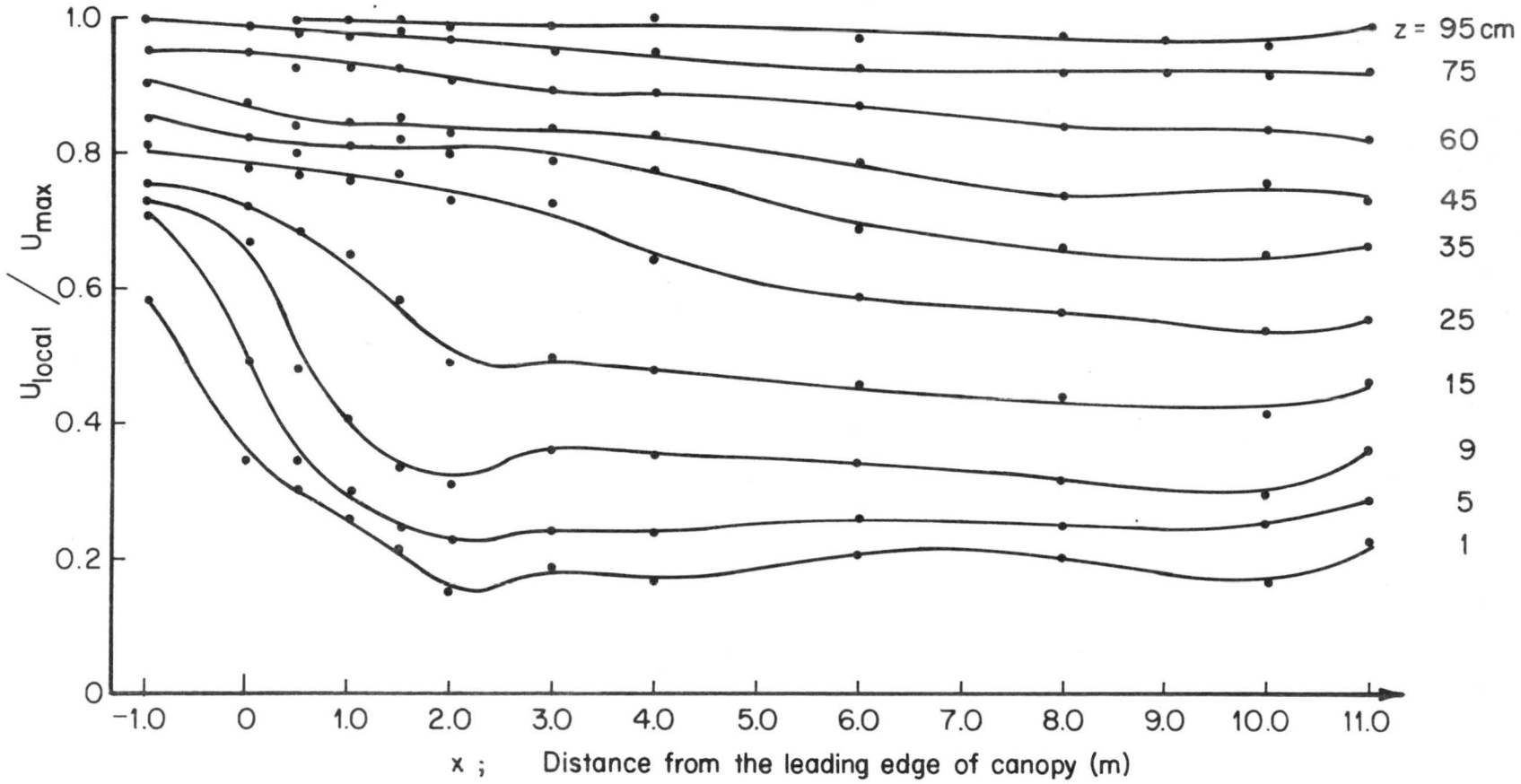

Fig. 6. Non-dimensional isoheight of the flow along the canopy (5.08 x 5.08 cm sq.)

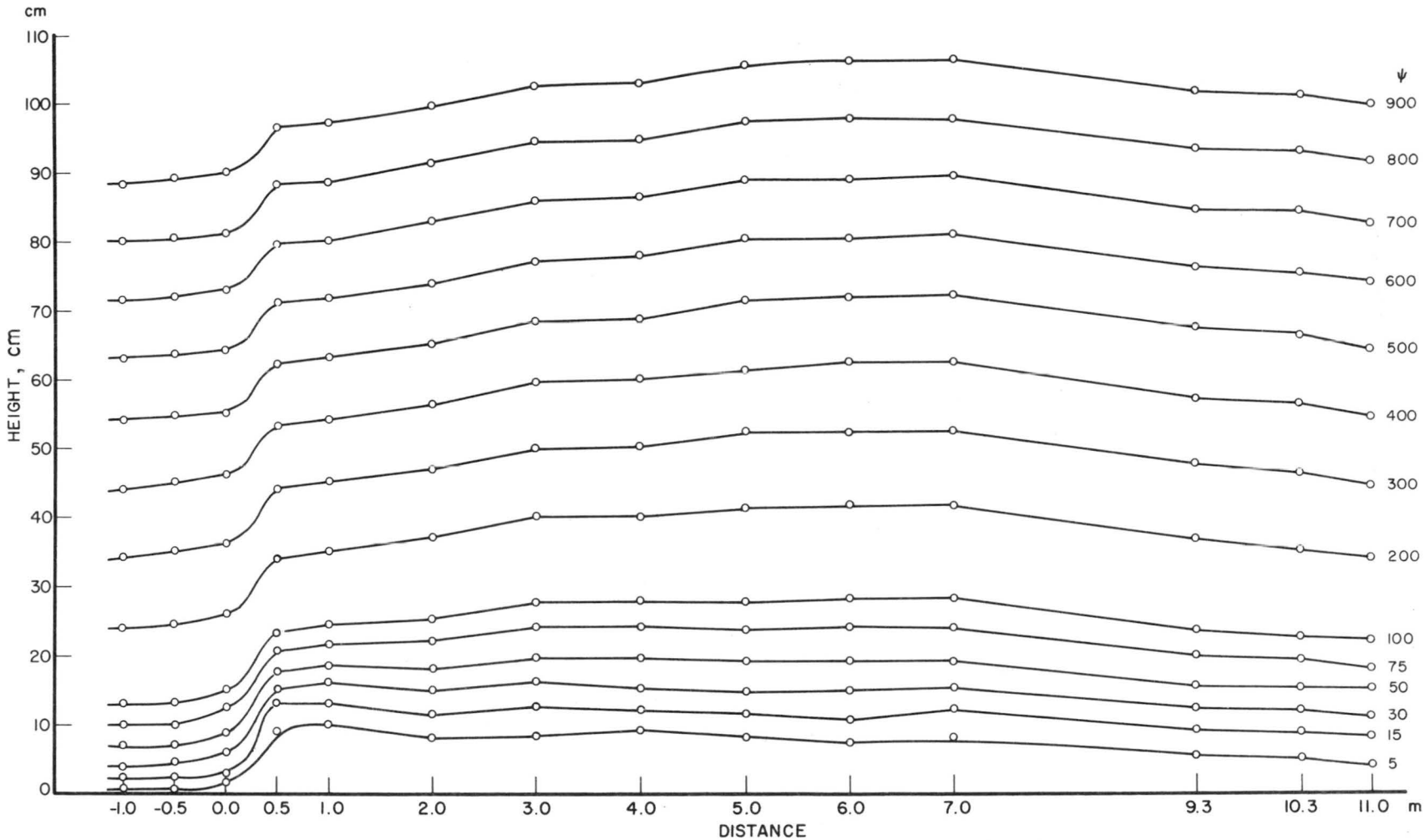

Fig. 7. Streamlines above and within the canopy (1.27 x 1.27 cm diag.)

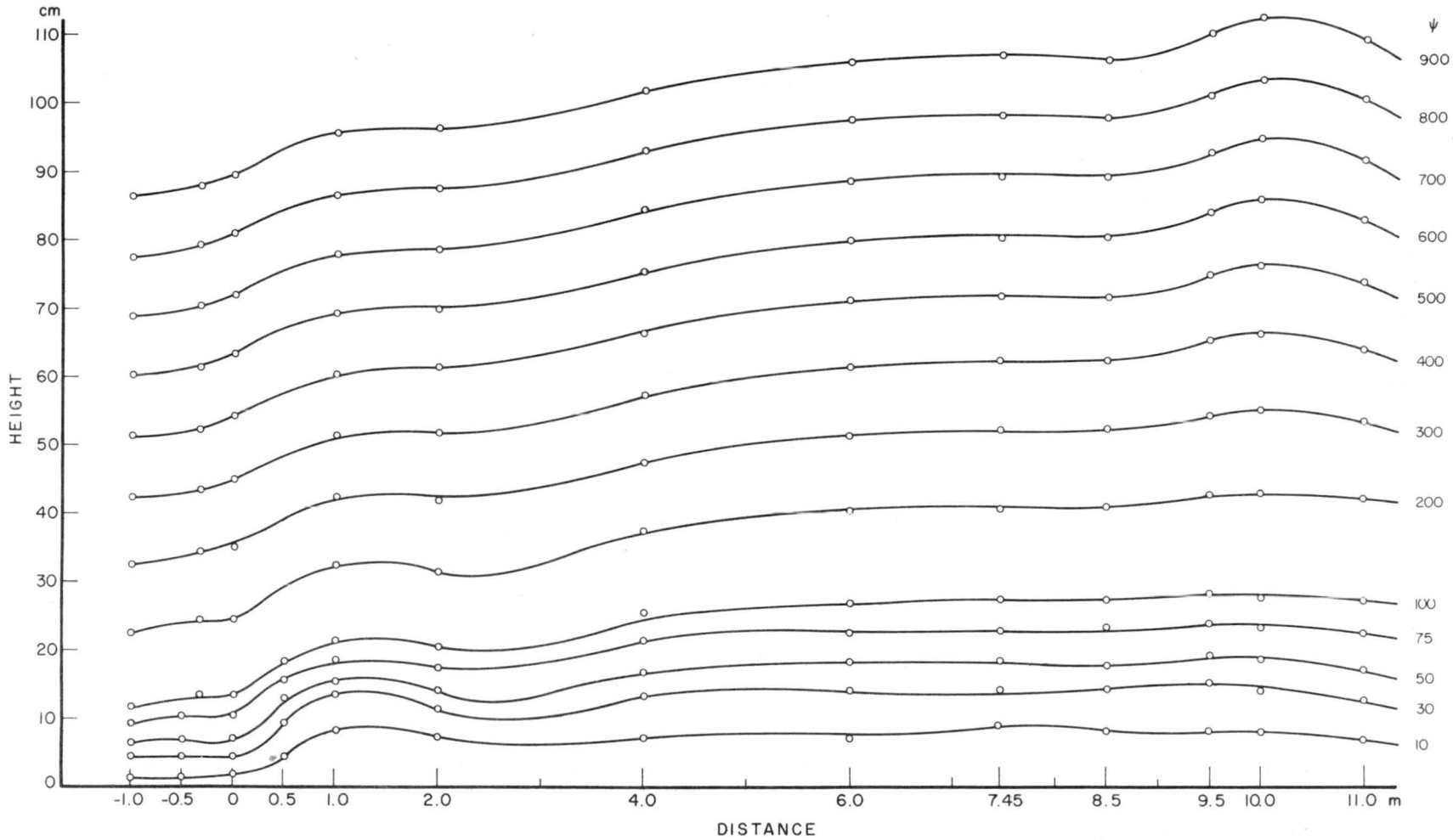

Fig. 8. Streamlines above and within the canopy (2.54 x 2.54 cm sq)

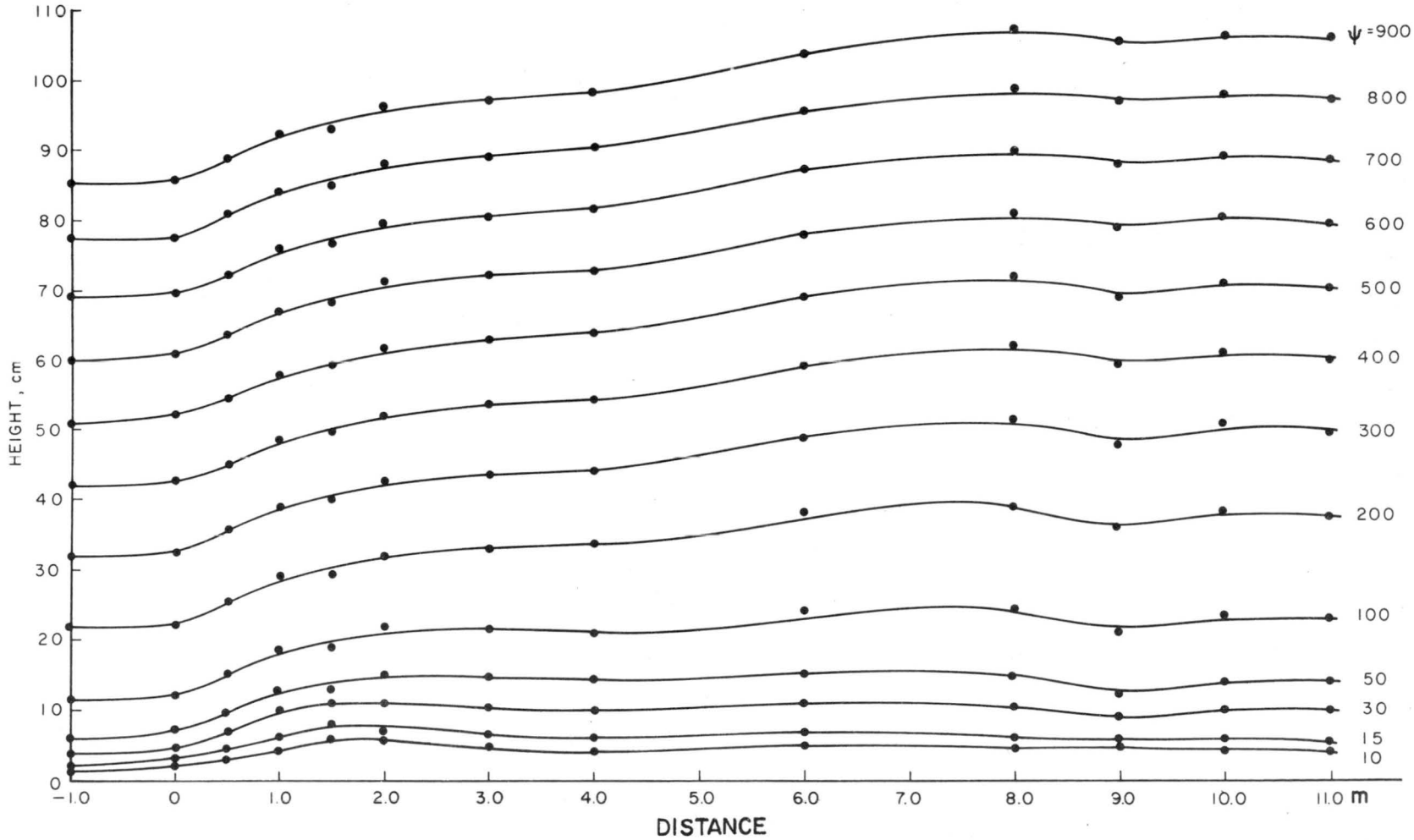

Fig. 9. Streamlines above and within the canopy (2.54 x 2.54 cm diag.)

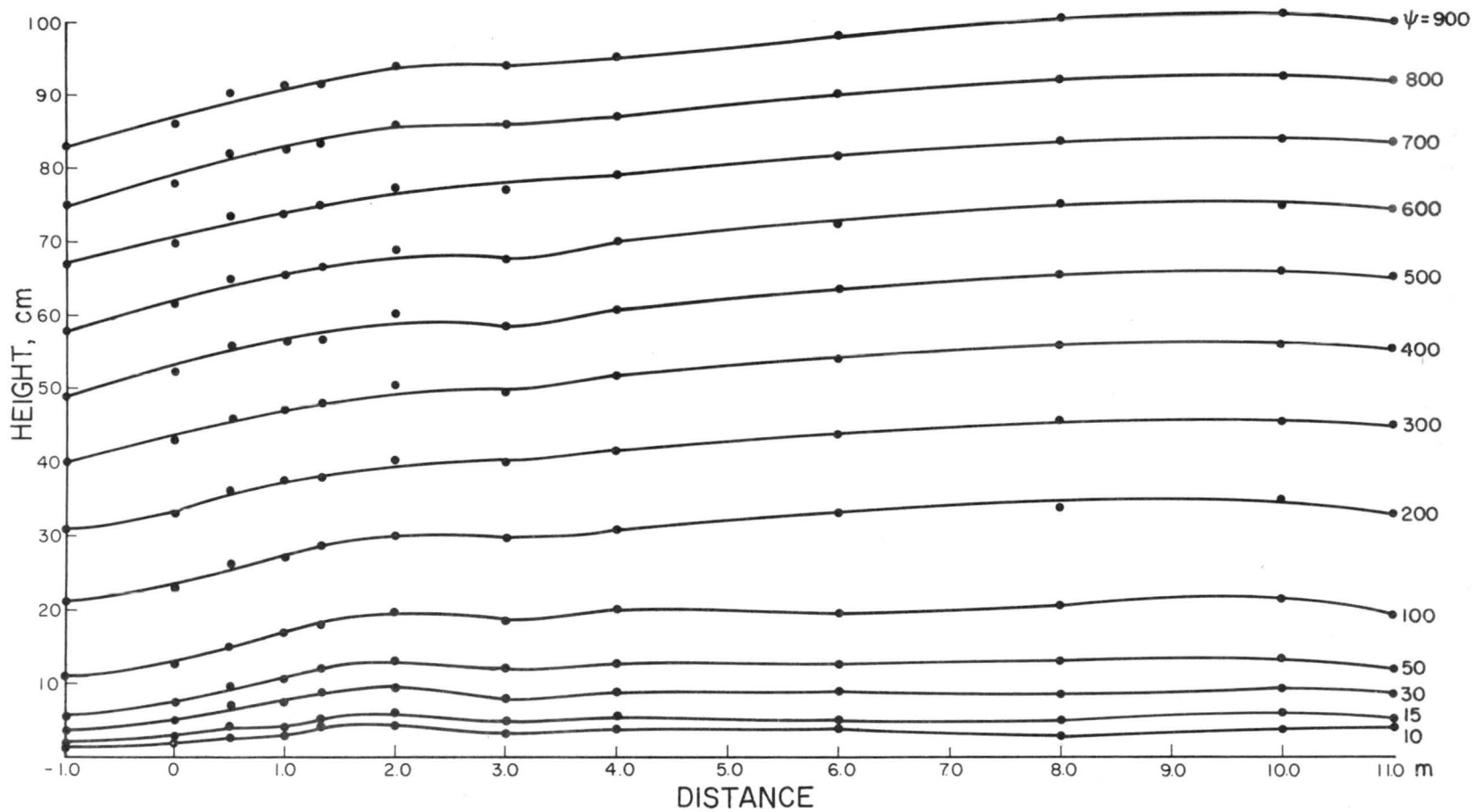

Fig. 10. Streamlines above and within the canopy (5.08 x 5.08 cm sq.)

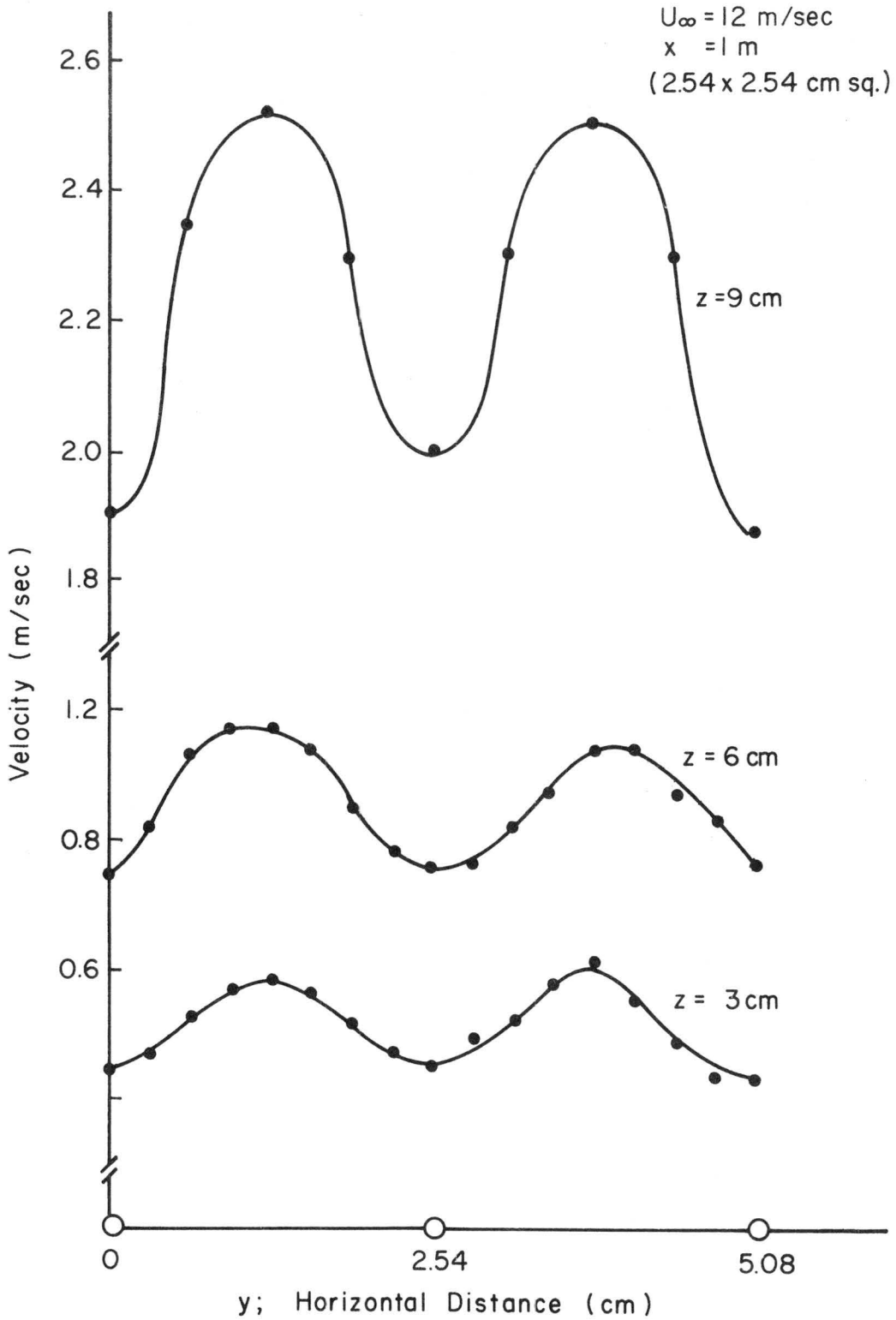

Fig. 11. Horizontal velocity distribution within canopy (2.54 x 2.54 cm sq)

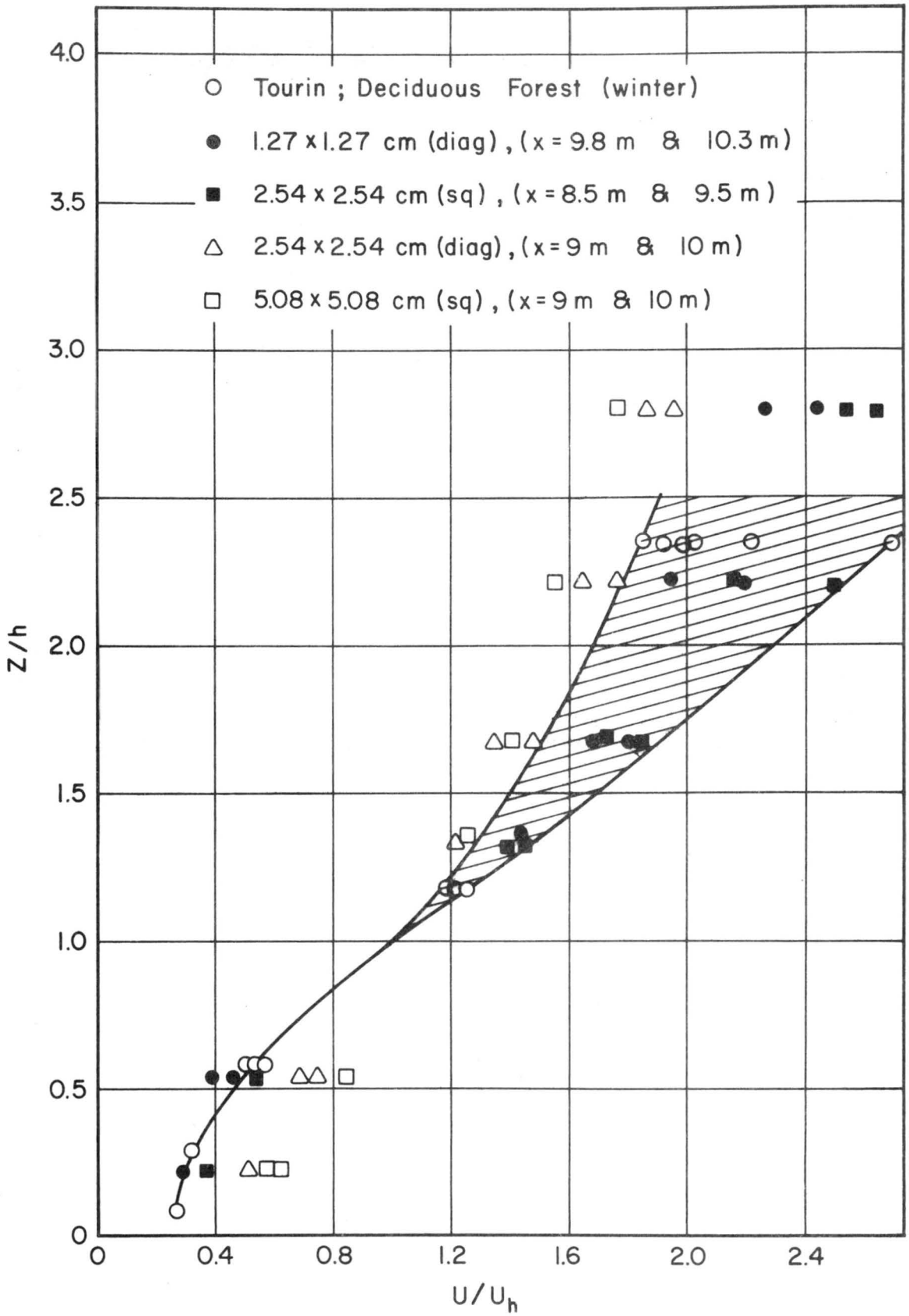

Fig. 12. Comparison of the wind tunnel data of velocity profiles with field data

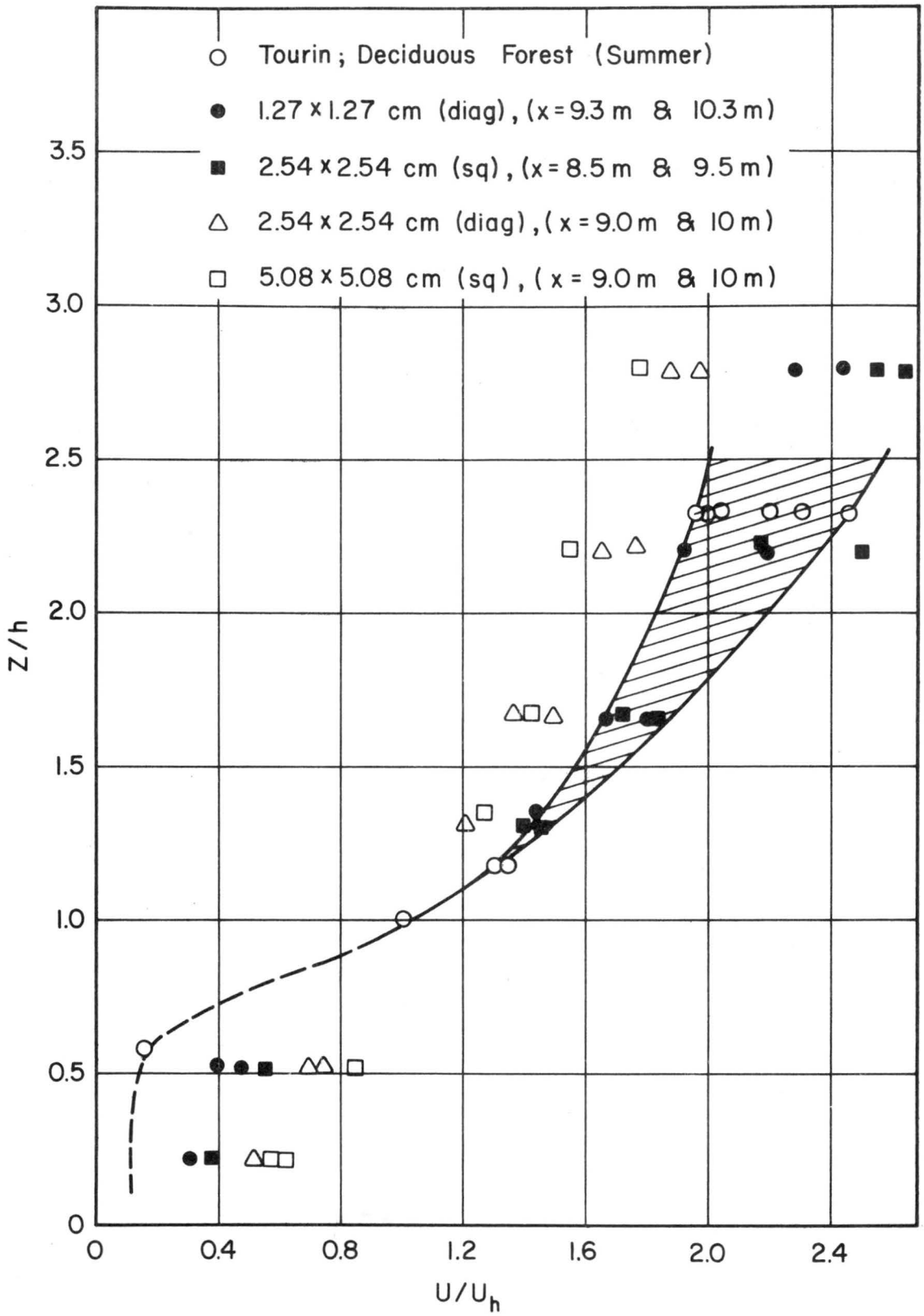

Fig. 13. Comparison of the wind tunnel data of velocity profiles with field data

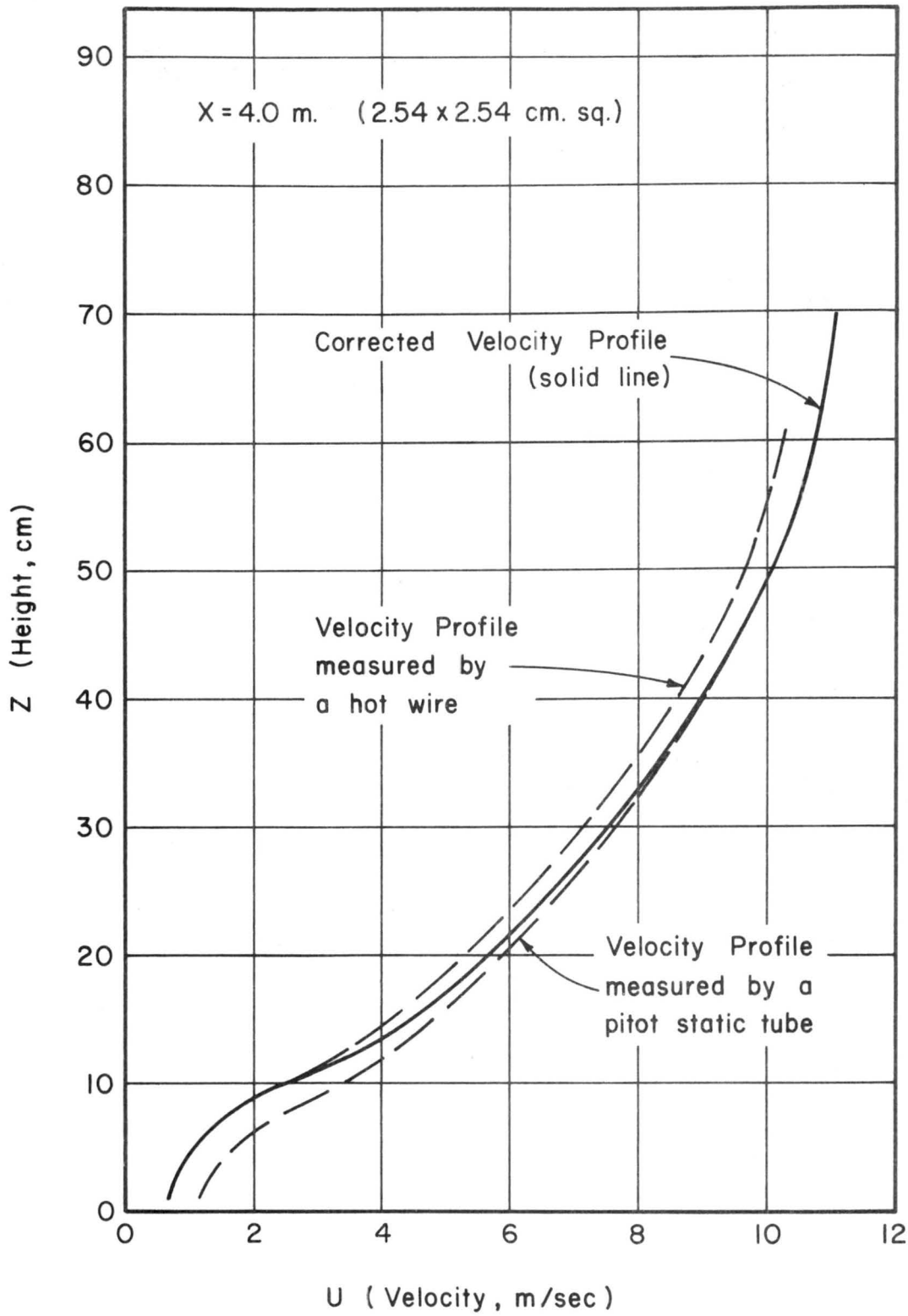

Fig. 14. Corrected velocity profile

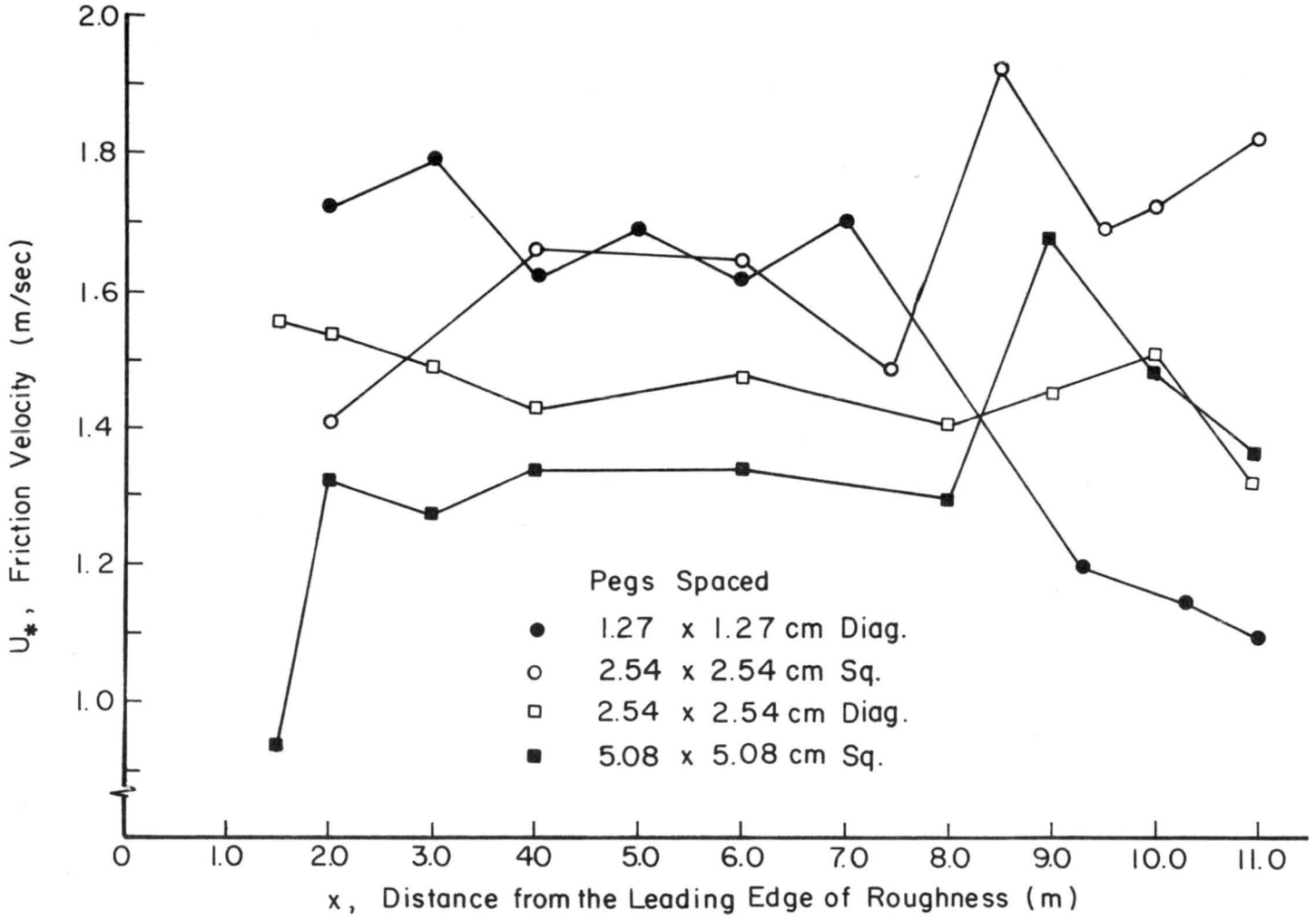

Fig. 15. Friction velocity U_* calculated from above canopy velocity profiles

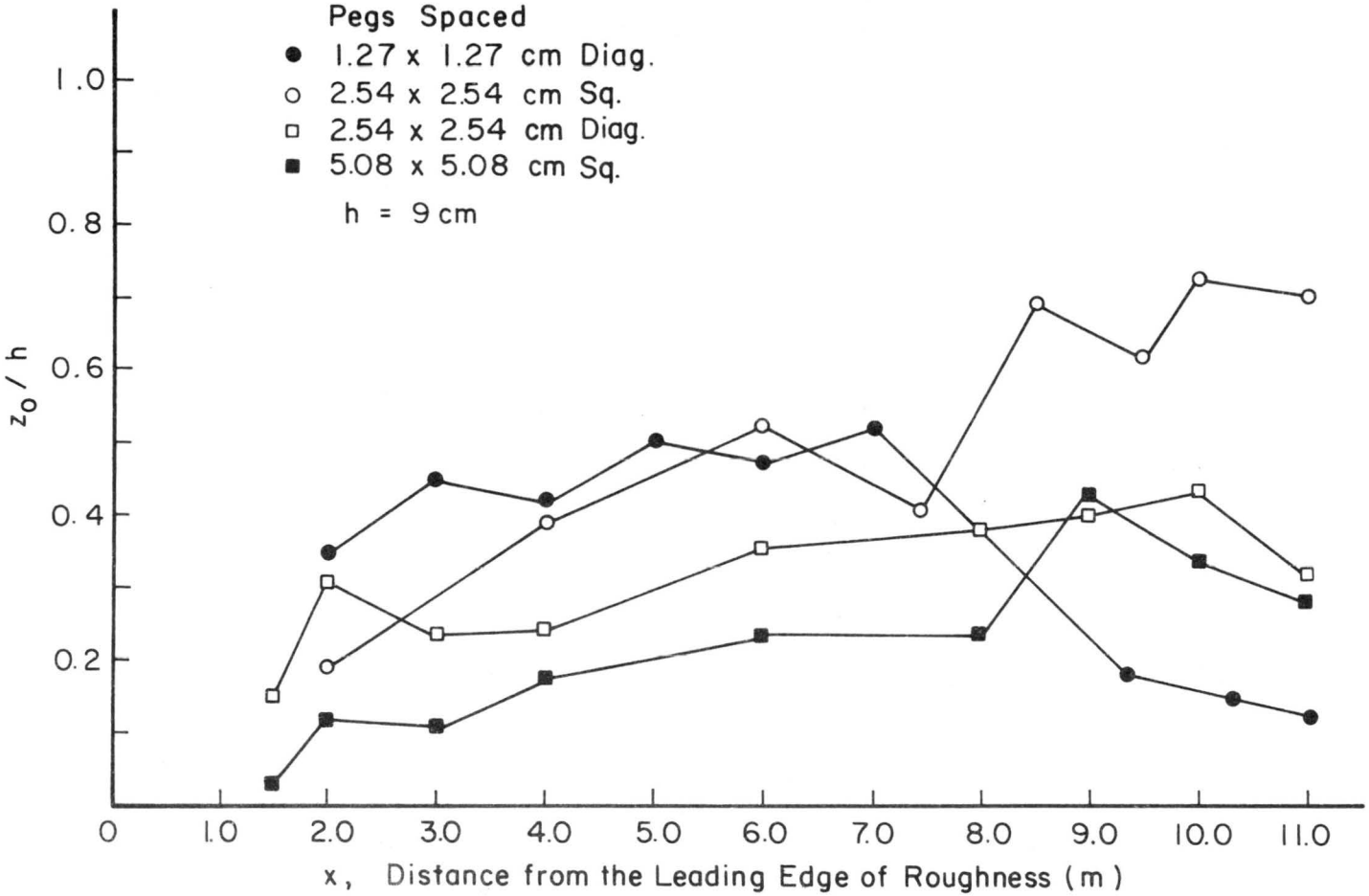

Fig. 16. Roughness length Z_o calculated from above canopy velocity profiles

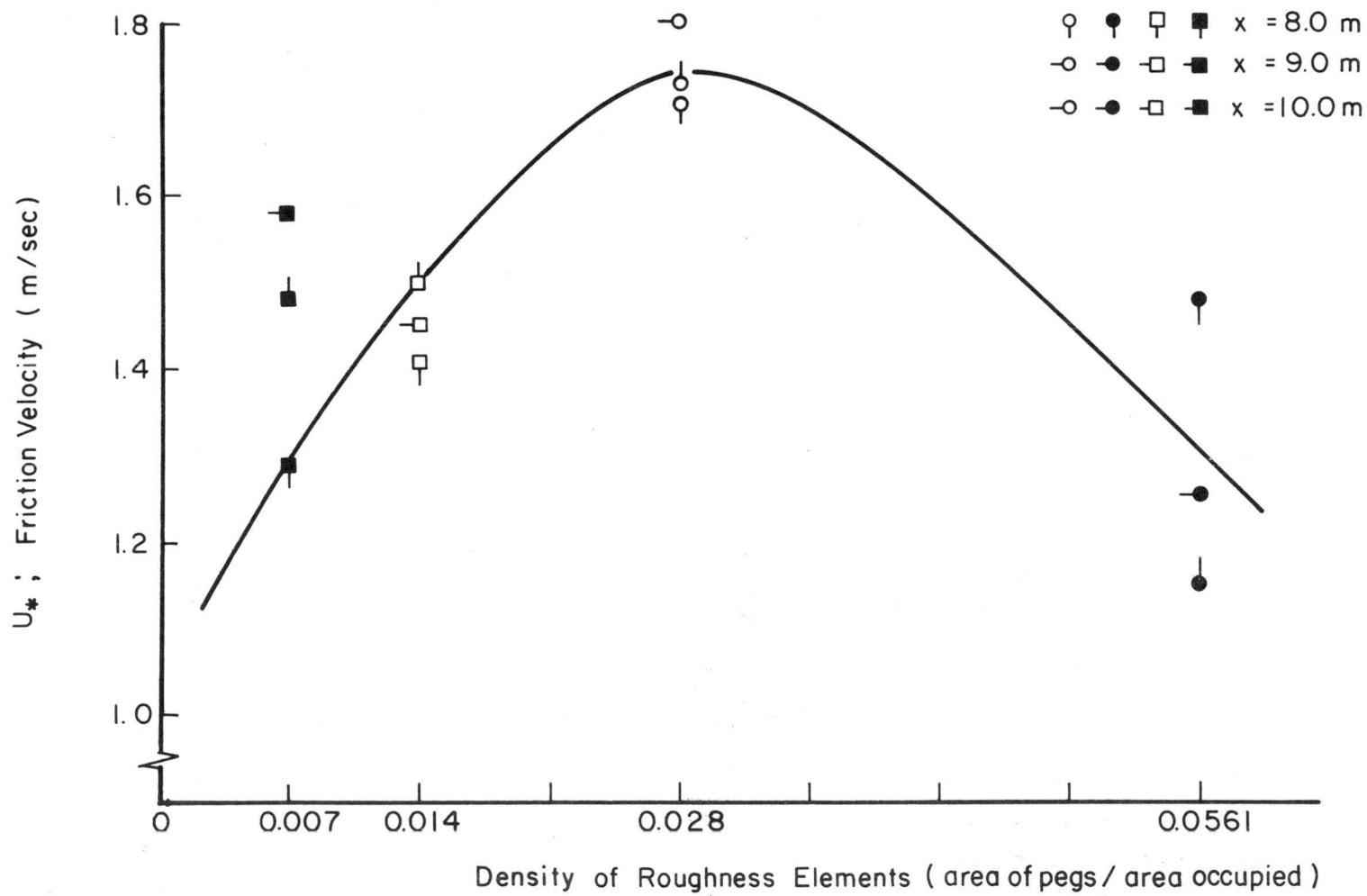

Fig. 17. Friction velocity U_* vs density of roughness elements

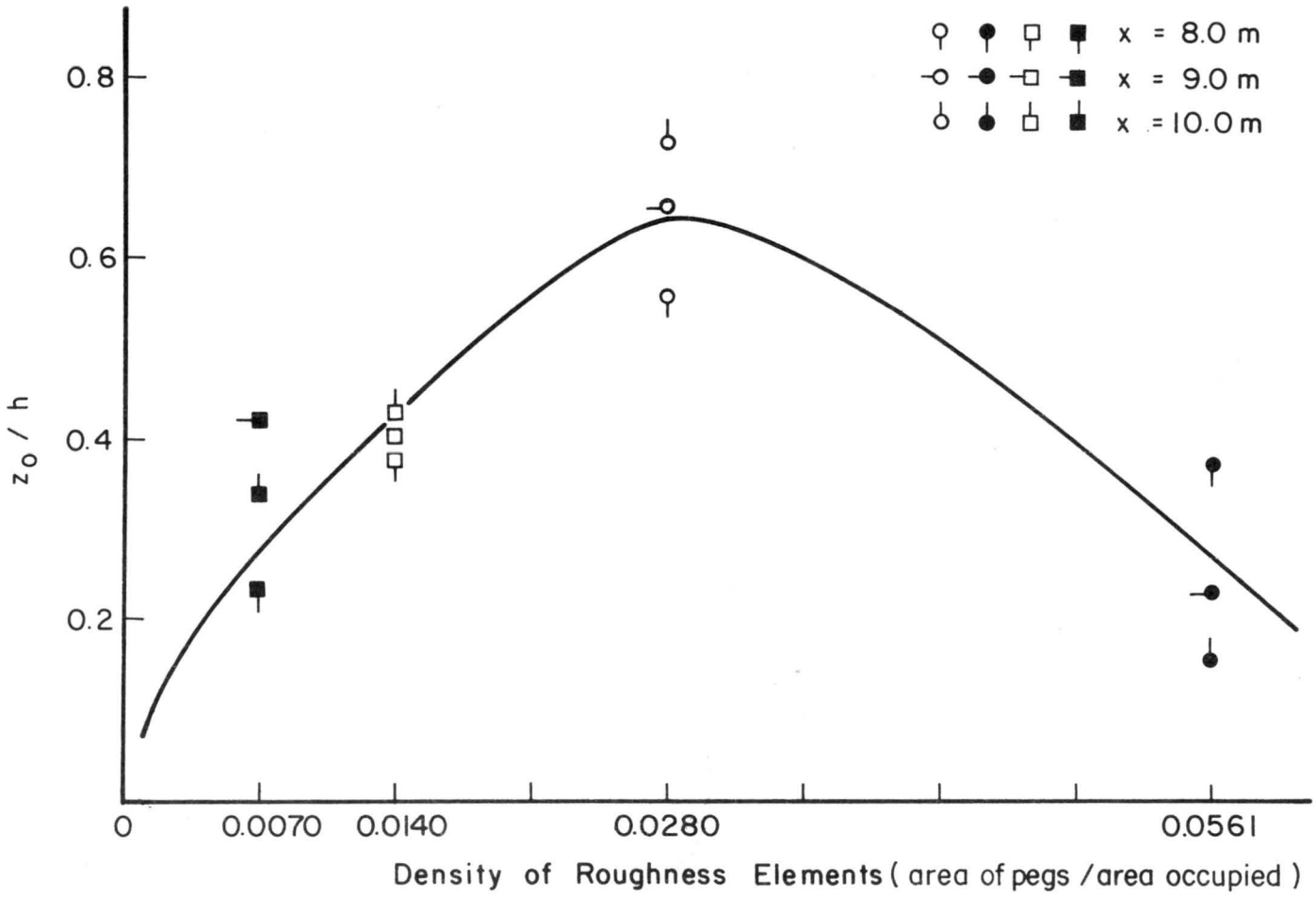

Fig. 18. Roughness length Z_o vs density of roughness elements

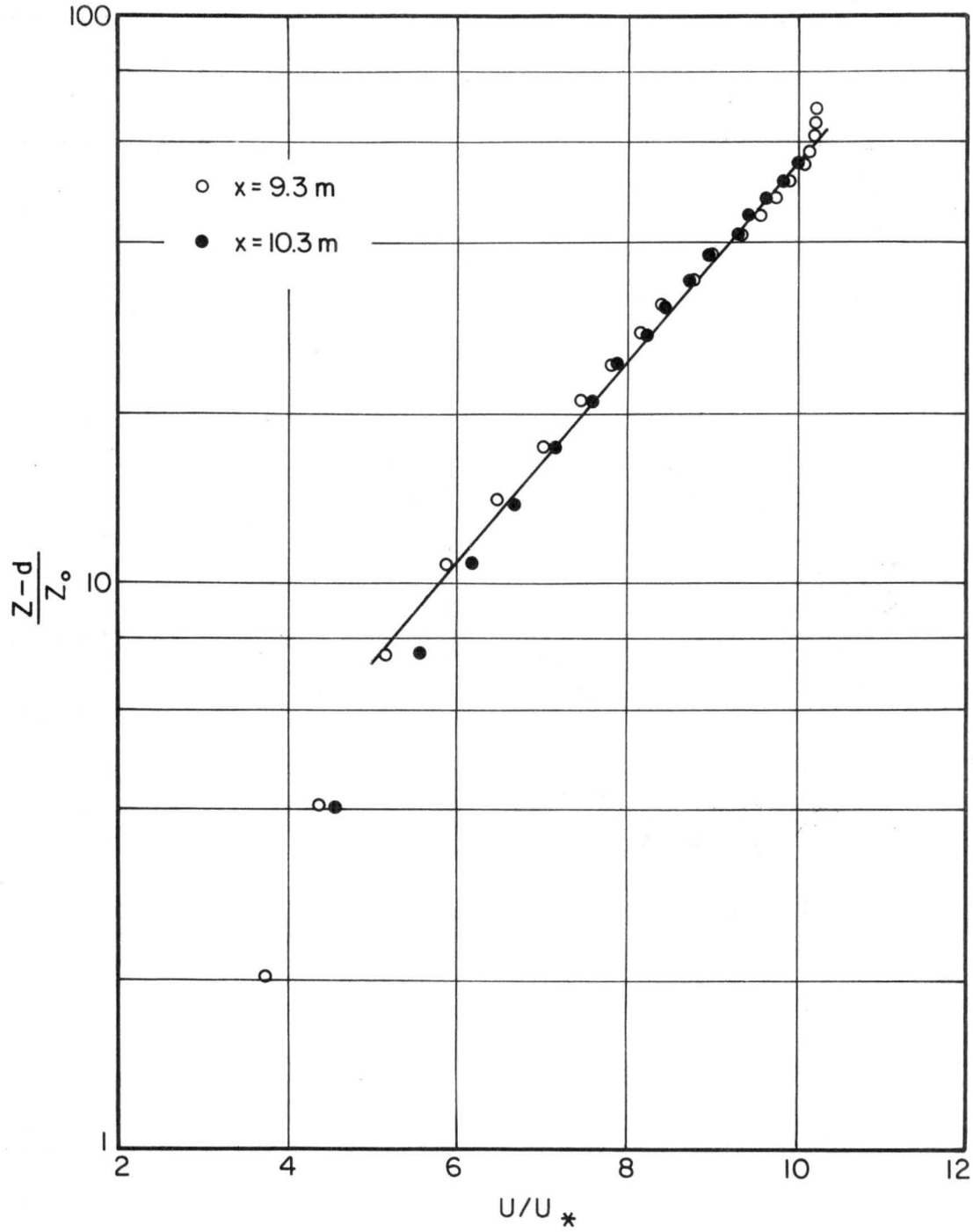

Fig. 19. Mean velocity profile above canopy (1.27 x 1.27 cm diag)

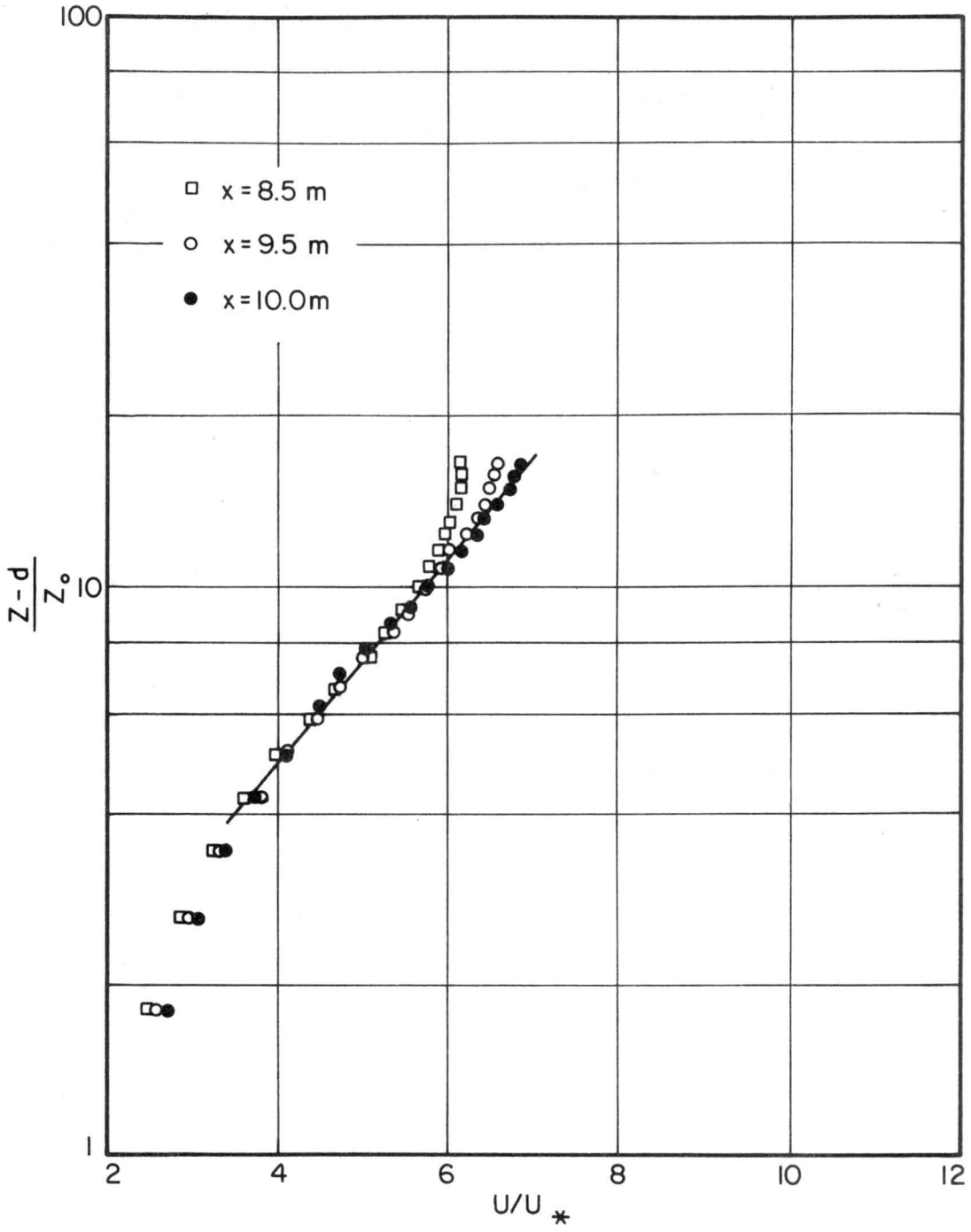

Fig. 20. Mean velocity profile above canopy (2.54 x 2.54 cm sq)

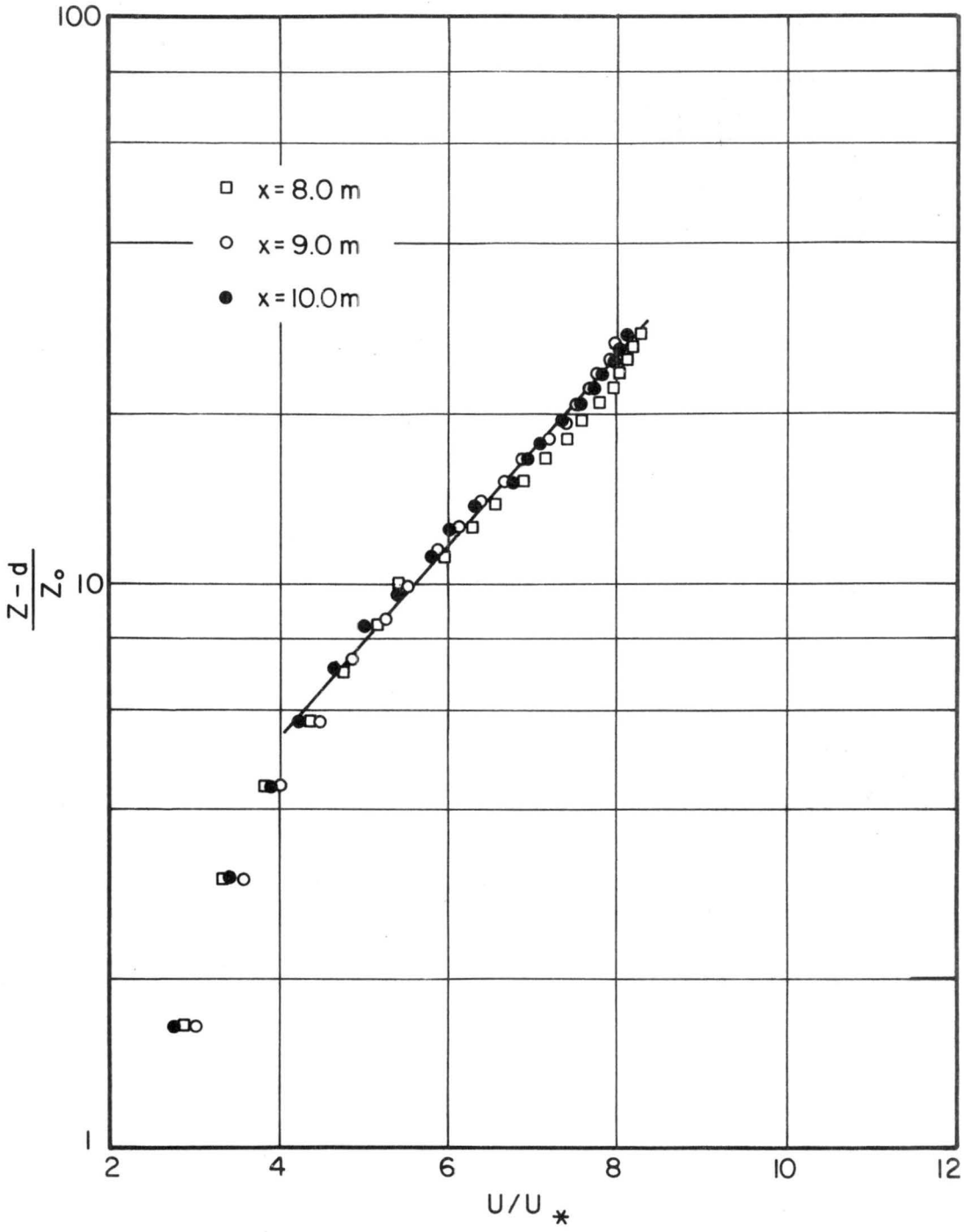

Fig. 21. Mean velocity profile above canopy (2.54 x 2.54 cm diag)

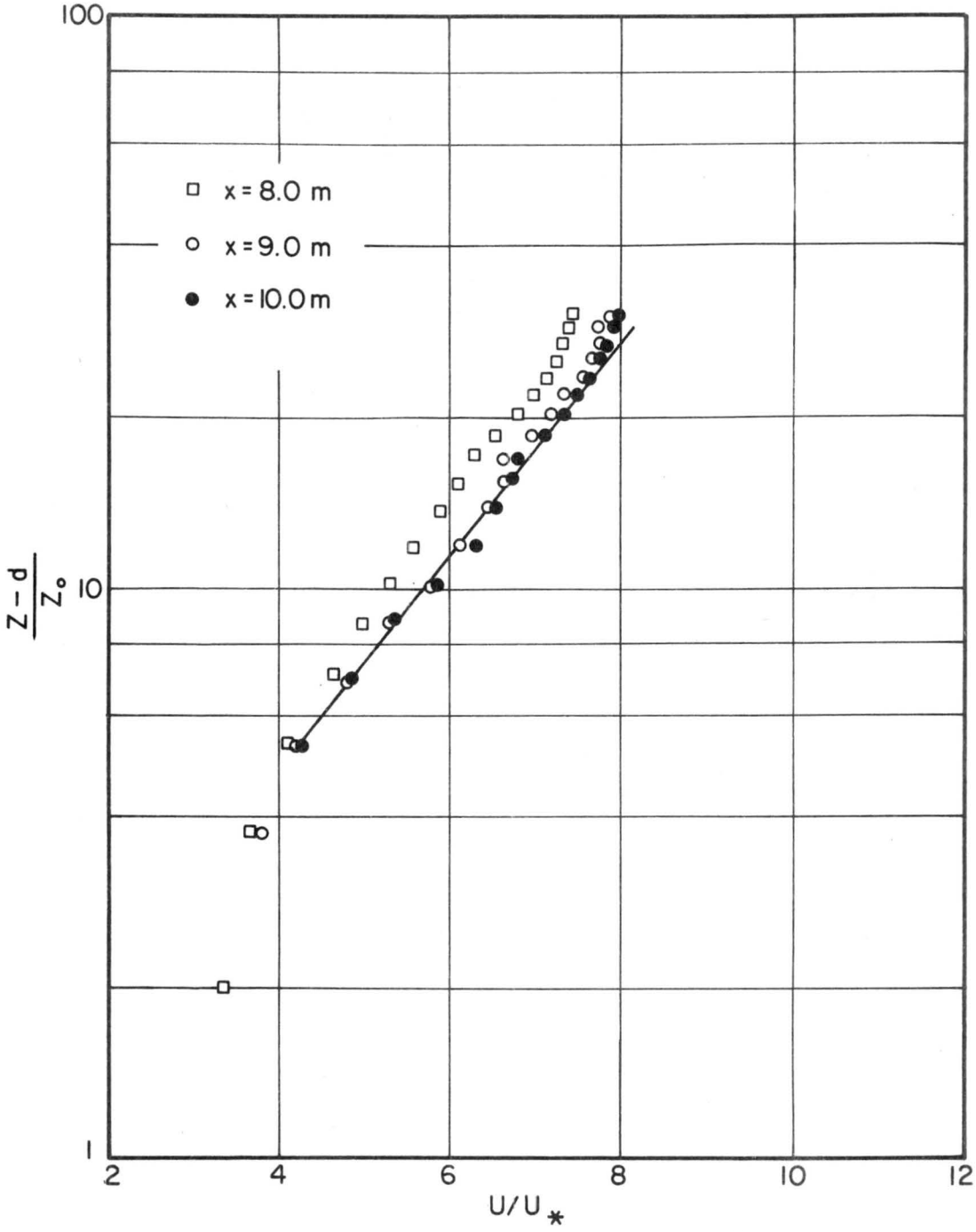

Fig. 22. Mean velocity profile above canopy (5.08 x 5.08 cm sq)

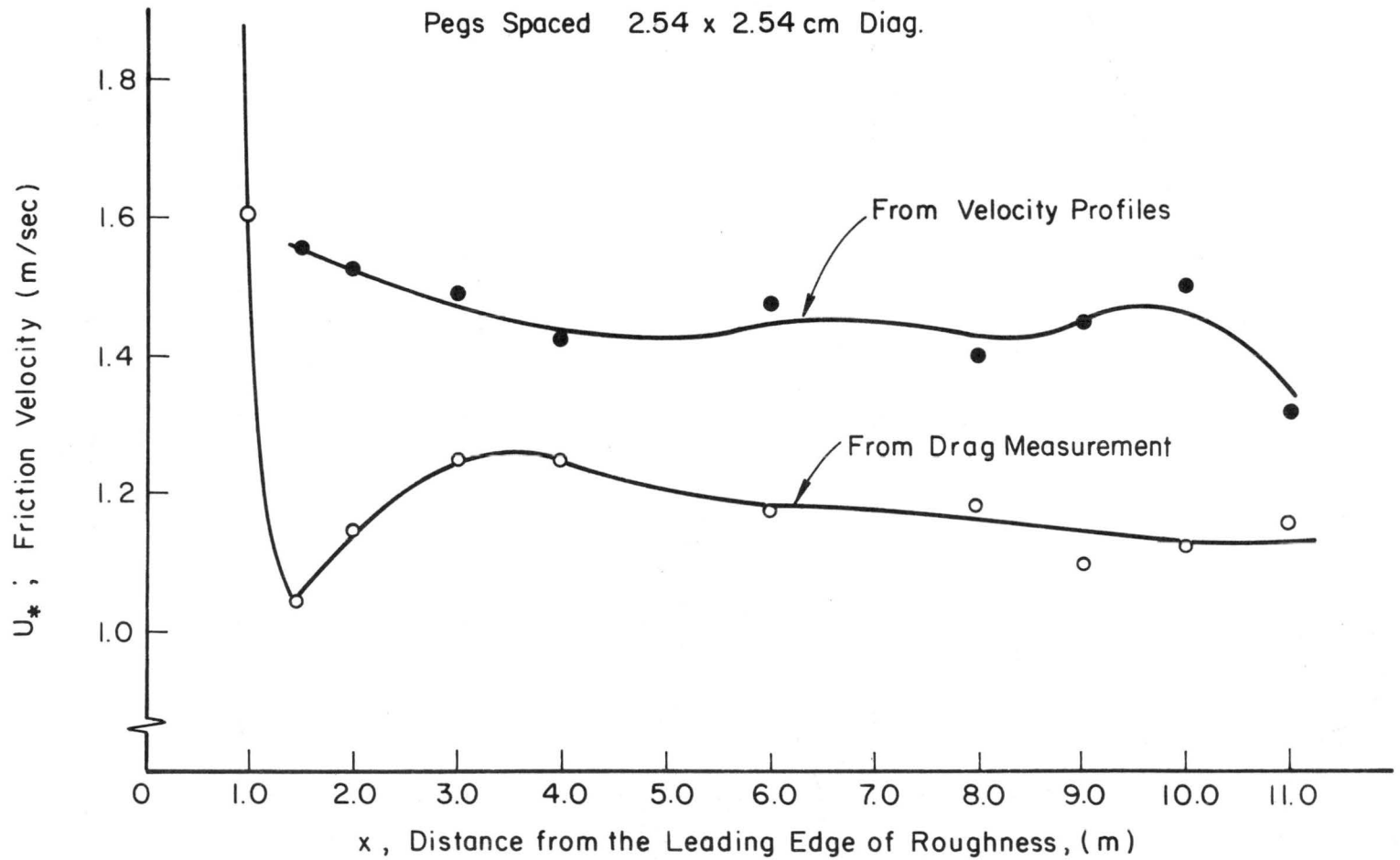

Fig. 23. Comparison of friction velocity obtained from drag measurement with that from velocity profiles (2.54 x 2.54 cm diag)

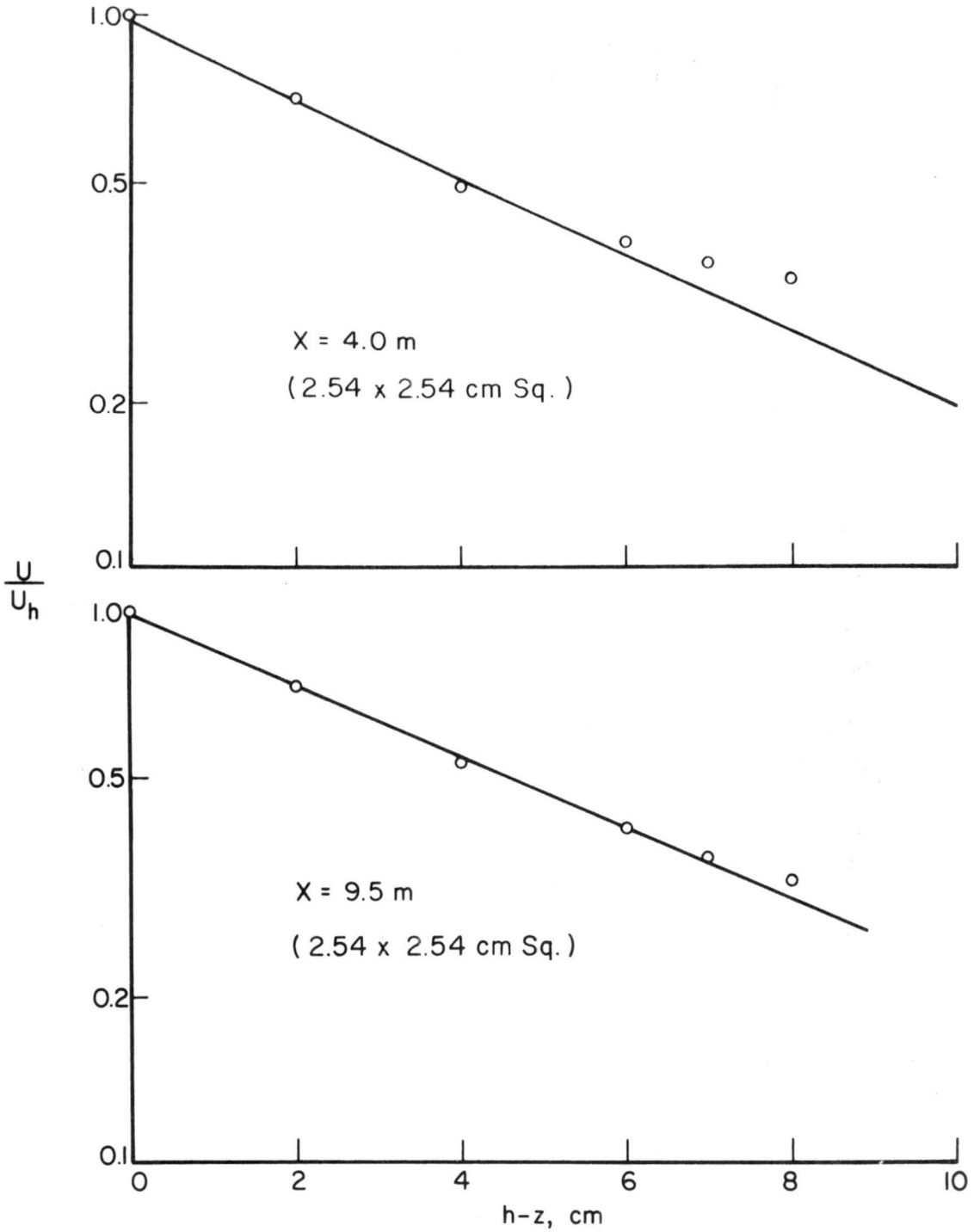

Fig. 24. Velocity profiles within canopy x = 4.0 m and 9.5 m (2.54 x 2.54 cm sq)

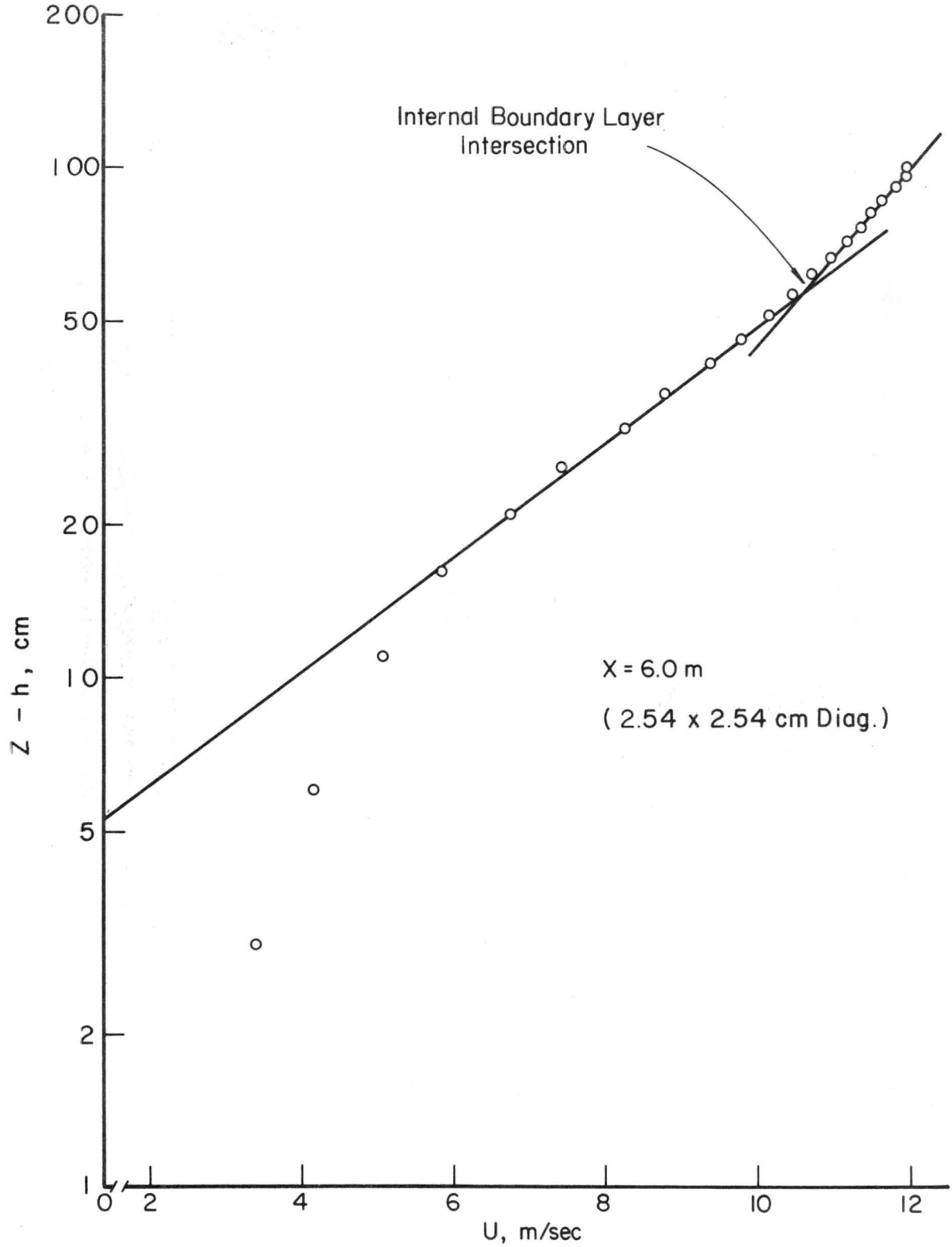

Fig. 25. Logarithmic velocity profile (inner boundary layer intersection)

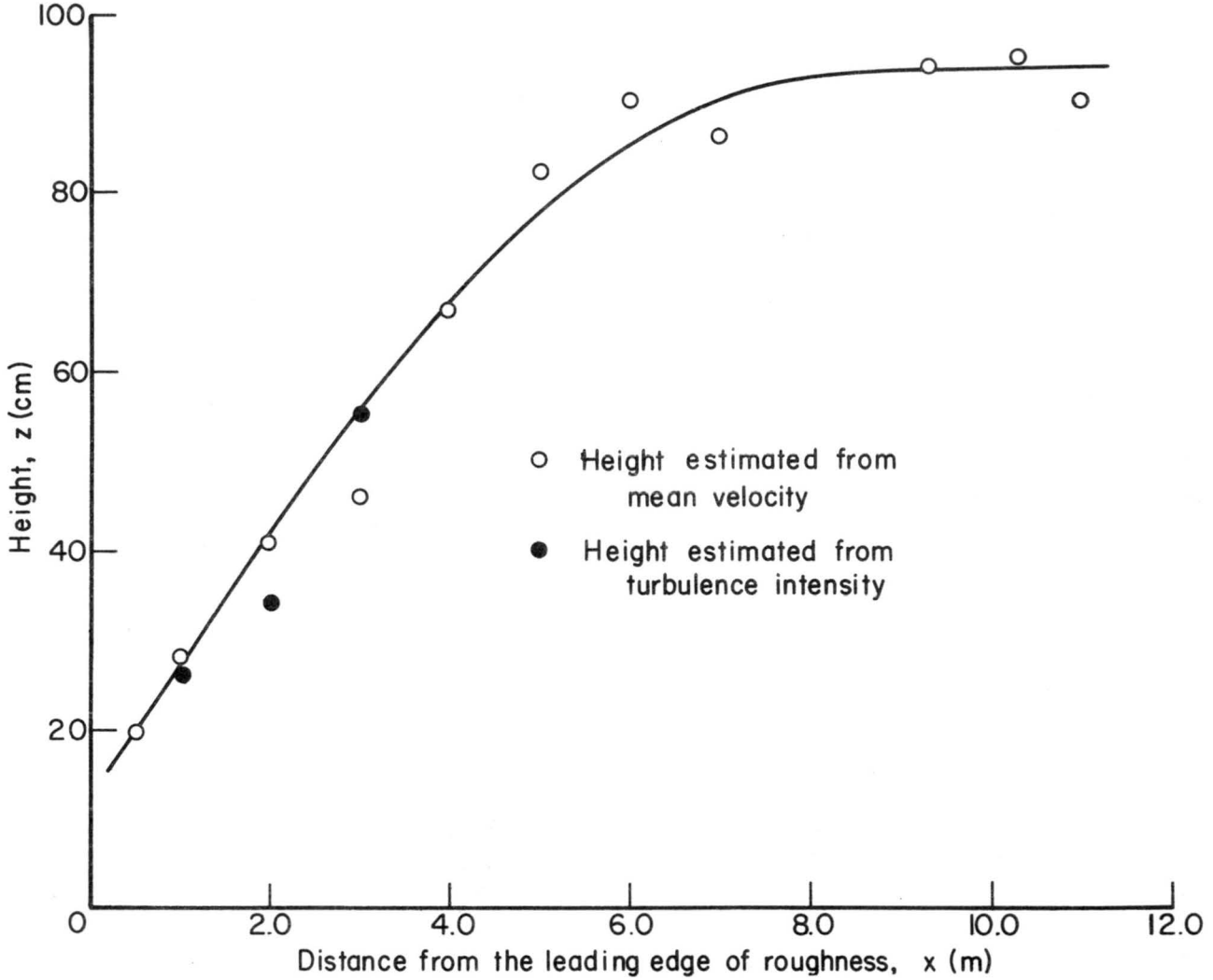

Fig. 26. Height of internal boundary layer (1.27 x 1.27 cm diag)

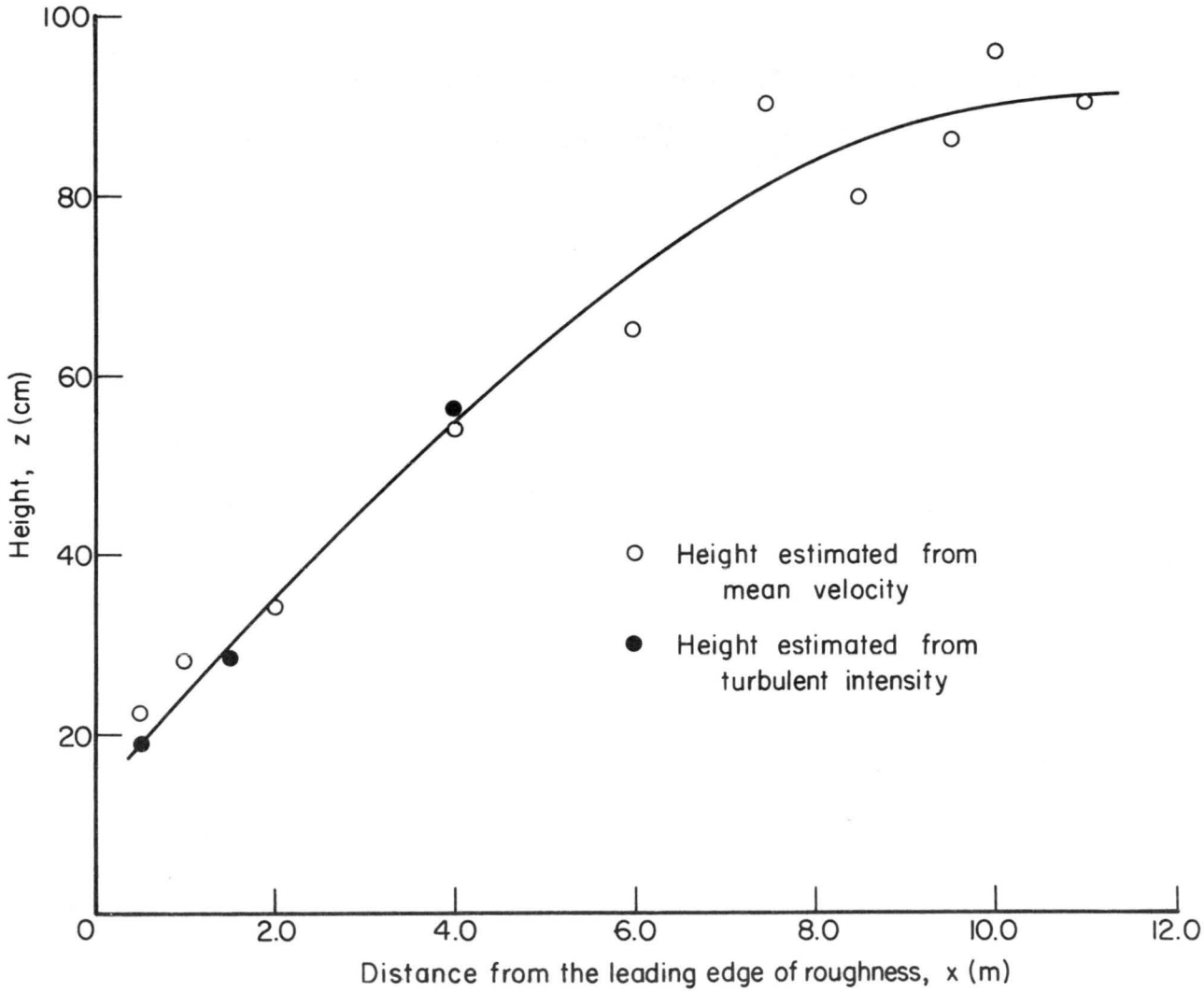

Fig. 27. Height of internal boundary layer (2.54 x 2.54 cm sq)

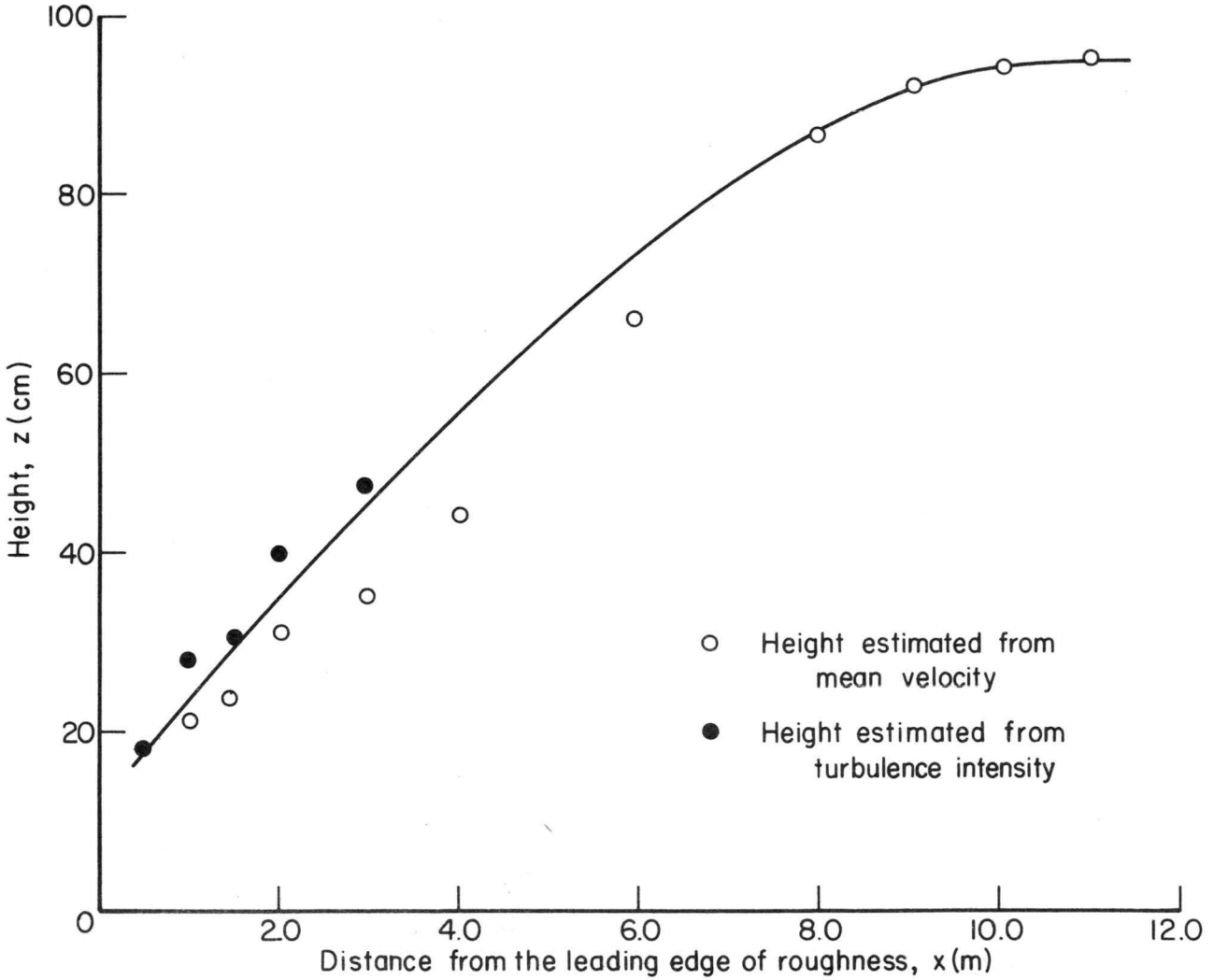

Fig. 28. Height of internal boundary layer (2.54 x 2.54 cm diag)

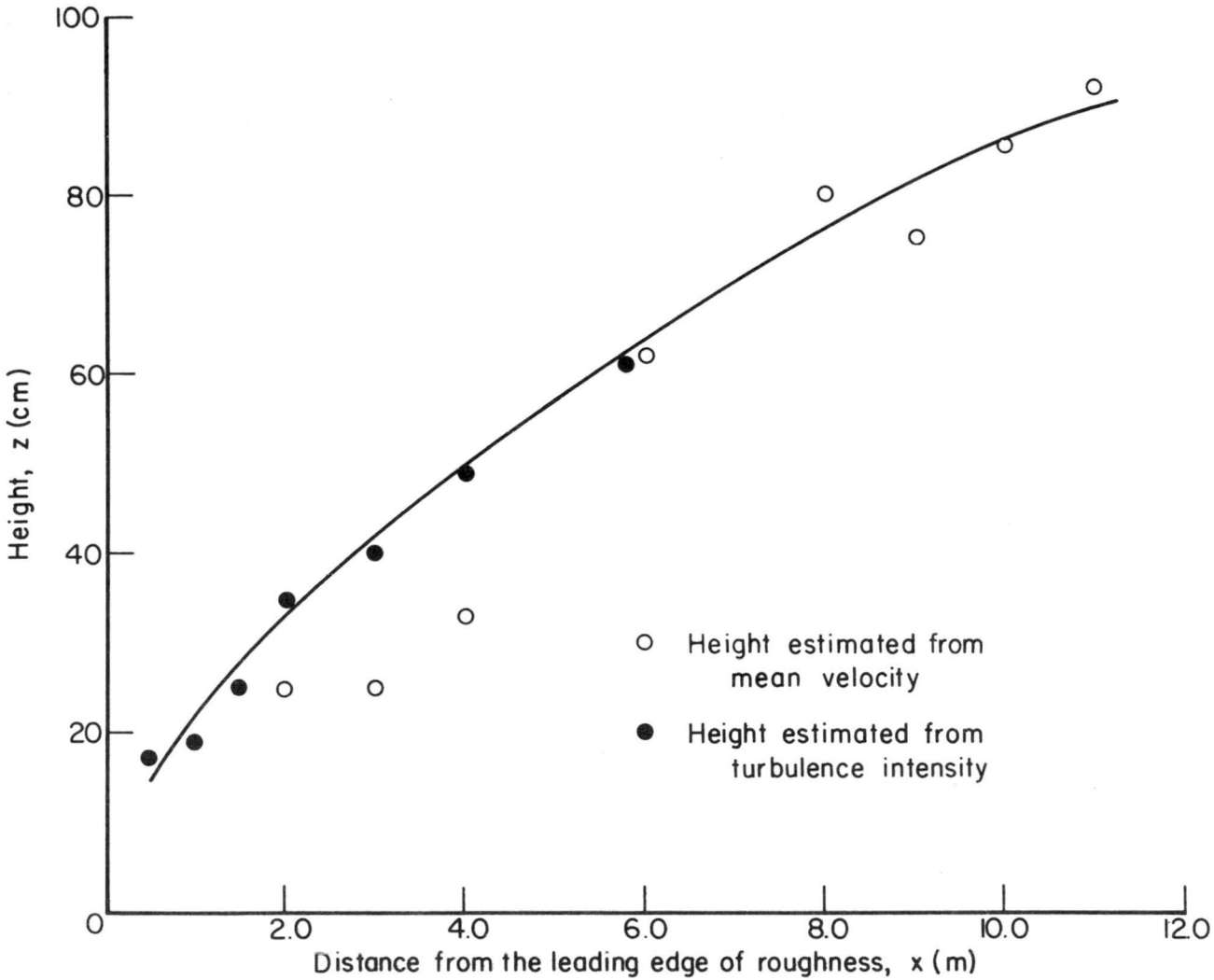

Fig. 29. Height of internal boundary layer (5.08 x 5.08 cm sq)

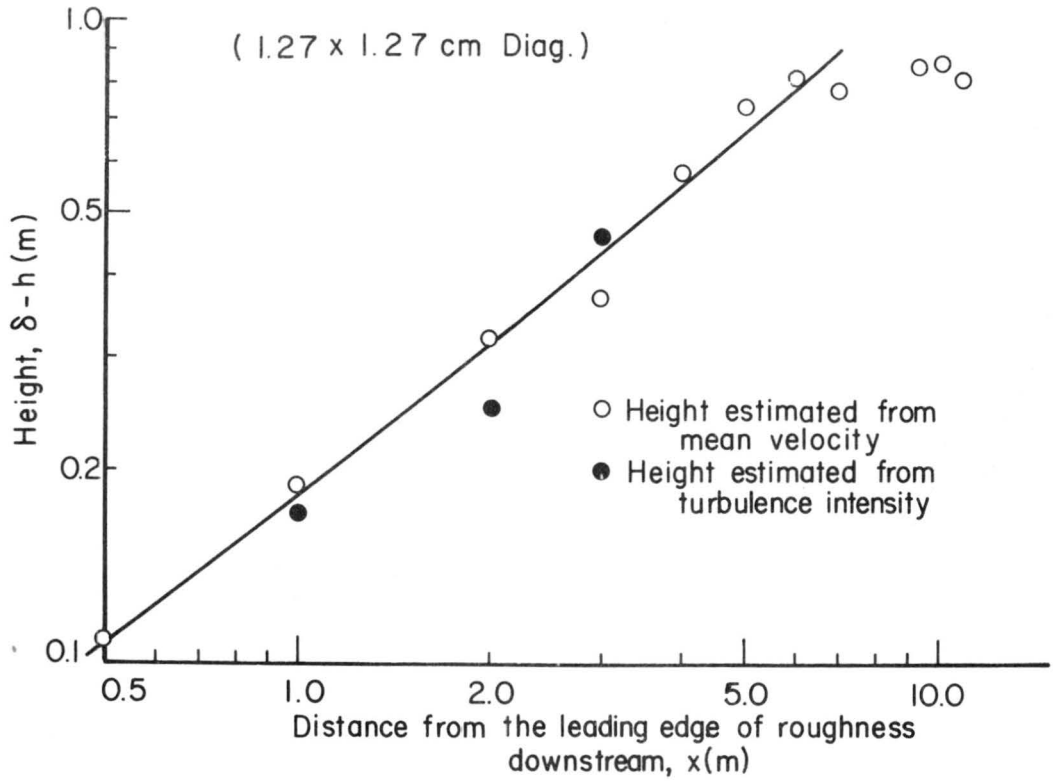

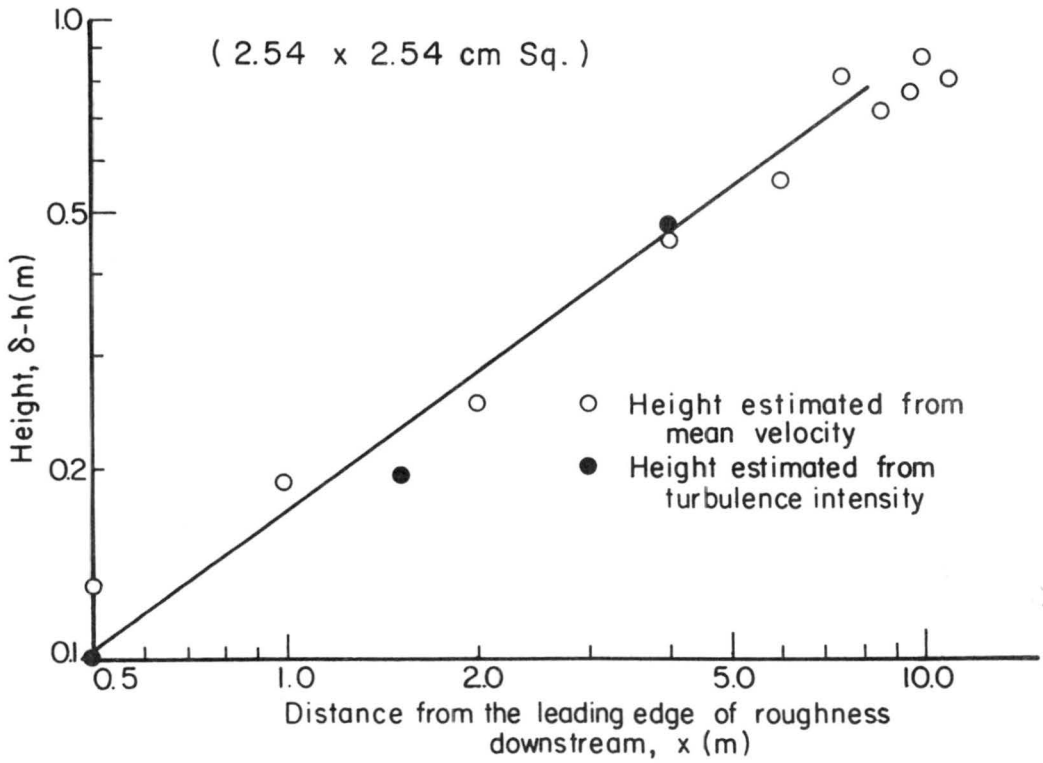

Fig. 30. Height of internal boundary layer
(1.27 x 1.27 cm diag)
(2.54 x 2.54 cm sq)

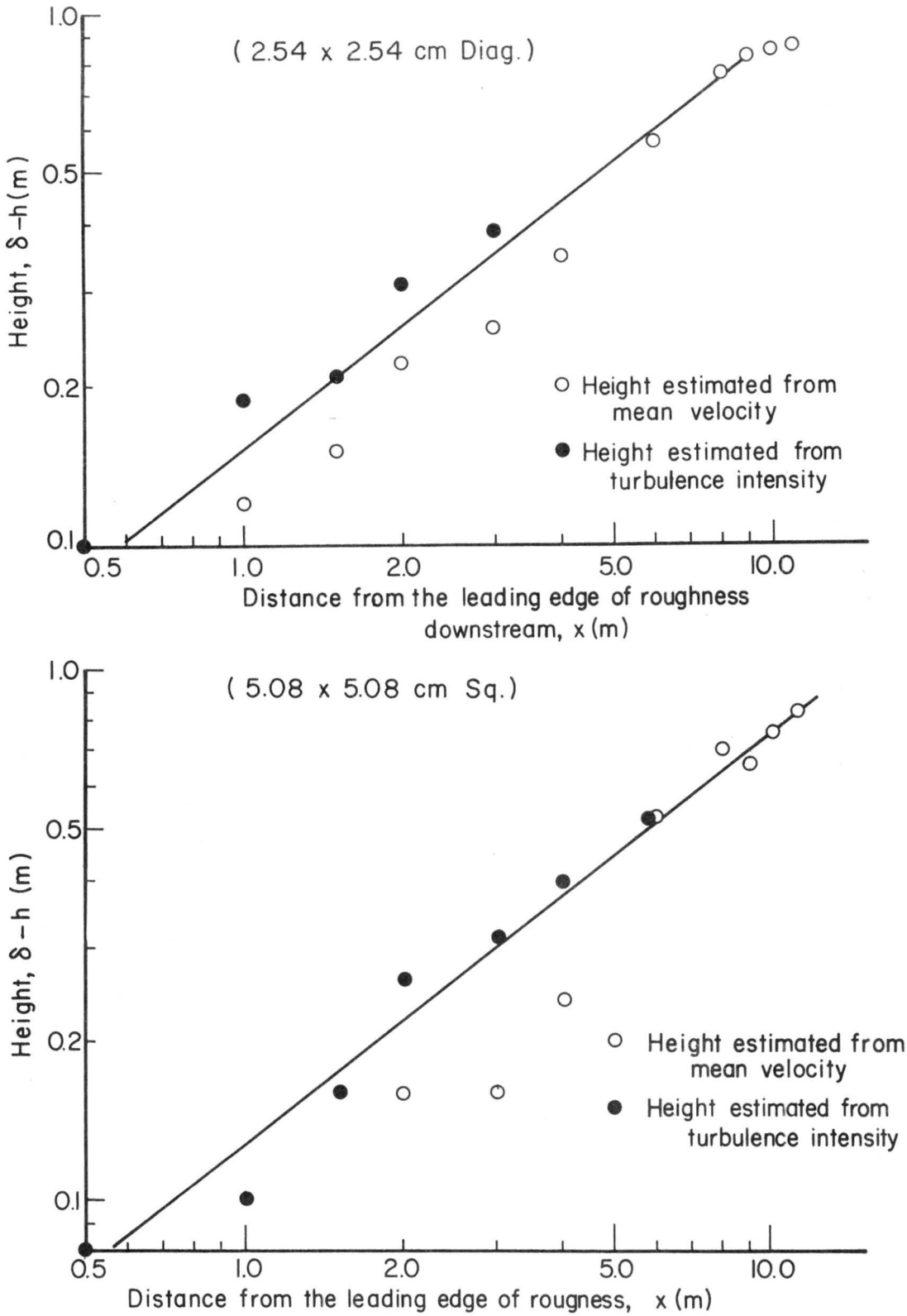

Fig. 31. Height of internal boundary layer
(2.54 x 2.54 cm diag)
(5.08 x 5.08 cm sq)

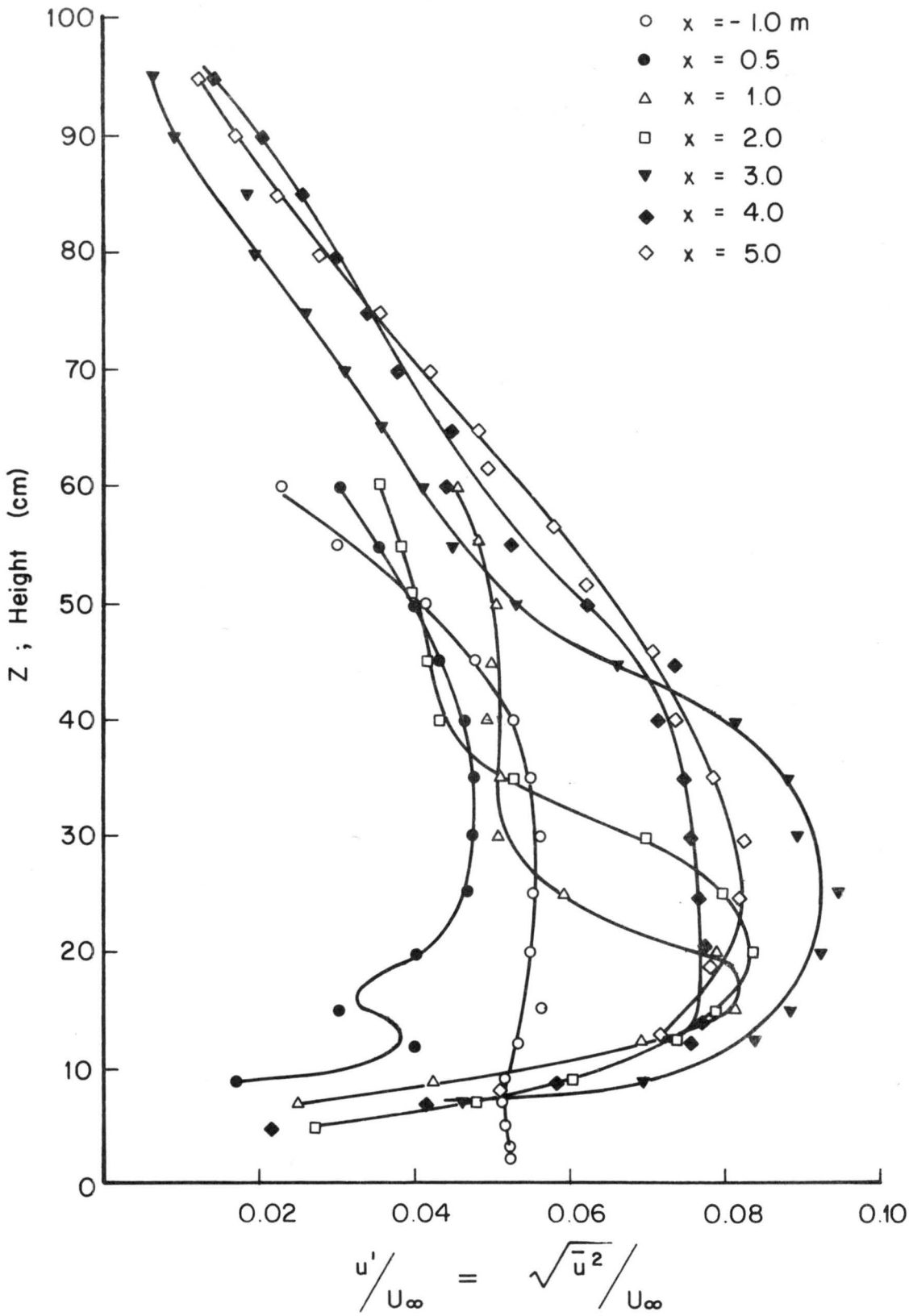

Fig. 32. Turbulent velocity profile (1.27 x 1.27 cm diag)

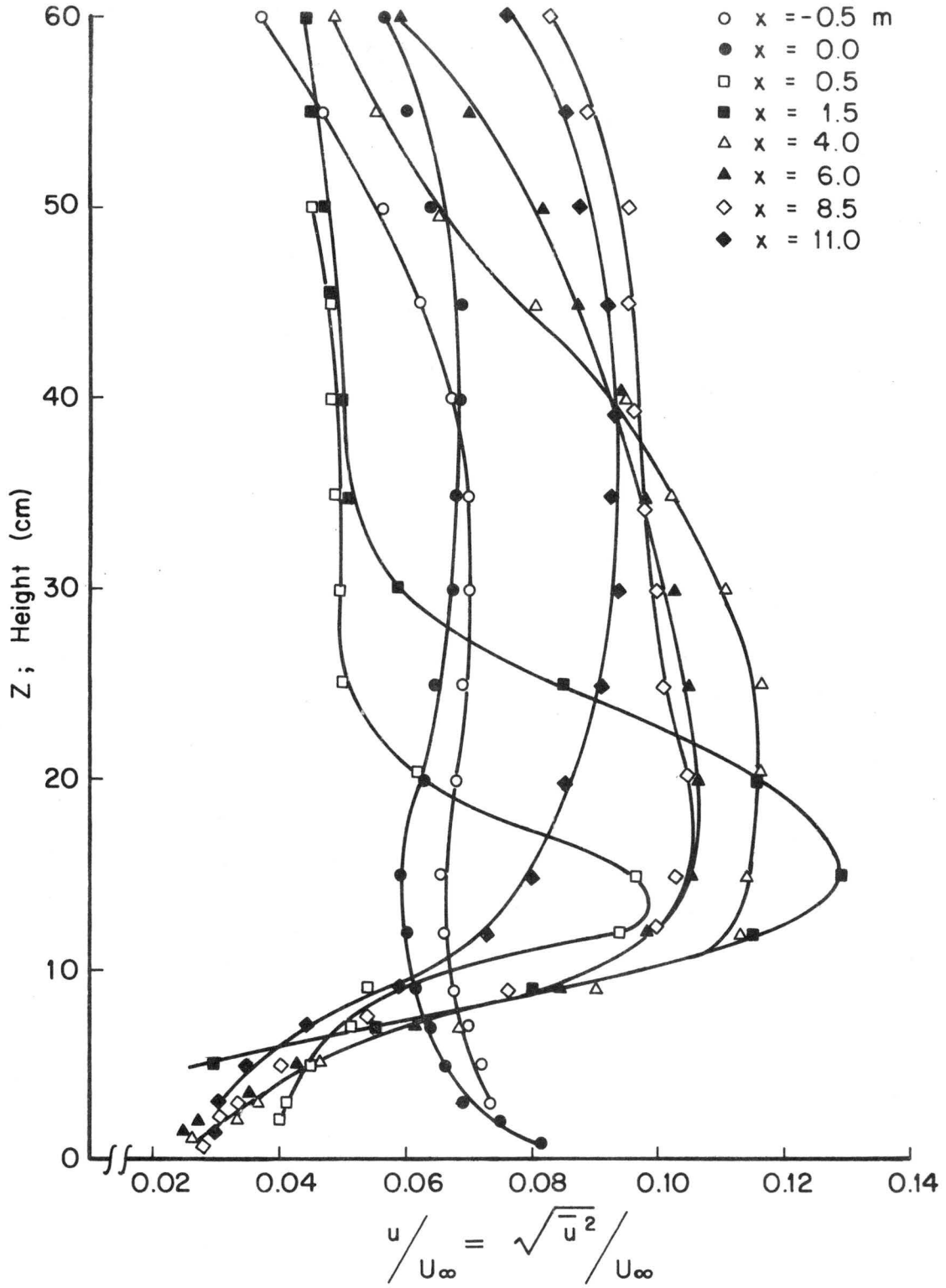

Fig. 33. Turbulent velocity profile (2.54 x 2.54 cm sq)

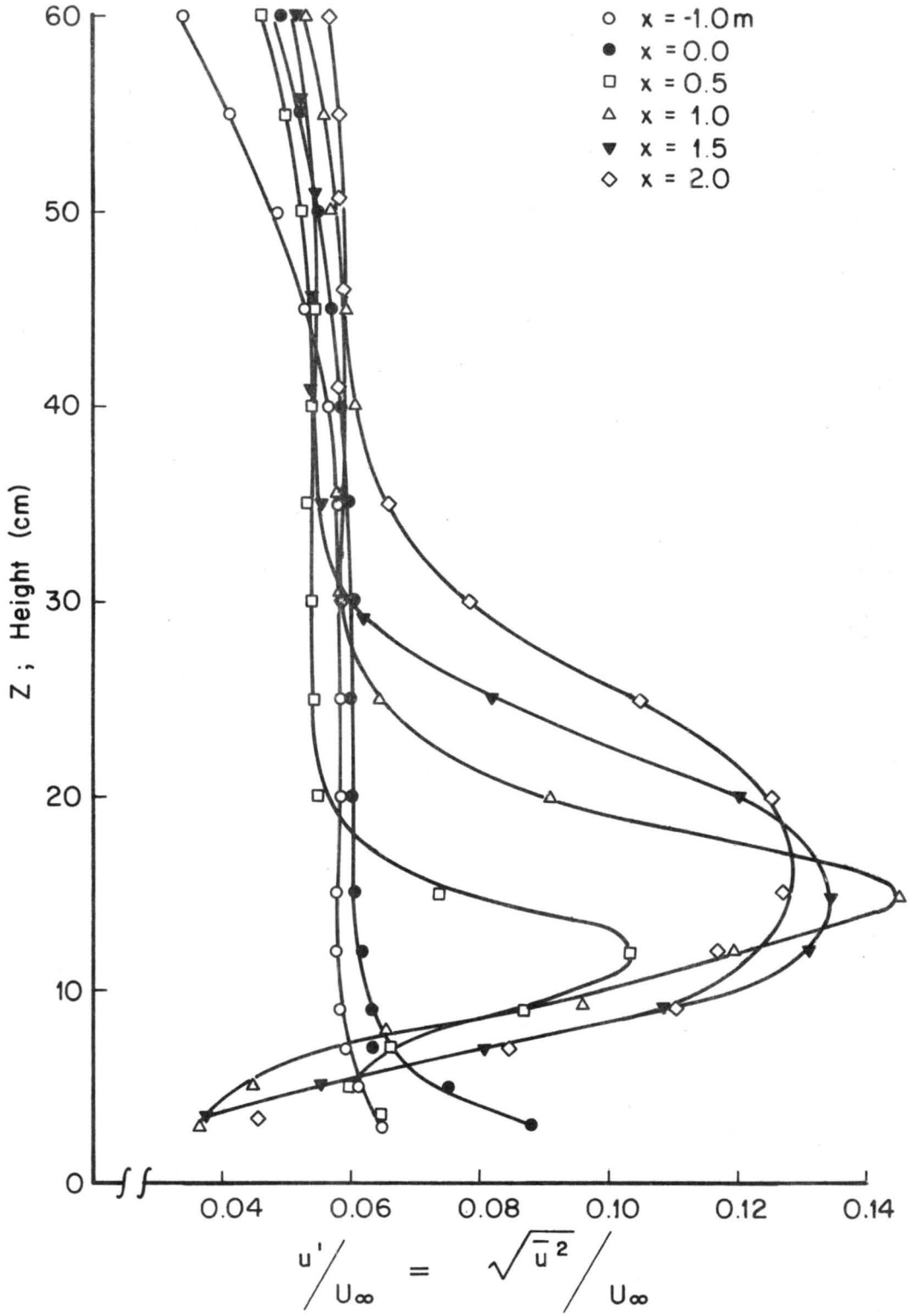

Fig. 34a. Turbulent velocity profile (2.54 x 2.54 cm diag)

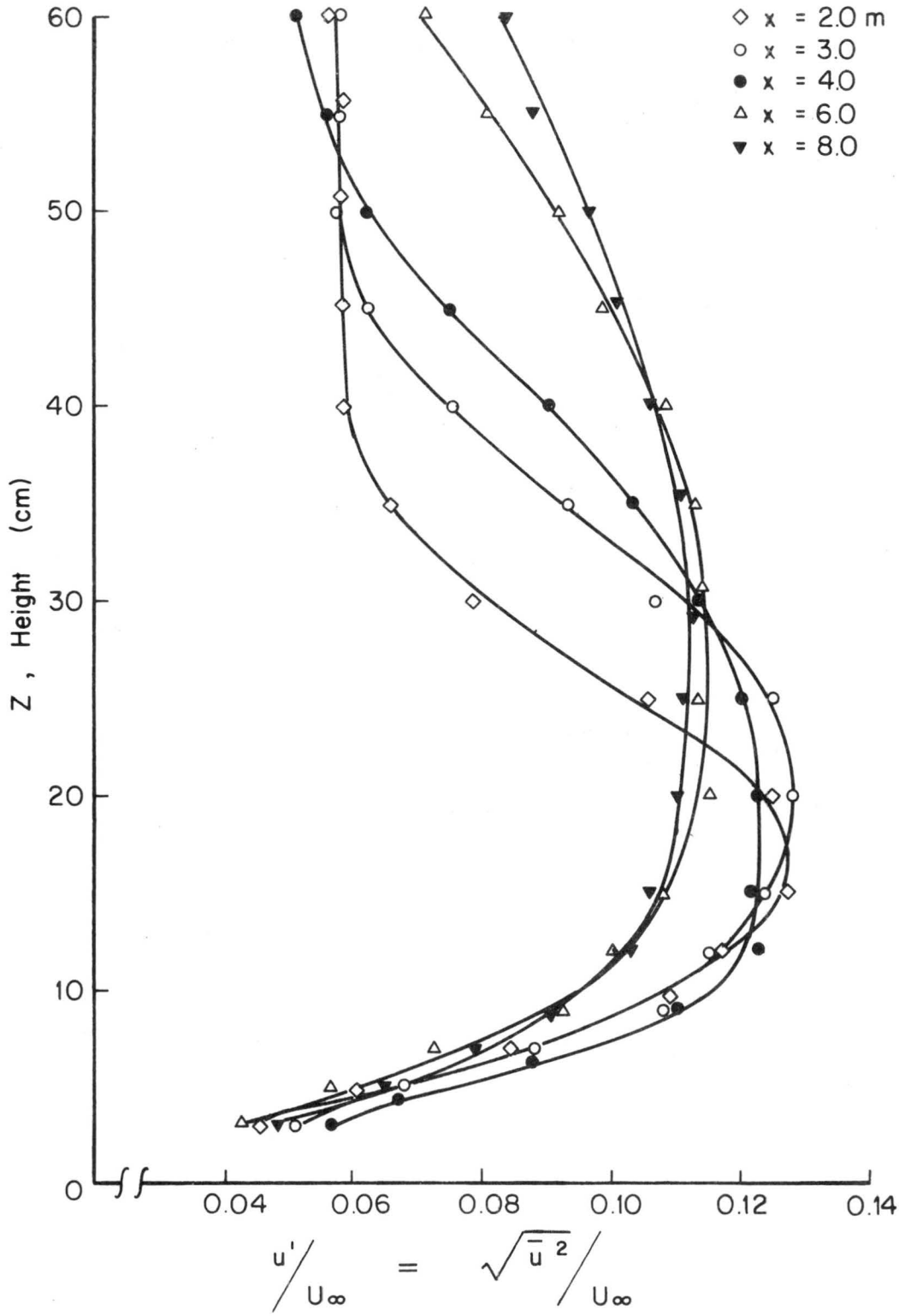

Fig. 34b. Turbulent velocity profile (2.54 x 2.54 dm diag)

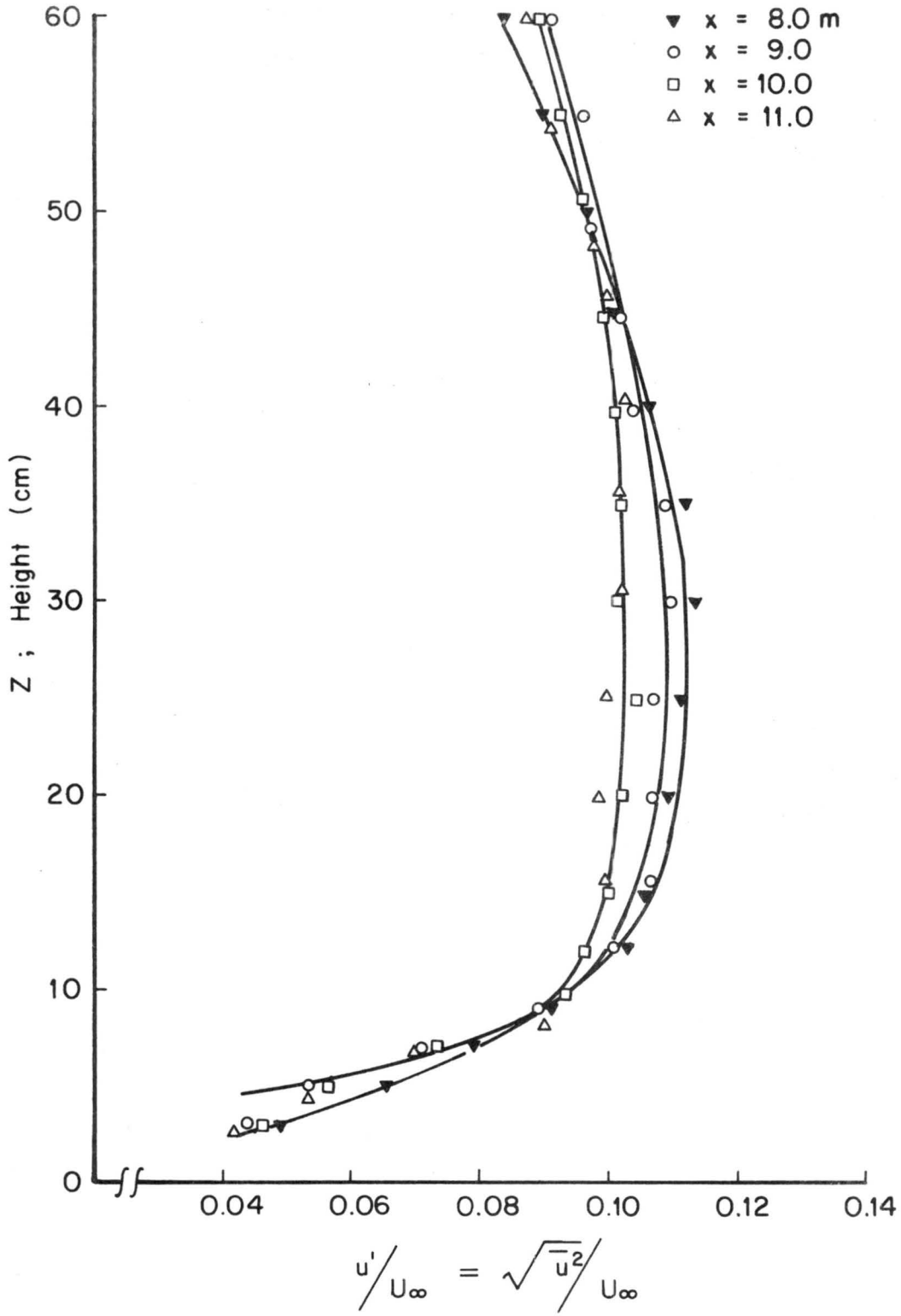

Fig. 34c. Turbulent velocity profile (2.54 x 2.54 cm diag)

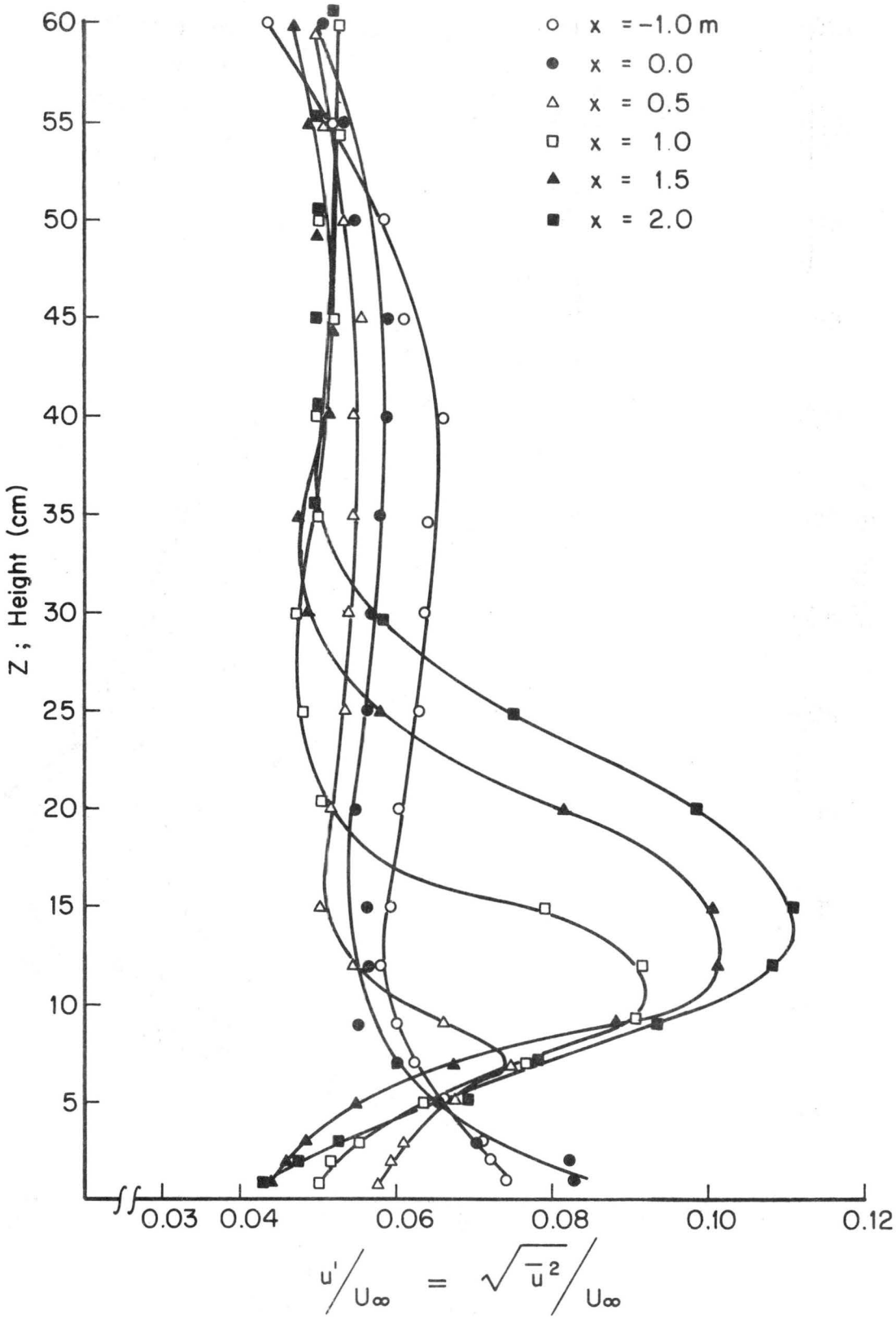

Fig. 35a. Turbulent velocity profile (5.08 x 5.08 cm sq)

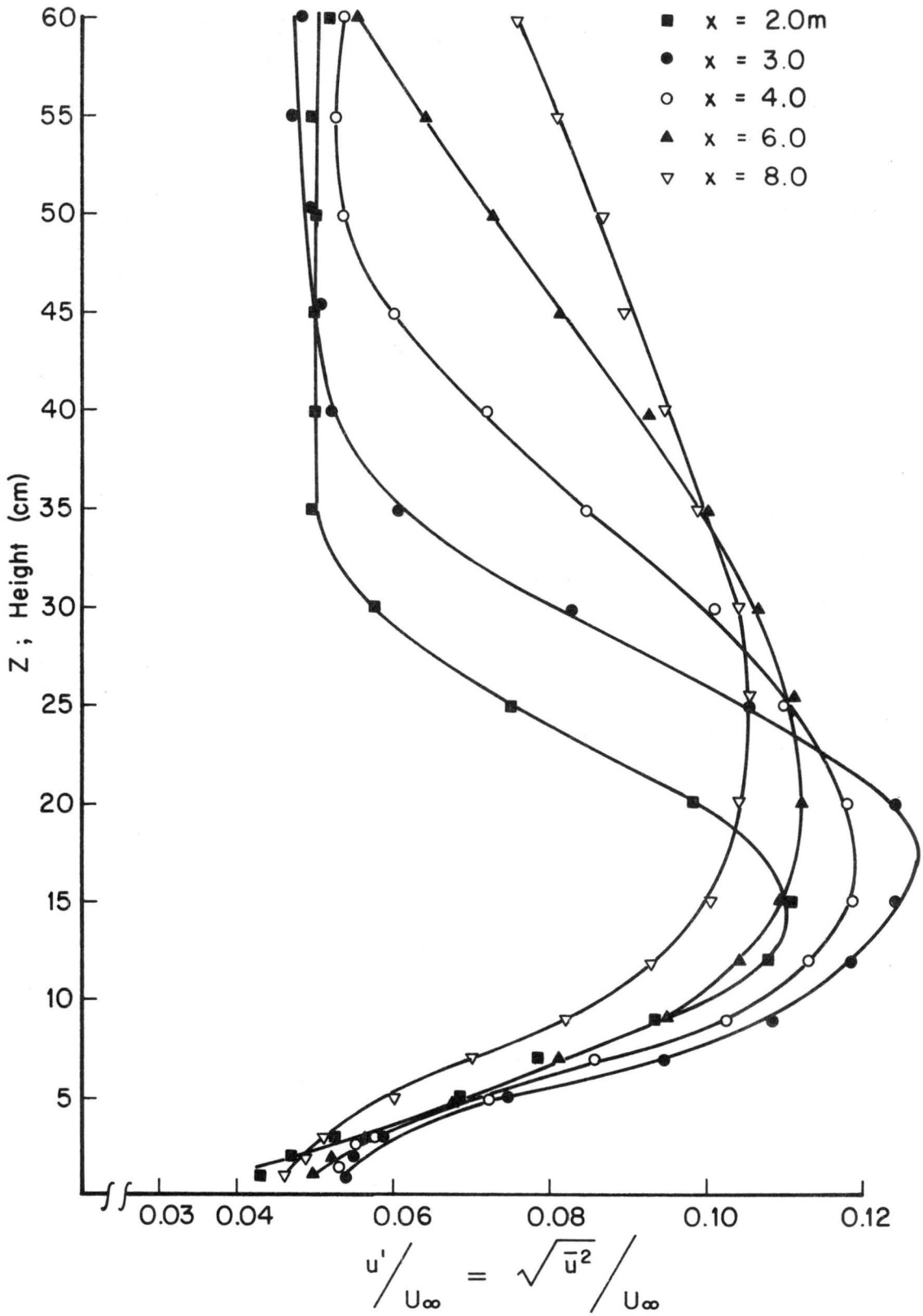

Fig. 35b. Turbulent velocity profile (5.08 x 5.08 cm sq)

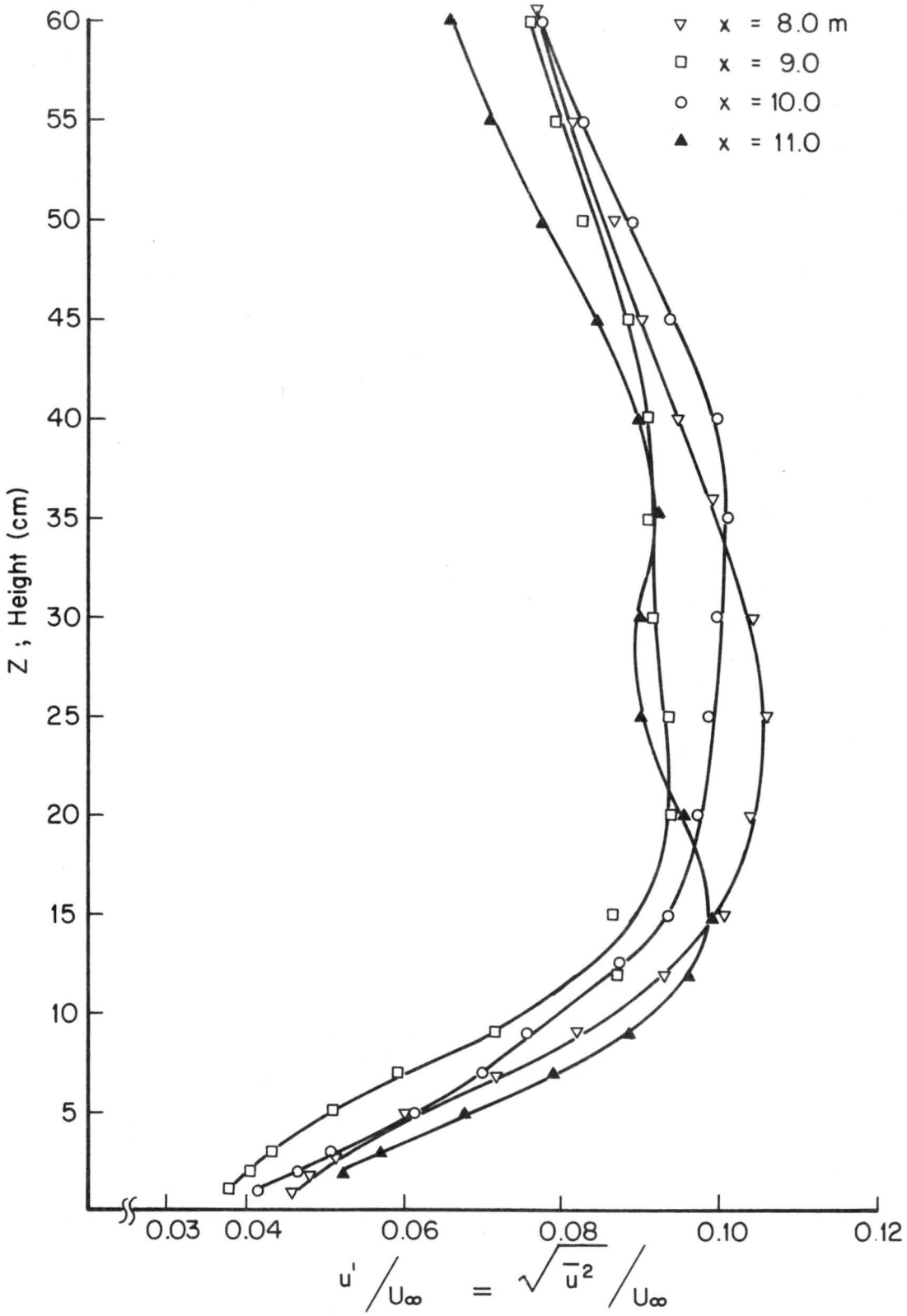

Fig. 35c. Turbulent velocity profile (5.08 x 5.08 cm sq)

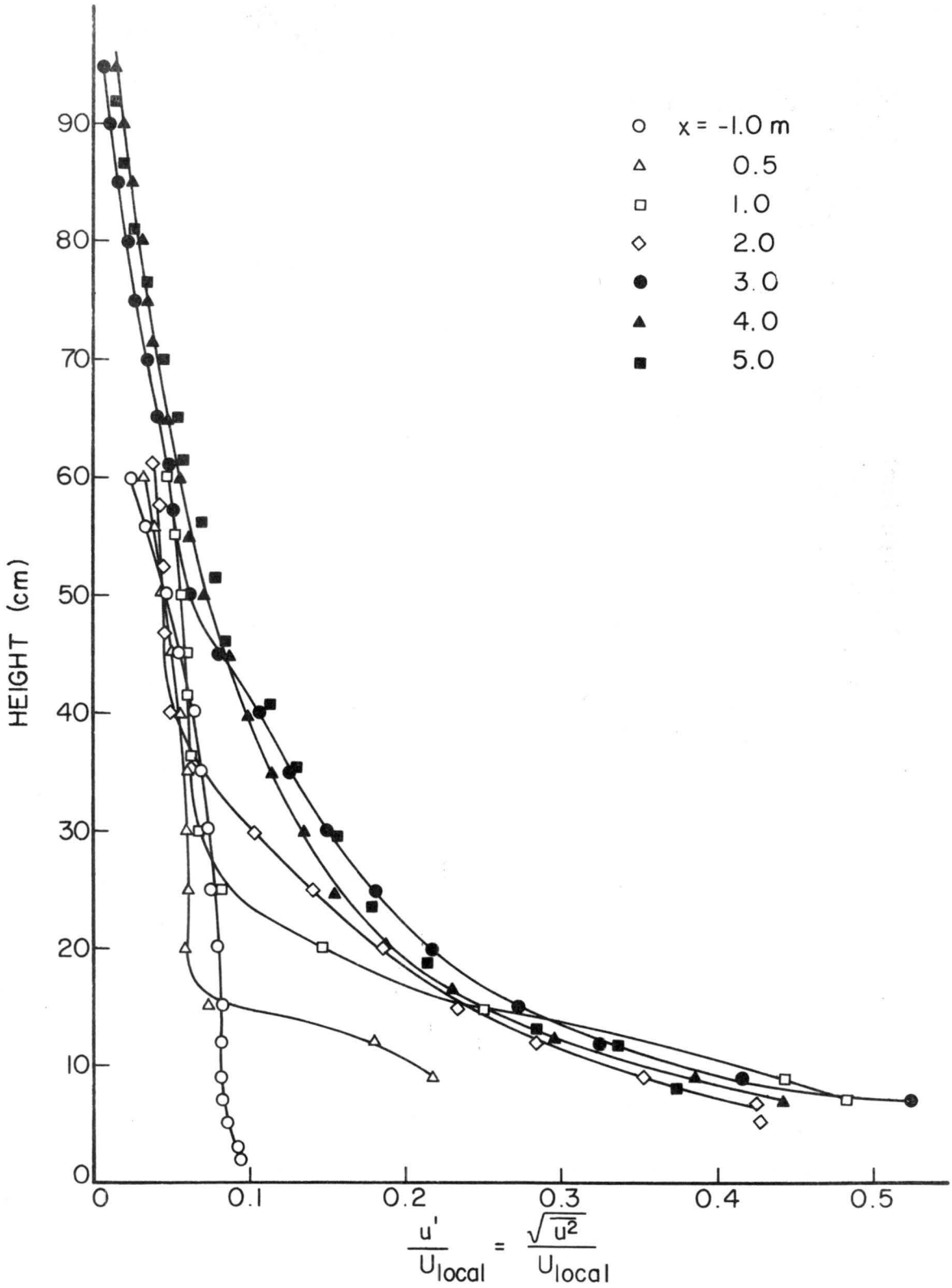

Fig. 36. Turbulence intensity (1.27 x 1.27 cm diag)

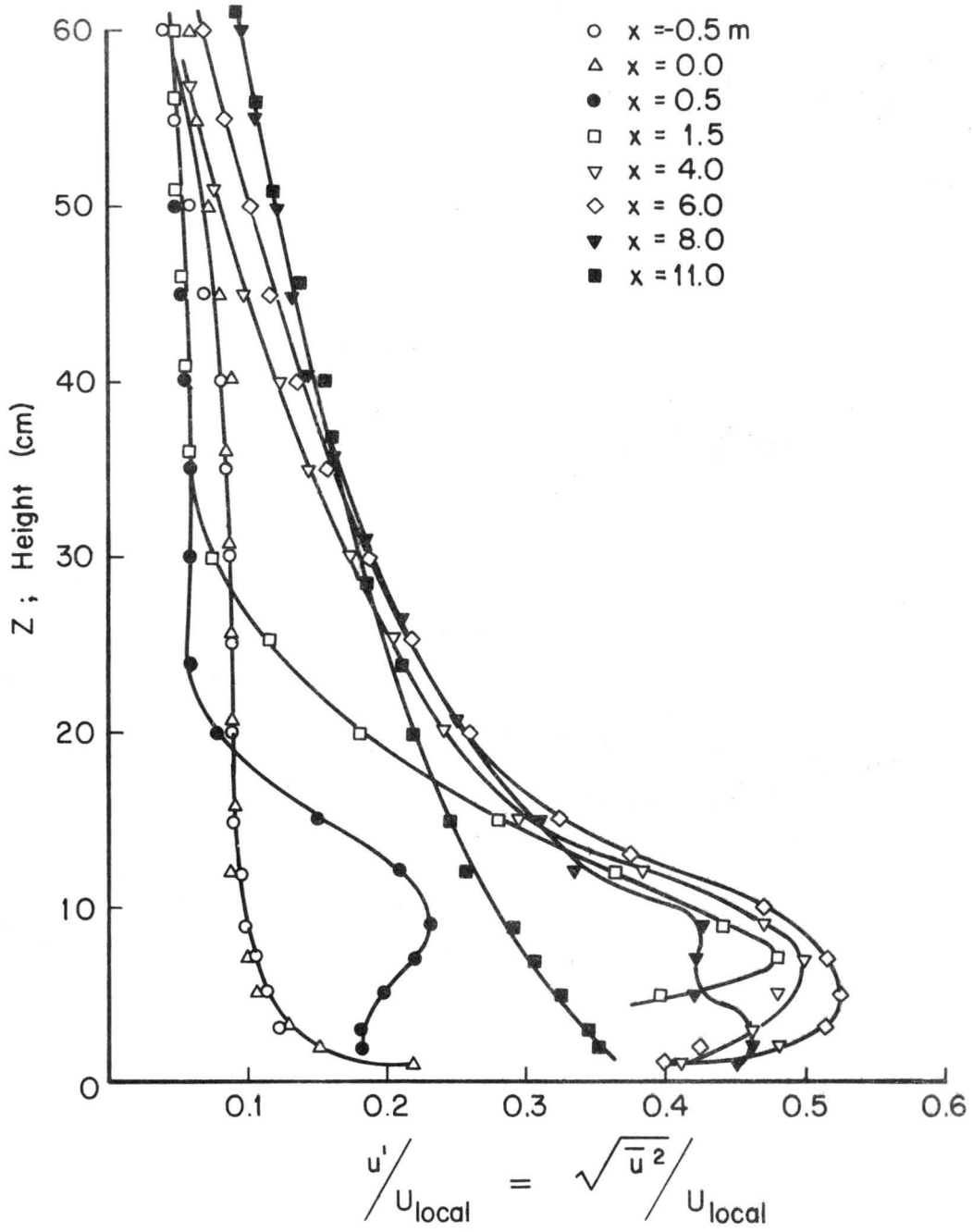

Fig. 37. Turbulence intensity (2.54 x 2.54 cm sq)

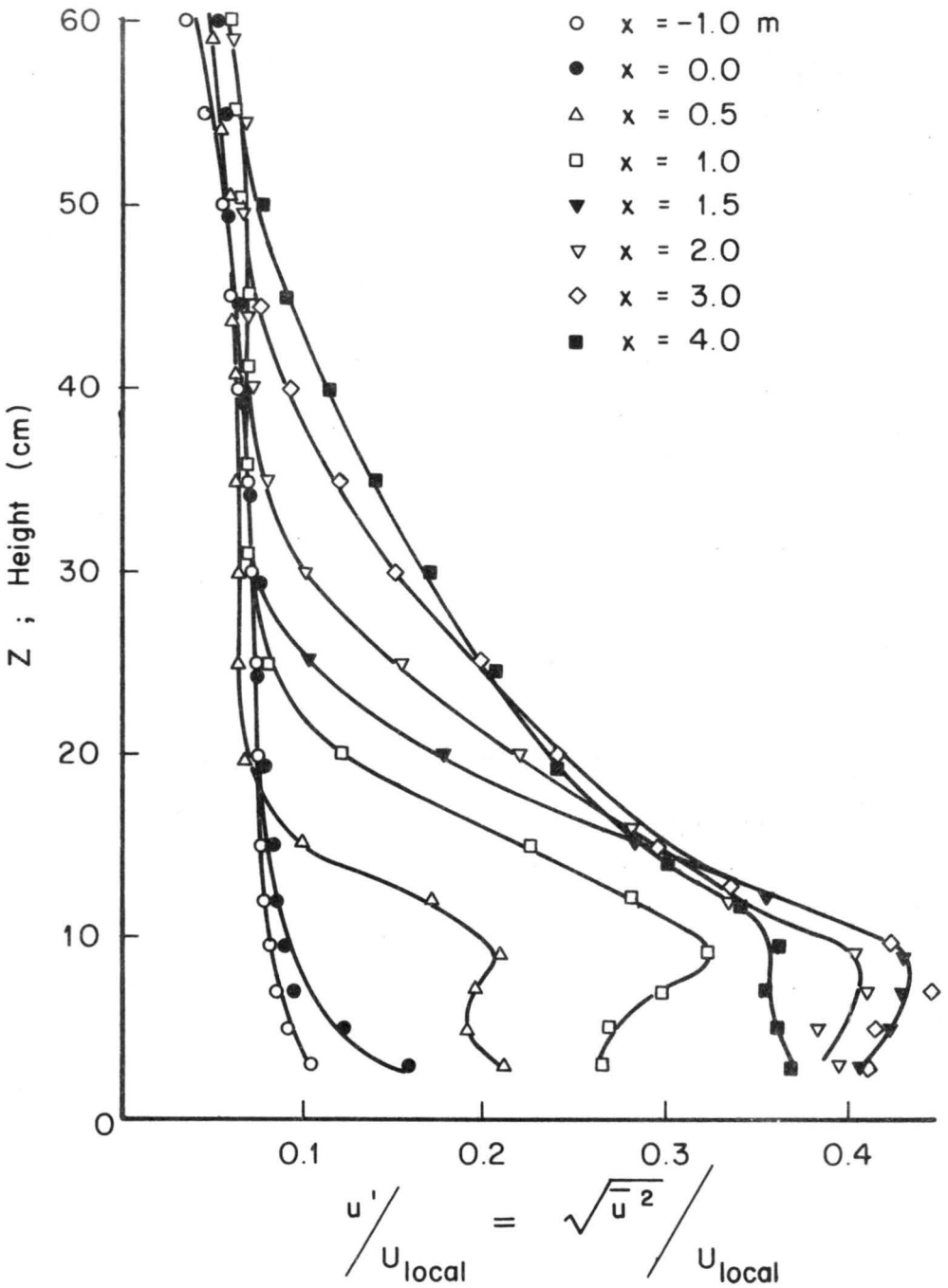

Fig. 38a. Turbulence intensity (2.54 x 2.54 cm diag)

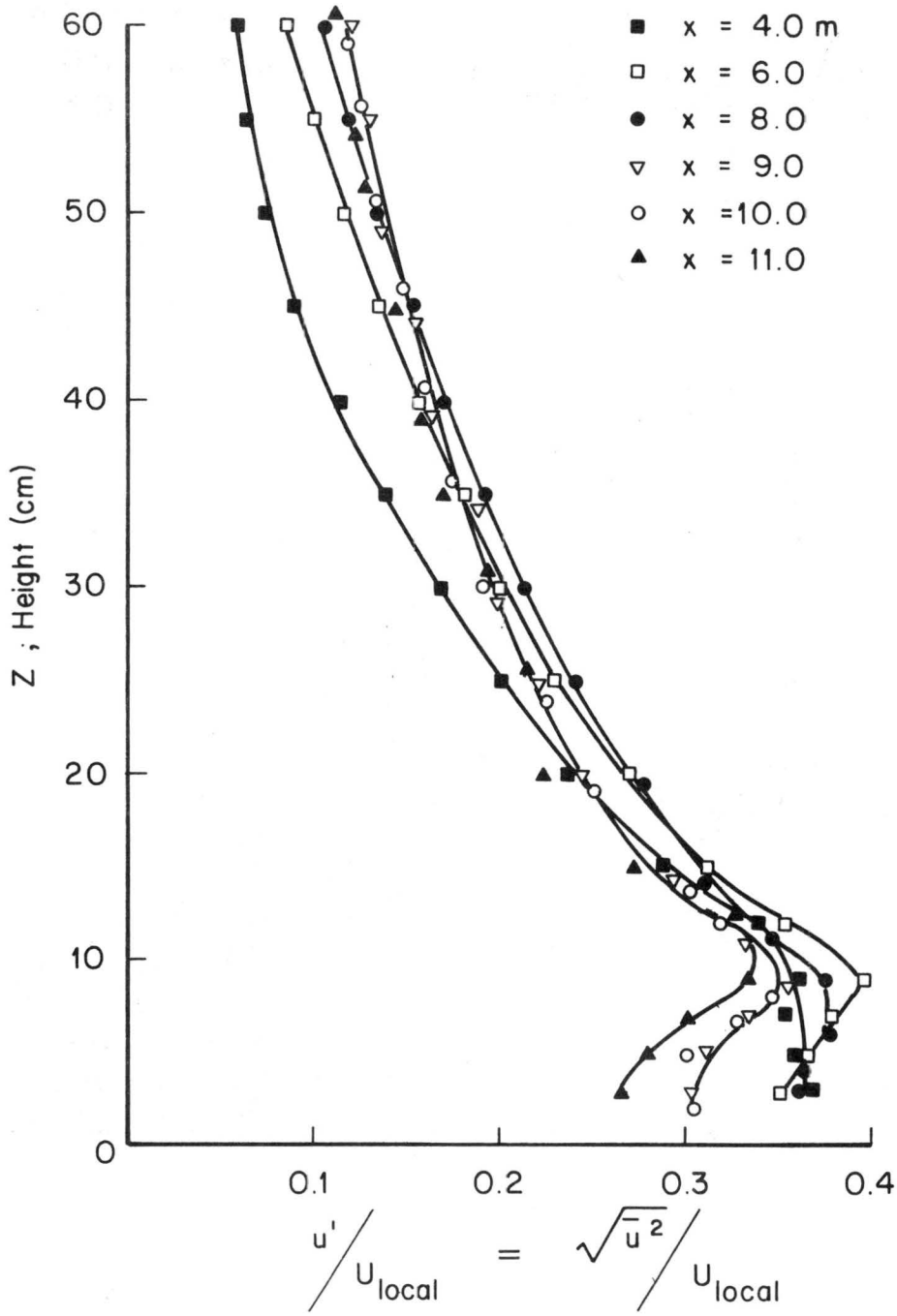

Fig. 38b. Turbulence intensity (2.54 x 2.54 cm diag)

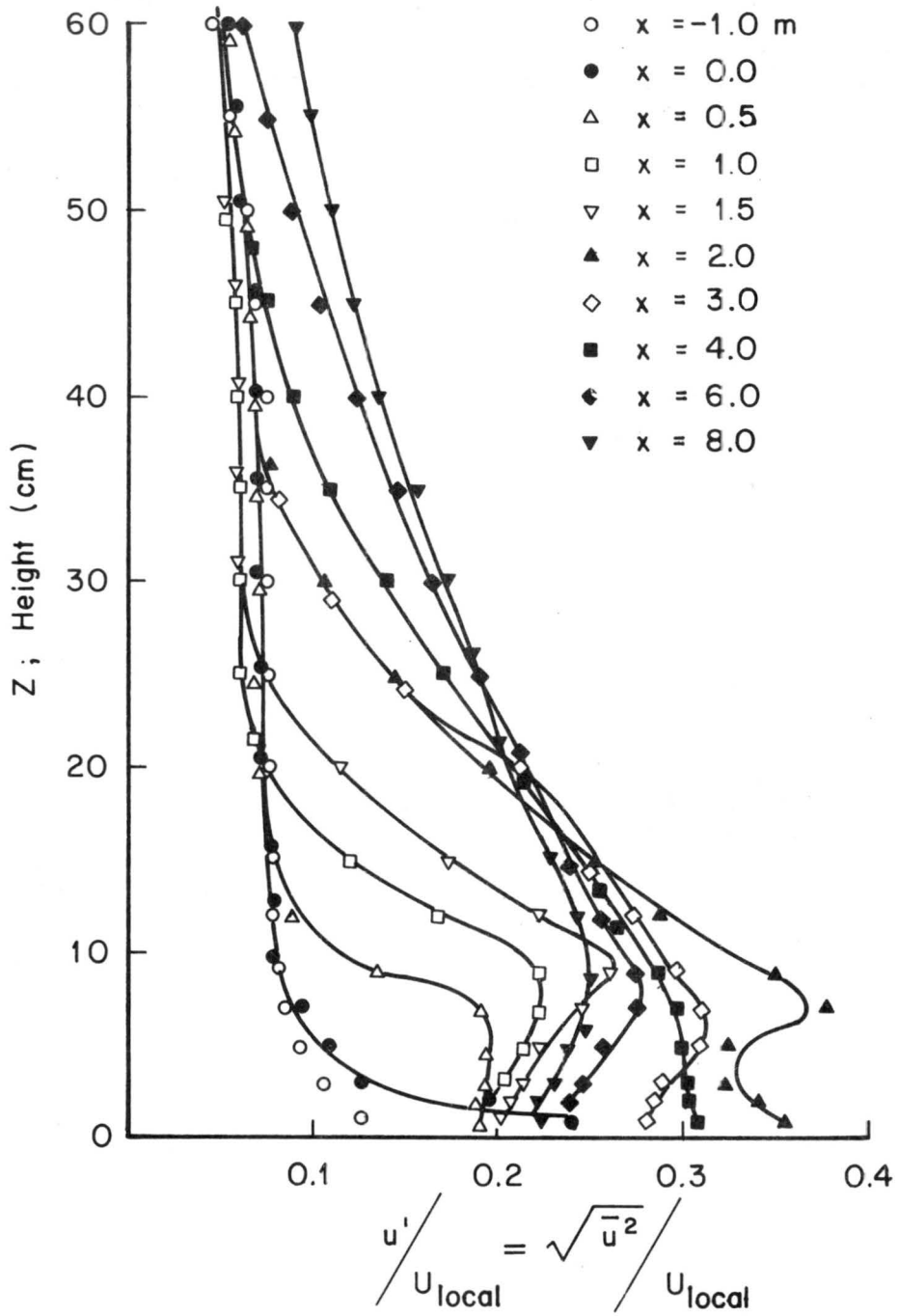

Fig. 39a. Turbulence intensity (5.08 x 5.08 cm sq)

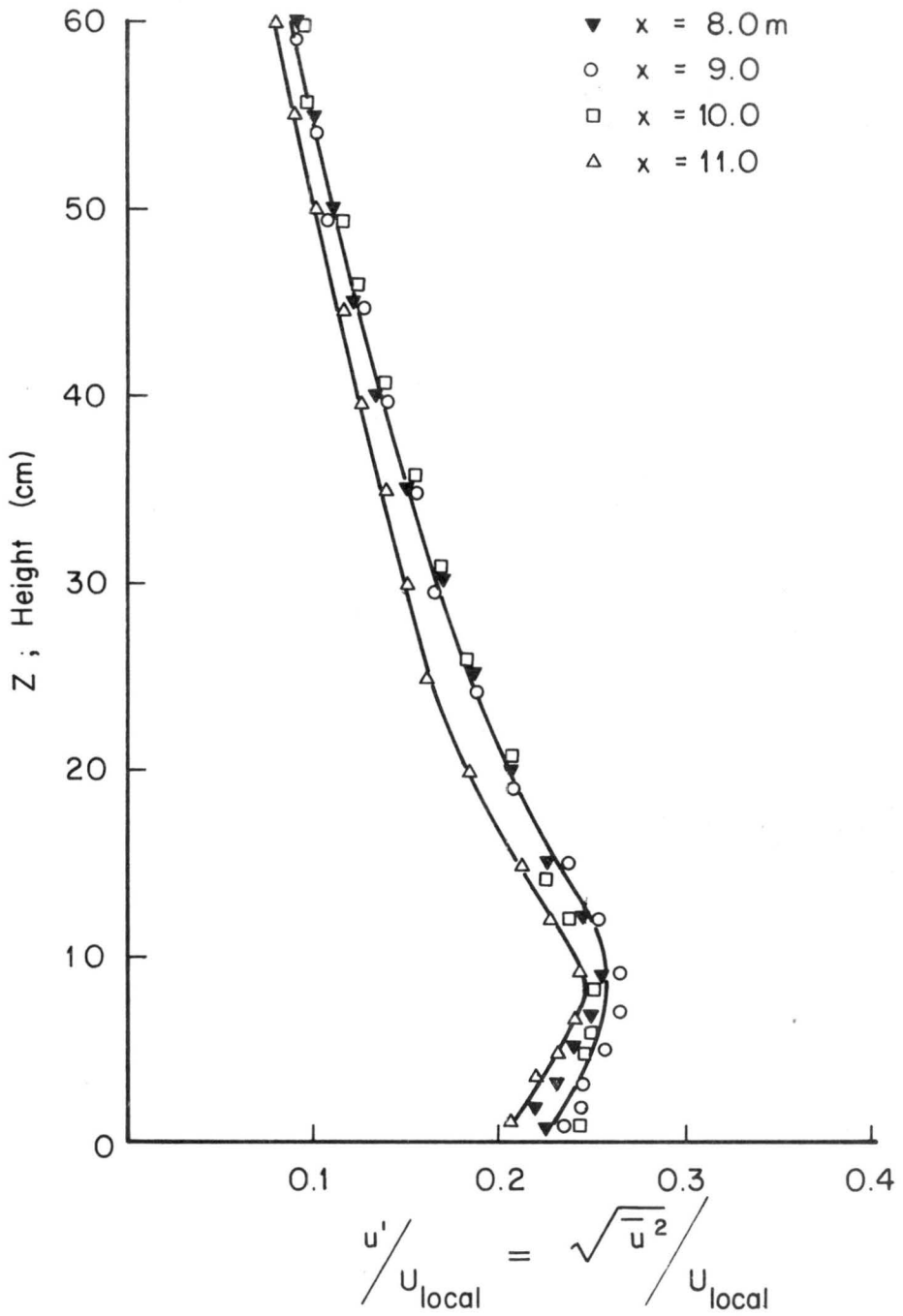

Fig. 39b. Turbulence intensity (5.08 x 5.08 cm sq)

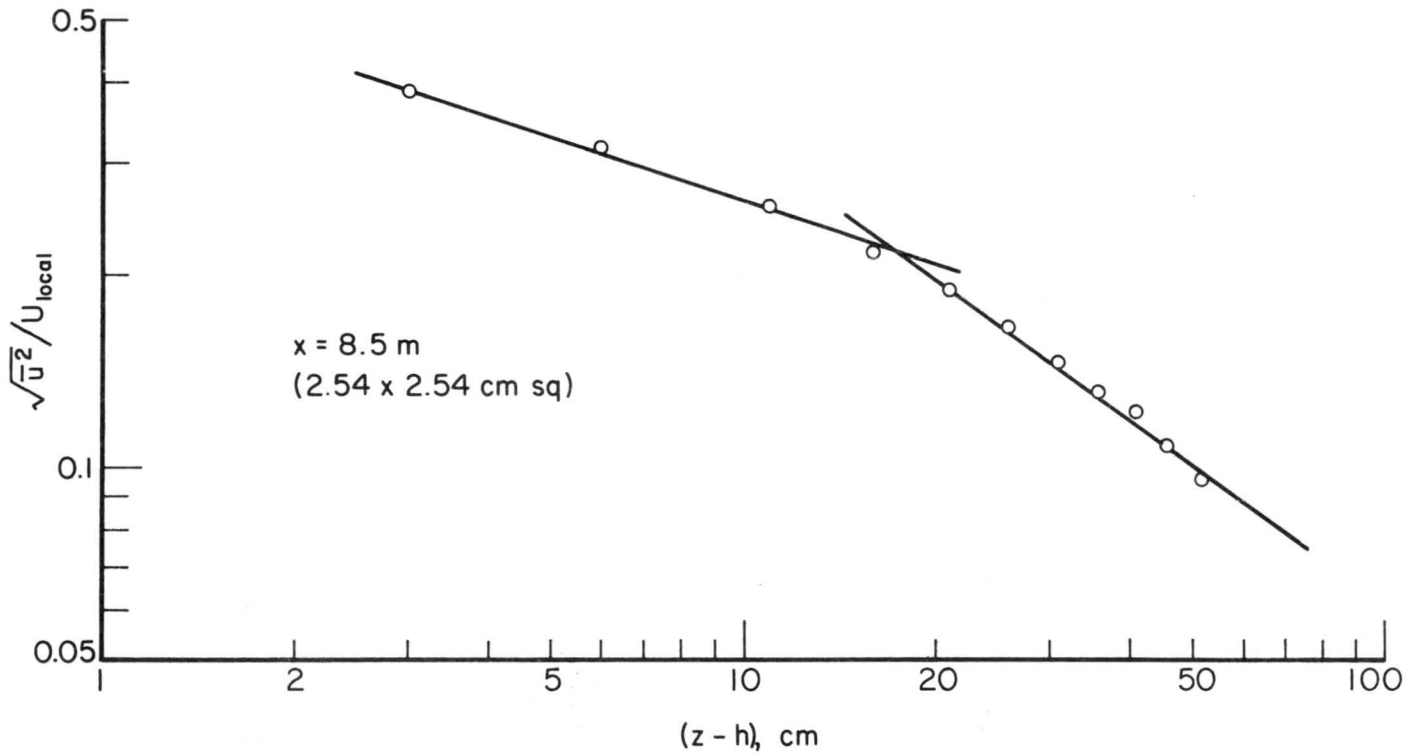

Fig. 40. Turbulence intensity profile above canopy

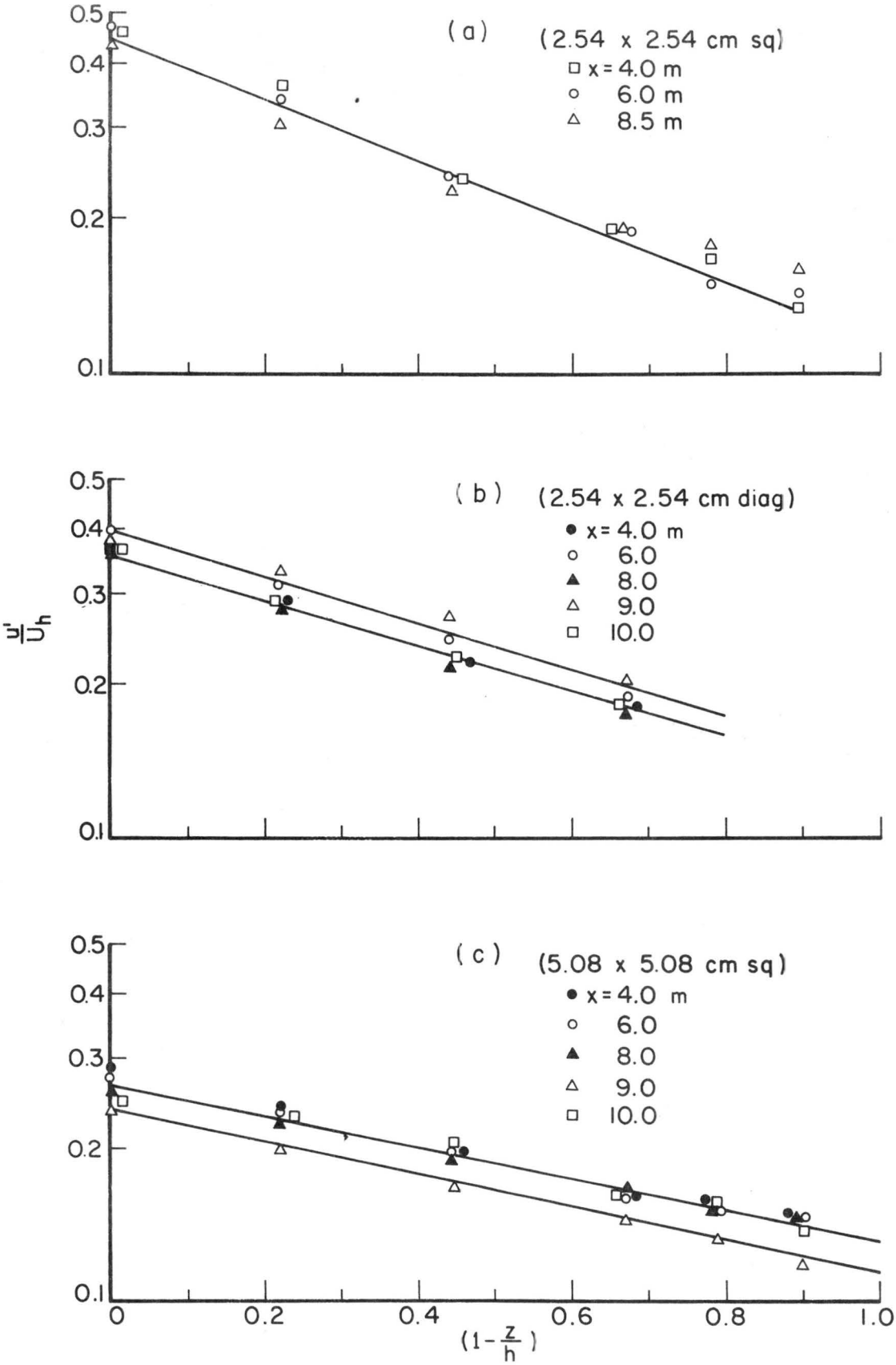

Fig. 41a,b,c. Turbulent velocity within canopy

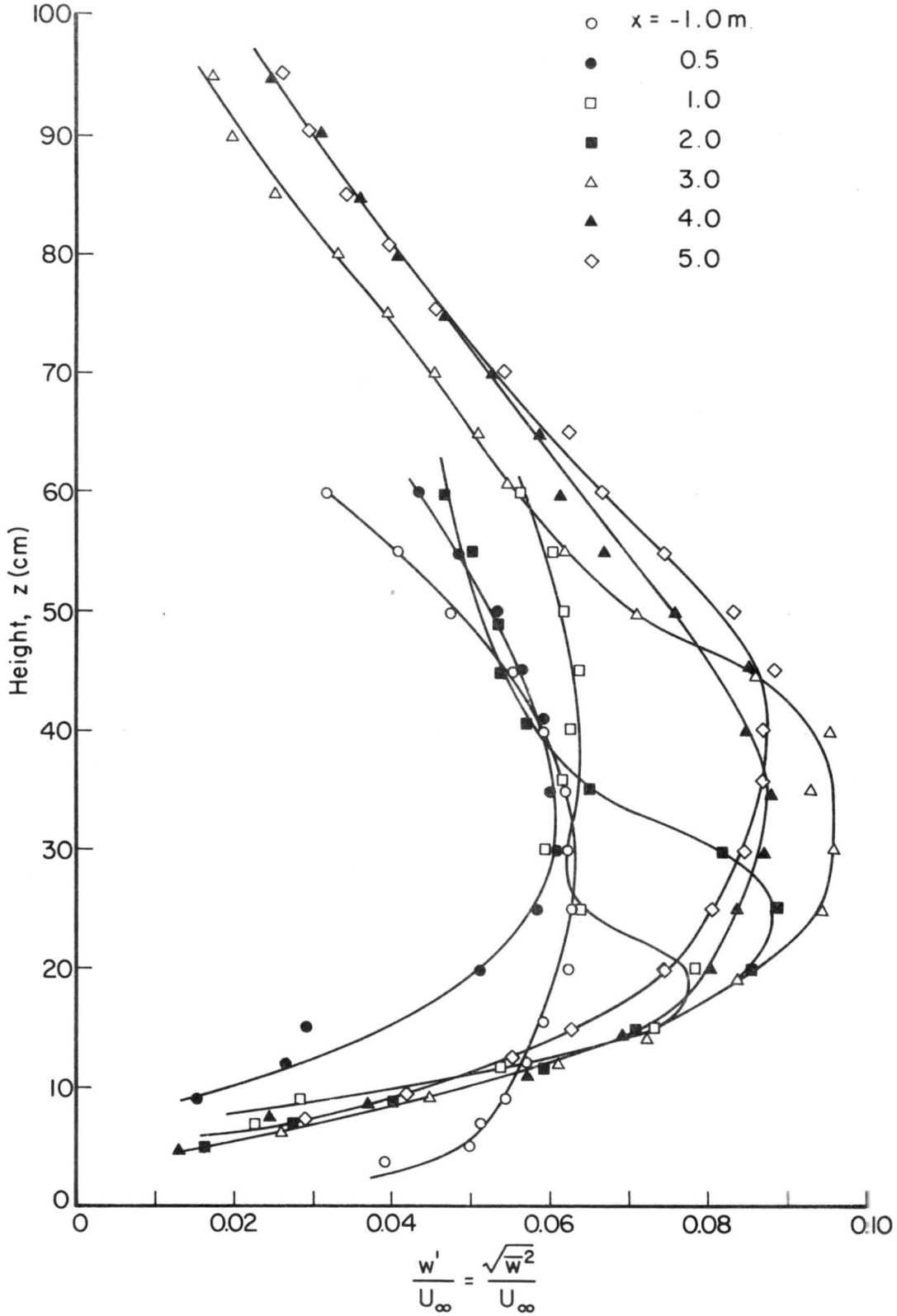

Fig. 42. Vertical component of turbulent velocity (1.27 x 1.27 cm diag)

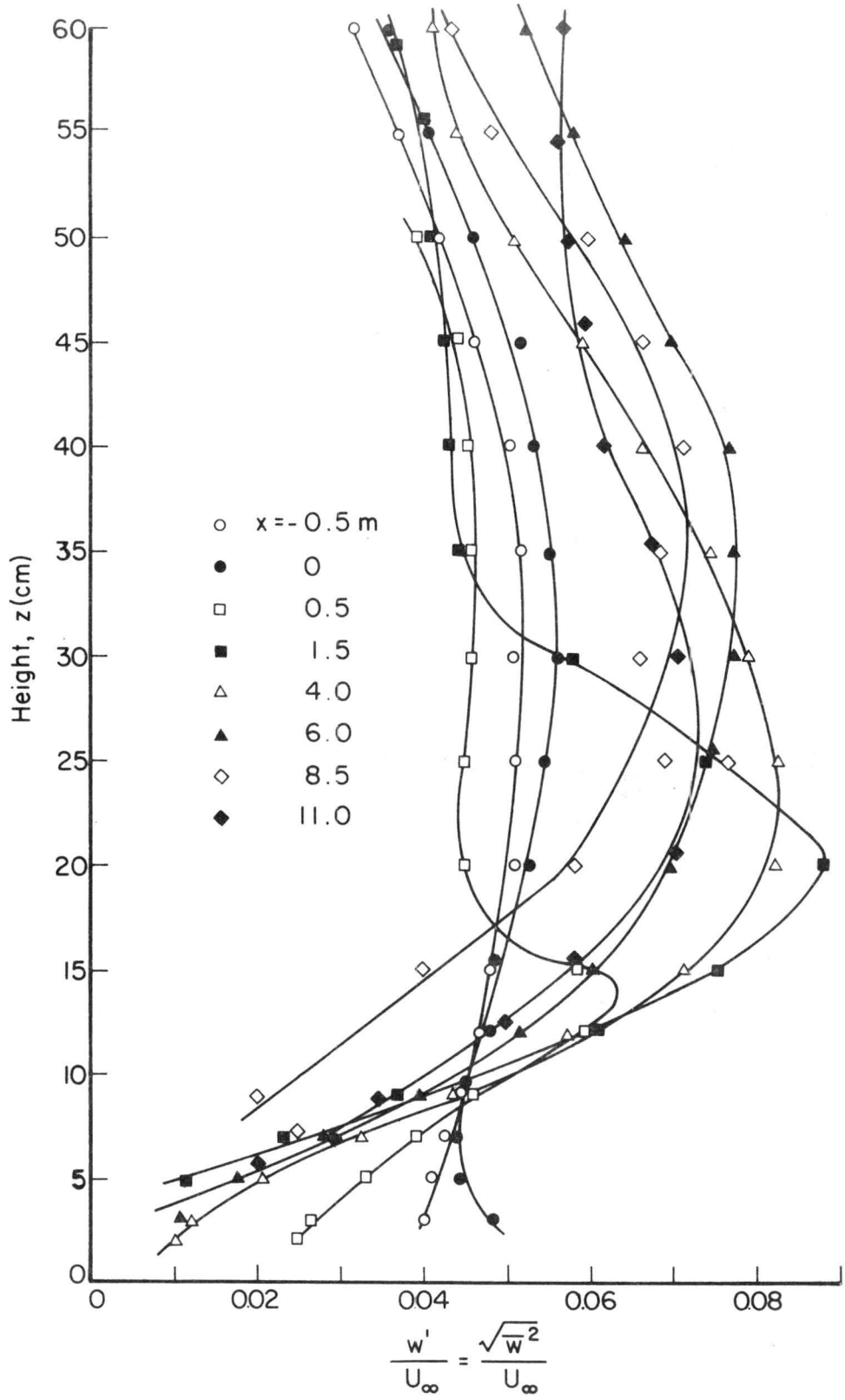

Fig. 43. Vertical component of turbulent velocity (2.54 x 2.54 cm sq)

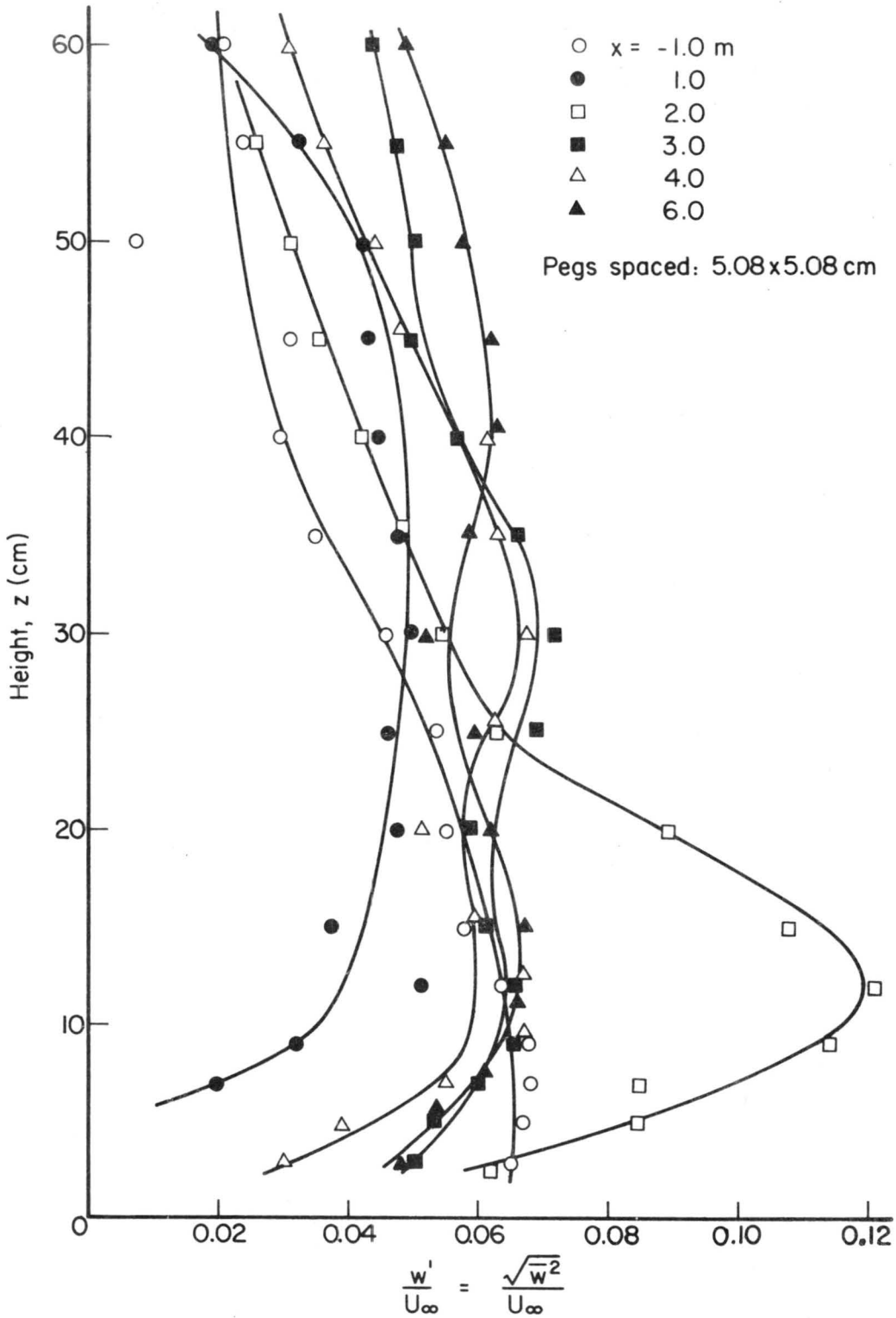

Fig. 44a. Vertical component of turbulent velocity (5.08 x 5.08 cm sq)

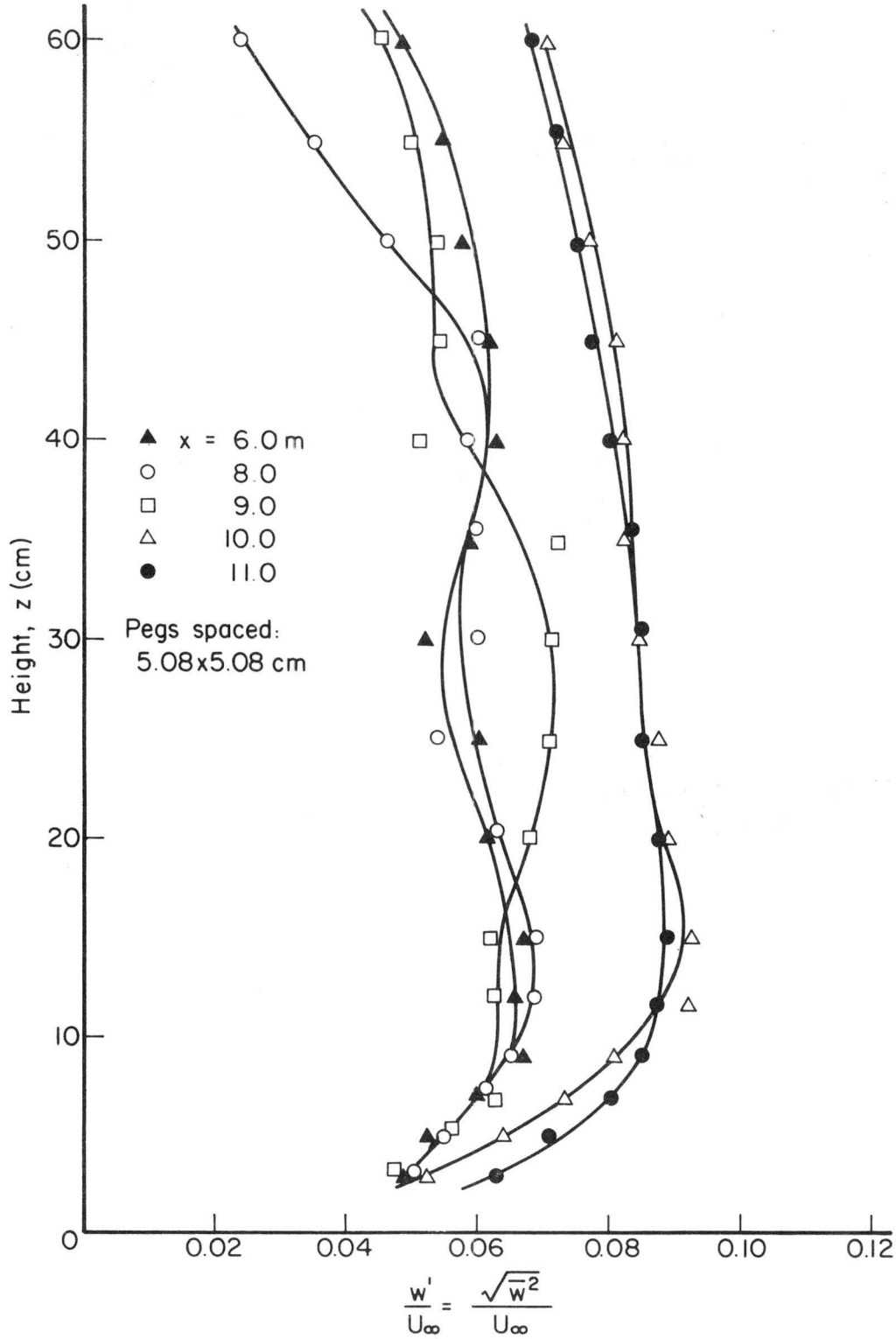

Fig. 44b. Vertical component of turbulent velocity (5.08 x 5.08 cm sq)

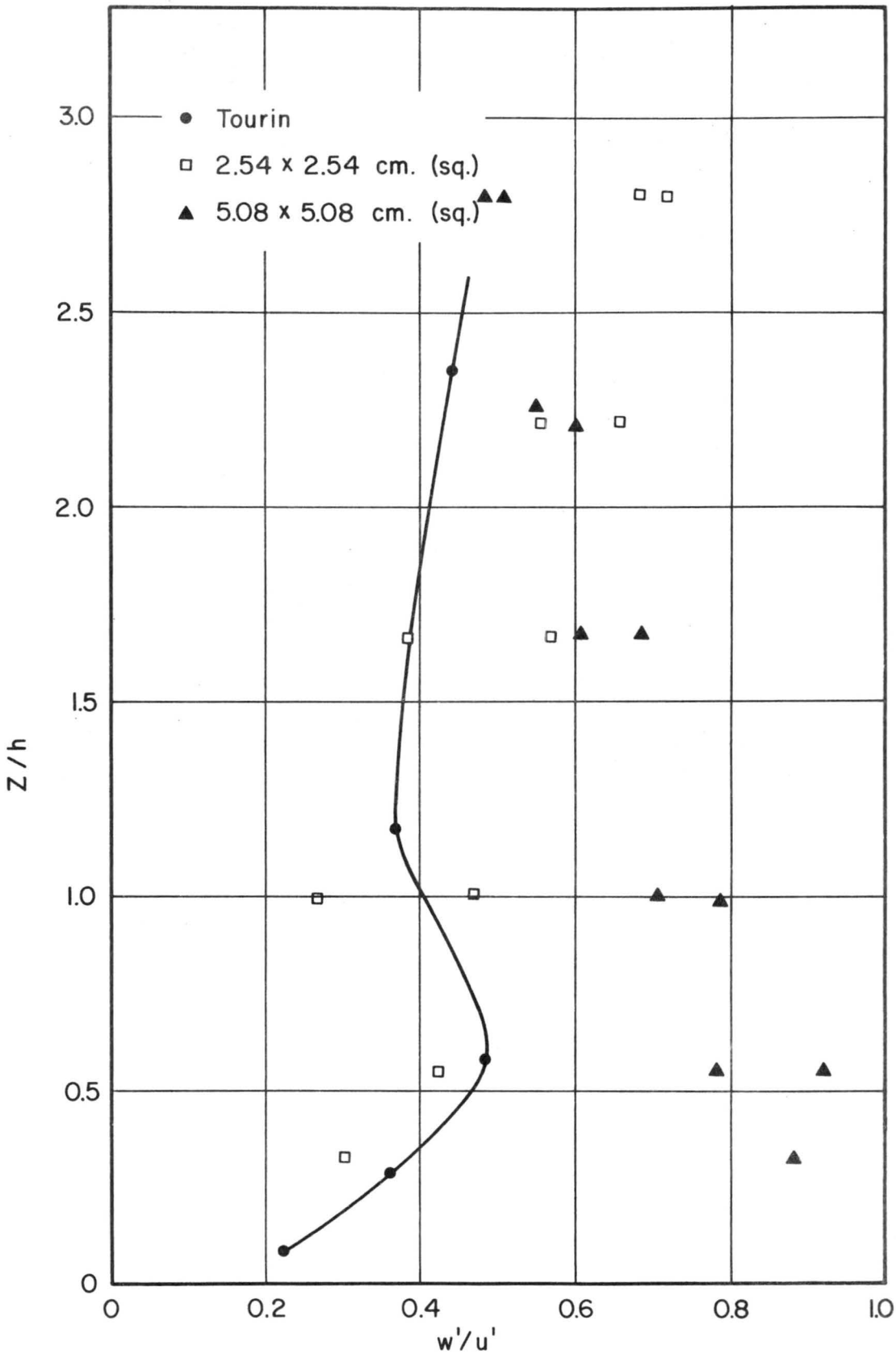

Fig. 45 Distribution of the coefficient of anisotropy

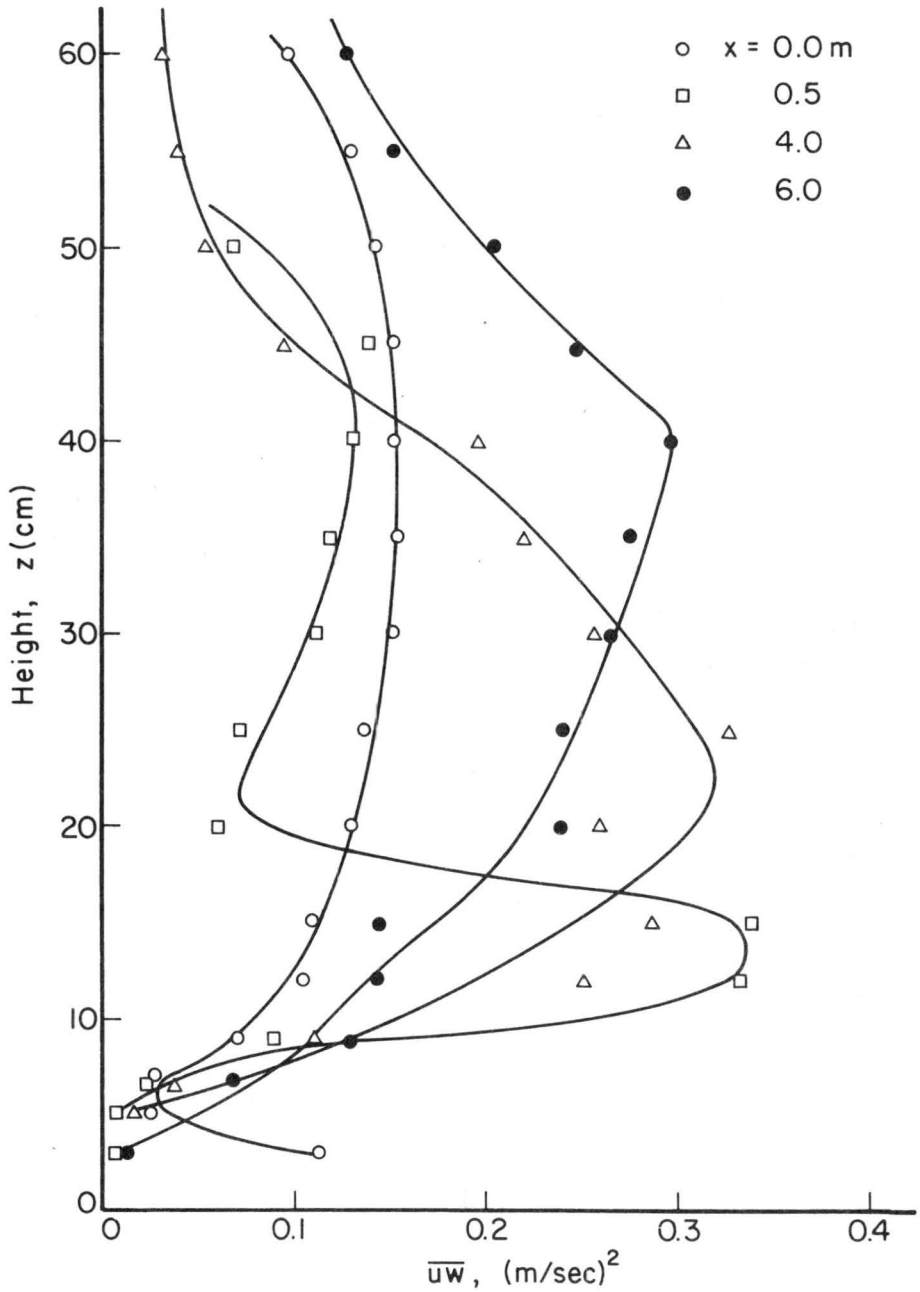

Fig. 46a Turbulent shear stress
(2.54 x 2.54 cm sq)

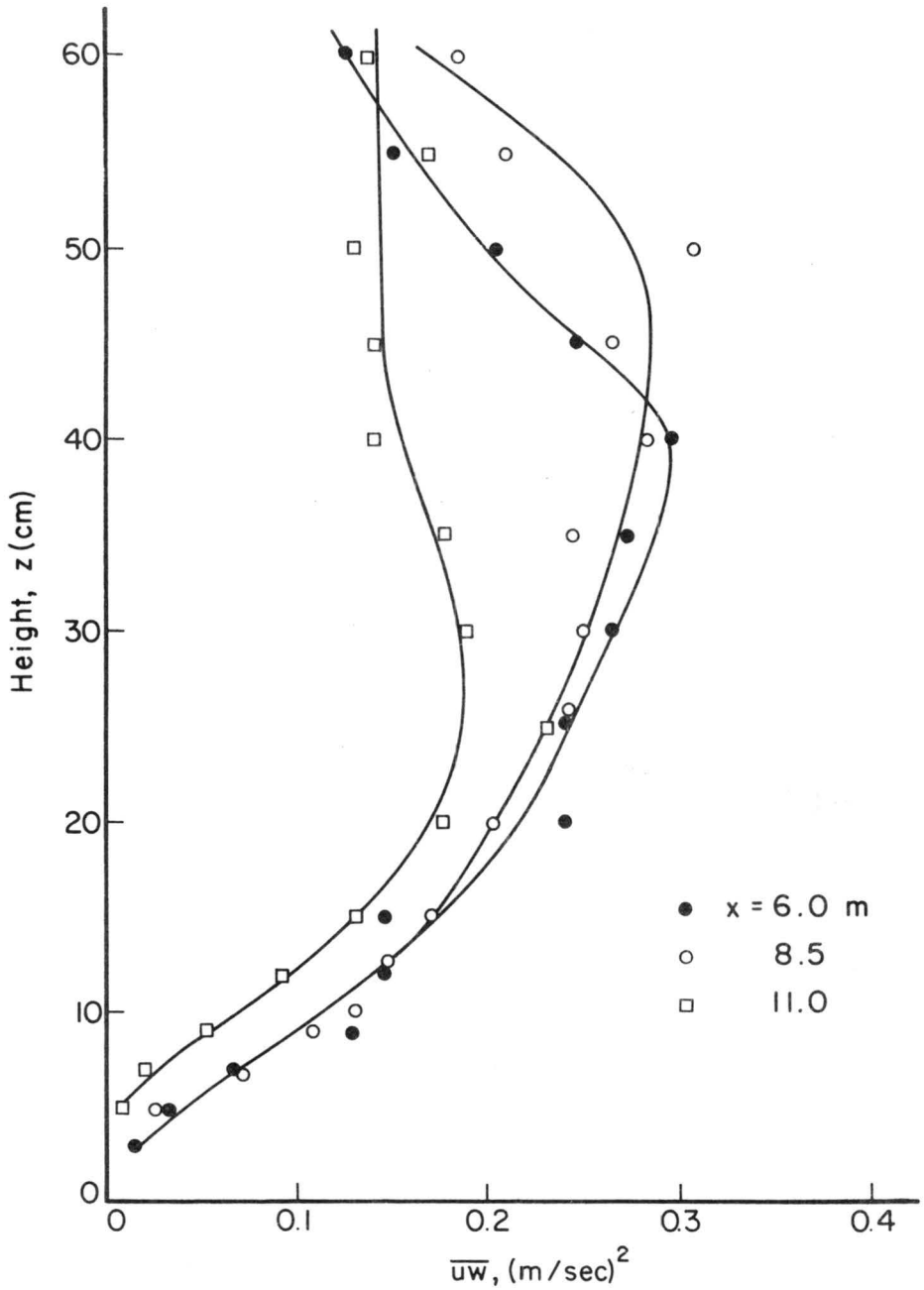

Fig. 46b Turbulent shear stress
(2.54 x 2.54 cm sq)

TABLE 1. VALUES OF MEAN VELOCITY

(1.27 x 1.27 cm diag.)

Z cm	X=-1.0m	X=-0.5m	X=0m	X=0.5m	X=1.0m	X=2.0m	X=3.0m	X=4.0m	X=5.0m
	m/s	m/s	m/s	m/s	m/s	m/s	m/s	m/s	m/s
1.0	6.25	6.00	3.25	--	--	--	--	--	--
2.0	6.60	6.22	3.97	--	--	--	--	--	--
3.0	6.82	6.42	4.45	--	0.33	0.27	0.27	0.27	--
5.0	7.15	6.73	5.15	--	0.38	0.75	0.45	0.60	--
7.0	7.38	7.02	5.77	0.30	0.62	1.35	1.05	1.12	1.25
9.0	7.60	7.25	6.38	0.95	1.14	2.05	2.00	1.82	1.97
12.0	7.85	7.56	7.17	2.65	2.45	3.10	3.10	3.00	2.80
15.0	8.08	7.83	7.78	4.85	3.90	4.03	3.90	3.90	3.50
20.0	8.38	8.24	8.32	8.15	6.50	5.40	5.07	4.95	4.55
25.0	8.74	8.64	8.77	9.14	8.75	6.75	6.18	5.85	5.52
30.0	9.13	9.03	9.27	9.37	9.53	8.15	7.23	6.77	6.42
35.0	9.53	9.42	9.78	9.57	9.82	9.13	8.22	7.77	7.27
40.0	9.90	9.77	10.20	9.80	10.08	9.82	9.11	8.77	8.10
45.0	10.25	10.12	10.57	10.10	10.35	10.32	9.80	9.43	8.79
50.0	10.59	10.50	10.91	10.42	10.63	10.60	10.23	9.95	9.28
55.0	10.95	10.90	10.14	10.75	10.92	10.80	10.52	10.35	9.78
60.0	11.18	11.25	11.30	11.11	11.18	10.95	10.69	10.72	10.23
65.0	11.40	11.47	11.52	11.45	11.40	11.08	10.85	10.98	10.68
70.0	11.62	11.67	11.75	11.68	11.62	11.25	11.03	11.24	11.03
75.0	11.70	11.75	11.85	11.85	11.82	11.43	11.30	11.43	11.30
80.0	11.80	11.82	11.92	11.87	11.90	11.65	11.42	11.66	11.48
85.0	11.85	11.85	11.95	11.95	11.95	11.88	11.65	11.78	11.67
90.0	11.90	11.90	11.97	11.97	11.97	11.95	11.85	11.90	11.80
95.0	11.93	11.93	11.97	11.97	11.97	11.97	11.92	11.95	11.92
100.0	11.95	11.95	11.97	11.97	11.97	11.97	11.95	11.95	11.95
105.0	11.97	11.97	11.97	11.97	11.97	11.97	11.97	11.97	11.97
110.0	11.97	11.97	11.97	11.97	11.97	11.97	11.97	11.97	11.97

Z cm	X=6.0m	X=7.0m	X=9.3m	X=10.3m	X=11.0m
	m/s	m/s	m/s	m/s	m/s
1.0	--	--	0.82	0.78	1.02
2.0	--	--	0.90	0.85	1.09
3.0	--	--	0.97	0.97	1.17
5.0	--	0.47	1.18	1.37	1.48
7.0	1.00	0.85	1.87	1.97	2.12
9.0	2.06	1.70	3.04	2.96	3.33
12.0	3.10	2.90	4.40	4.35	5.05
15.0	3.82	3.74	5.10	5.32	5.82
20.0	4.67	4.82	6.00	6.50	6.80
25.0	5.52	5.63	6.85	7.22	7.53
30.0	6.42	6.38	7.57	7.83	8.15
35.0	7.27	7.18	8.20	8.35	8.63
40.0	8.02	8.00	8.72	8.80	9.06
45.0	8.71	8.66	9.12	9.18	9.45
50.0	9.28	9.20	9.50	9.60	9.78
55.0	9.75	9.68	9.86	9.88	10.10
60.0	10.12	10.10	10.20	10.20	10.40
65.0	10.44	10.52	10.52	10.50	10.68
70.0	10.72	10.88	10.83	10.81	10.95
75.0	11.00	11.20	11.15	11.08	11.22
80.0	11.31	11.45	11.40	11.33	11.48
85.0	11.57	11.65	11.60	11.55	11.69
90.0	11.83	11.80	11.75	11.70	11.85
95.0	11.92	11.92	11.85	11.83	11.92
100.0	11.95	11.95	11.92	11.92	11.95
105.0	11.97	11.97	11.95	11.95	11.97
110.0	11.97	11.97	11.97	11.97	11.97

TABLE 2. VALUES OF MEAN VELOCITY

(2.54 x 2.54 cm sq.)

Height	X=-1.0m	X=-0.5m	X=0m	X=0.5m	X=1.0m	X=2.0m	X=4.0m	X=6.0m
Z cm								
	m/s	m/s	m/s	m/s	m/s	m/s	m/s	m/s
1.0	6.60	6.35	4.33	2.55	0.73	0.73	0.75	0.75
2.0	6.95	6.67	5.75	2.55	0.73	0.75	0.80	0.75
3.0	7.25	6.93	6.40	2.58	0.73	0.80	0.88	0.80
5.0	7.75	7.33	6.94	2.63	0.76	0.96	1.12	0.97
7.0	8.12	7.64	7.22	2.72	1.32	1.38	1.62	1.38
9.0	8.37	7.83	7.42	3.20	2.25	2.00	2.25	2.10
12.0	8.63	8.16	7.68	5.23	3.85	3.55	3.45	3.02
15.0	8.83	8.40	7.93	7.50	5.67	5.13	4.50	3.81
20.0	9.10	8.68	8.35	9.30	8.35	6.58	5.65	4.80
25.0	9.39	8.97	8.80	9.55	9.28	7.85	6.60	5.65
30.0	9.72	9.31	9.20	9.72	9.65	8.85	7.42	6.50
35.0	10.05	9.70	9.55	9.95	9.89	9.42	8.27	7.30
40.0	10.40	10.05	9.85	10.30	10.12	9.75	9.02	8.05
45.0	10.78	10.35	10.15	10.60	10.35	9.97	9.65	8.73
50.0	11.09	10.70	10.45	10.83	10.62	10.20	10.10	9.26
55.0	11.27	11.00	10.74		10.87	10.37	10.43	9.75
60.0	11.40	11.20	10.98		11.07	10.57	10.67	10.13
65.0	11.48	11.38	11.23		11.25	10.79	10.88	10.50
70.0	11.55	11.49	11.45		11.48	11.05	11.05	10.75
75.0	11.60	11.57	11.57		11.57	11.25	11.22	10.93
80.0	11.63	11.61	11.61		11.61	11.43	11.35	11.13
85.0	11.63	11.63	11.63		11.63	11.55	11.49	11.30
90.0	11.63	11.63	11.63		11.63	11.60	11.58	11.42
95.0		11.63	11.63		11.63	11.65	11.65	11.55
100.0						11.68	11.68	11.68
105.0						11.68	11.68	11.73
110.0						11.68	11.68	11.73

Height	X=7.45m	X=8.5m	X=9.5m	X=10m	X=11m
Z cm					
	m/s	m/s	m/s	m/s	m/s
1.0	0.75	0.73	0.68	0.60	0.95
2.0	0.75	0.80	0.75	0.65	1.00
3.0	0.80	0.87	0.85	0.80	1.05
5.0	0.97	1.12	1.12	1.12	1.27
7.0	1.38	1.50	1.53	1.60	1.70
9.0	2.10	2.08	2.10	2.07	2.43
12.0	3.02	3.02	2.90	3.00	3.33
15.0	3.81	3.81	3.54	3.65	3.80
20.0	4.80	4.80	4.50	4.48	4.52
25.0	5.65	5.51	5.33	5.15	5.21
30.0	6.50	6.18	6.05	5.77	5.90
35.0	7.30	6.90	6.75	6.35	6.60
40.0	7.98	7.67	7.27	6.90	7.23
45.0	8.55	8.44	7.85	7.37	7.85
50.0	9.00	9.13	8.34	7.90	8.43
55.0	9.42	9.70	8.88	8.42	8.98
60.0	9.81	10.13	9.40	8.82	9.45
65.0	10.17	10.50	9.77	9.27	9.92
70.0	10.50	10.82	10.12	9.66	10.31
75.0	10.75	11.05	10.37	10.02	10.62
80.0	11.00	11.25	10.65	10.28	10.85
85.0	11.22	11.41	10.95	10.55	11.05
90.0	11.42	11.55	11.18	10.75	11.20
95.0	11.55	11.67	11.33	10.98	11.33
100.0	11.68	11.73	11.45	11.23	11.45
105.0	11.73	11.73	11.55	11.37	11.55
110.0	11.73	11.73	11.60	11.50	11.60

TABLE 3. VALUES OF MEAN VELOCITY

(2.54 x 2.54 cm diag.)

Z cm	X=-1.0m	X=0.0m	X=0.5m	X=1.0m	X=1.5m	X=2.0m	X=3.0m
	m/s	m/s	m/s	m/s	m/s	m/s	m/s
1.0	7.05	4.50	3.52	1.45	0.97	0.88	1.10
2.0	7.30	5.68	3.52	1.50	0.99	1.12	1.30
3.0	7.50	6.53	3.65	1.63	1.08	1.38	1.50
5.0	7.90	7.40	3.75	2.00	1.58	1.92	1.95
7.0	8.23	7.92	4.03	2.57	2.25	2.48	2.37
9.0	8.55	8.25	4.95	3.56	3.02	3.23	3.00
12.0	8.77	8.65	7.23	5.20	4.42	4.18	4.10
15.0	8.95	8.80	8.80	6.95	5.80	5.35	5.05
20.0	9.30	9.25	9.50	8.95	8.15	6.80	6.40
25.0	9.55	9.45	9.75	9.55	9.37	8.20	7.63
30.0	9.80	9.77	9.90	9.80	9.80	9.25	8.50
35.0	10.10	10.00	10.05	10.00	9.92	9.70	9.35
40.0	10.45	10.25	10.18	10.12	10.02	9.93	9.77
45.0	10.65	10.53	10.35	10.30	10.35	10.00	9.90
50.0	10.87	10.75	10.57	10.55	10.52	10.20	10.20
55.0	11.08	11.00	10.85	10.75	10.67	10.35	10.40
60.0	11.30	11.20	11.10	10.95	10.88	10.65	10.55
65.0	11.58	11.43	11.33	11.15	11.15	10.87	10.73
70.0	11.77	11.70	11.58	11.43	11.43	11.10	11.00
75.0	11.92	11.86	11.75	11.67	11.70	11.40	11.30
80.0	12.00	11.97	11.90	11.80	11.90	11.65	11.54
85.0	12.00	11.97	11.97	11.97	12.00	11.77	11.65
90.0	12.00	12.00	12.00	12.00	12.03	11.90	11.78
95.0		12.00	12.00	12.00	12.05	12.00	11.90
100.0					12.05	12.00	12.00
105.0							12.00
110.0							

Z cm	X=4.0m	X=6.0m	X=8.0m	X=9.0m	X=10.0m	X=11.0m
	m/s	m/s	m/s	m/s	m/s	m/s
1.0	1.35	1.13	1.23	1.23	1.38	1.53
2.0	1.58	1.32	1.45	1.47	1.60	1.76
3.0	1.83	1.48	1.63	1.72	1.85	1.95
5.0	2.25	1.85	2.15	2.05	2.25	2.30
7.0	3.00	2.30	2.52	2.55	2.64	2.80
9.0	3.63	2.77	2.93	2.98	3.05	3.30
12.0	4.32	3.42	3.60	3.65	3.62	3.95
15.10	5.02	4.15	4.12	4.40	4.15	4.37
20.0	6.20	5.11	4.77	5.27	5.02	5.25
25.0	7.07	5.90	5.55	5.85	5.71	5.88
30.0	8.00	6.78	6.33	6.51	6.30	6.65
35.0	8.80	7.45	6.95	7.05	6.95	7.25
40.0	9.40	8.27	7.45	7.55	7.45	7.85
45.0	9.85	8.80	7.80	8.05	8.05	8.35
50.0	10.20	9.40	8.55	8.55	8.55	8.67
55.0	10.40	9.80	8.98	8.95	8.97	9.10
60.0	10.57	10.14	9.45	9.35	9.40	9.47
65.0	10.75	10.44	9.90	9.72	9.90	9.80
70.0	11.00	10.73	10.25	10.10	10.25	10.17
75.0	11.25	10.97	10.63	10.50	10.56	10.53
80.0	11.50	11.20	10.90	10.80	10.88	10.82
85.0	11.65	11.38	11.14	11.05	11.17	11.04
90.0	11.76	11.50	11.34	11.25	11.37	11.28
95.0	11.84	11.70	11.50	11.43	11.55	11.43
100.0	11.92	11.86	11.62	11.60	11.73	11.68
105.0	12.00	11.95	11.75	11.75	11.80	11.78
110.0	12.00	12.00	11.85	11.83	11.85	11.83

TABLE 4. VALUES OF MEAN VELOCITY

(5.08 x 5.08 cm sq)

Z cm	X=-1.0m	X=0.0m	X=0.5m	X=1.0m	X=1.5m	X=2.0m	X=3.0m
	m/s	m/s	m/s	m/s	m/s	m/s	m/s
1.0	7.05	4.17	3.65	3.15	2.62	1.83	2.32
2.0	7.52	5.12	3.79	3.22	2.70	1.95	2.35
3.0	8.13	6.00	3.85	3.35	2.77	2.20	2.46
5.0	8.57	7.20	4.15	3.62	2.97	2.80	2.92
7.0	8.75	7.65	4.75	4.12	3.35	3.03	3.67
9.0	8.85	8.13	5.83	4.93	4.07	3.75	4.43
12.0	9.02	8.52	7.51	6.58	5.50	5.00	5.25
15.0	9.17	8.75	8.30	7.87	7.05	5.97	6.05
20.0	9.40	9.12	8.75	9.95	9.57	7.62	7.60
25.0	9.85	9.40	9.30	9.22	9.35	8.85	8.78
30.0	10.10	9.57	9.50	9.50	9.67	9.40	9.23
35.0	10.27	10.00	9.67	9.80	9.97	9.67	9.55
40.0	10.75	10.27	9.85	9.92	10.15	9.80	9.85
45.0	10.95	10.62	10.17	10.25	10.35	9.97	10.16
50.0	11.27	10.95	10.27	10.53	10.55	10.04	10.43
55.0	11.43	11.15	10.80	11.00	10.95	10.50	10.62
60.0	11.60	11.50	11.27	11.20	11.20	10.98	10.80
65.0	11.81	11.80	11.48	11.41	11.42	11.33	11.04
70.0	11.92	11.92	11.72	11.58	11.62	11.58	11.28
75.0	12.05	12.00	11.81	11.78	11.85	11.78	11.52
80.0	12.09	12.08	11.92	11.92	11.92	11.92	11.73
85.0	12.09	12.09	11.97	11.97	12.00	11.98	11.83
90.0	12.09	12.09	11.97	11.99	12.02	11.98	11.95
95.0		12.09	11.97	12.00	12.02	12.00	12.00
100.0			12.00	12.00	12.02	12.00	12.00
105.0			12.00	12.00	12.02	12.00	12.04
110.0							

Z cm	X=4.0m	X=6.0m	X=8.0m	X=9.0m	X=10.0m	X=11.0m
	m/s	m/s	m/s	m/s	m/s	m/s
1.0	2.07	2.55	2.50	1.95	2.07	2.75
2.0	2.21	2.64	2.55	2.05	2.30	2.92
3.0	2.31	2.75	2.70	2.36	2.50	3.12
5.0	2.92	3.17	3.00	3.05	3.05	3.50
7.0	3.50	3.57	3.40	3.36	3.40	3.94
9.0	4.33	4.18	3.88	3.58	3.65	4.42
12.0	5.10	4.90	4.55	4.45	4.45	5.08
15.0	5.83	5.55	5.33	5.12	5.07	5.64
20.0	6.78	6.30	6.04	5.55	5.68	6.25
25.0	7.78	7.13	6.83	6.34	6.52	6.75
30.0	8.75	7.70	7.39	7.10	7.15	7.30
35.0	9.40	8.30	8.00	7.89	7.87	8.03
40.0	9.68	9.12	8.52	8.70	8.57	8.53
45.0	10.03	9.50	8.90	9.25	9.12	8.85
50.0	10.27	10.02	9.45	9.80	9.63	9.23
55.0	10.50	10.27	9.80	10.02	9.98	9.80
60.0	10.75	10.54	10.11	10.15	10.13	9.95
65.0	10.97	10.85	10.43	10.40	10.35	10.30
70.0	11.28	11.04	10.85	10.82	10.78	10.73
75.0	11.53	11.18	11.15	11.13	11.08	11.15
80.0	11.75	11.35	11.35	11.37	11.25	11.35
85.0	11.94	11.52	11.57	11.50	11.45	11.58
90.0	12.00	11.62	11.70	11.67	11.60	11.79
95.0	12.05	11.72	11.82	11.76	11.66	11.93
100.0	12.05	11.82	11.88	11.88	11.80	11.98
105.0		11.93	11.93	11.93	11.93	12.05

TABLE 5. TURBULENT VELOCITY; $u' = \sqrt{\overline{u}^2}$ (Unit; m/sec)

(1.27 x 1.27 cm diag.)

Z\X	-1.0m	0.5m	1.0m	2.0m	3.0m	4.0m	Z\X	5.0m
cm							cm	
1.0	--	--	--	--	--	--	8.0	.609
2.0	.626	--	--	--	--	--	13.0	.866
3.0	.631	--	--	--	--	--	19.0	.933
5.0	.623	--	--	.324	--	.259	24.5	.972
7.0	.615	--	.299	.576	.552	.496	29.5	.986
9.0	.622	.209	.507	.724	.833	.704	35.0	.939
12.0	.640	.478	.825	.883	1.007	.895	40.5	.878
15.0	.675	.357	.978	.946	1.063	.946	46.0	.846
20.0	.659	.477	.944	1.000	1.102	.934	51.5	.752
25.0	.662	.565	.706	.956	1.131	.915	56.5	.696
30.0	.676	.569	.608	.839	1.068	.905	61.5	.592
35.0	.661	.570	.613	.637	1.050	.899	65.0	.580
40.0	.635	.556	.587	.521	.978	.858	70.0	.502
45.0	.574	.521	.598	.500	.793	.883	75.0	.426
50.0	.498	.482	.604	.480	.629	.744	80.0	.333
55.0	.361	.426	.573	.462	.540	.630	85.0	.270
60.0	.275	.364	.544	.427	.492	.534	90.0	.204
65.0					.427	.537	95.0	.148
70.0					.374	.454		
75.0					.311	.407		
80.0					.233	.356		
85.0					.222	.305		
90.0					.110	.246		
95.0					.077	.170		

TABLE 6. TURBULENT VELOCITY; $u' = \sqrt{\overline{u^2}}$ (Unit; m/sec)

(2.54 x 2.54 cm sq.)

Z\X	-0.5m	0.0m	0.5m	1.5m	4.0m	6.0m	8.0m	11.0m
cm								
1.0	--	.956	--	--	.308	.300	.330	--
2.0	--	.881	.465	--	.385	.317	.370	.353
3.0	.864	.810	.472	--	.427	.410	.401	.363
5.0	.844	.774	.521	.345	.537	.509	.472	.412
7.0	.820	.744	.601	.645	.806	.713	.630	.523
9.0	.791	.723	.743	.938	1.054	.990	.890	.705
12.0	.773	.706	1.094	1.345	1.329	1.150	1.162	.853
15.0	.770	.696	1.123	1.512	1.333	1.230	1.203	.939
20.0	.797	.731	.726	1.356	1.362	1.242	1.231	1.000
25.0	.808	.765	.586	.997	1.361	1.224	1.180	1.066
30.0	.821	.790	.580	.694	1.296	1.200	1.164	1.095
35.0	.820	.810	.576	.592	1.192	1.143	1.142	1.084
40.0	.787	.800	.565	.583	1.111	1.101	1.120	1.102
45.0	.727	.805	.562	.564	.934	1.023	1.111	1.078
50.0	.655	.751	.528	.541	.763	.951	1.112	1.032
55.0	.545	.703	--	.531	.645	.816	1.040	1.000
60.0	.430	.663	--	.517	.563	.684	.969	.891

TABLE 7. TURBULENT VELOCITY; $u' = \sqrt{\overline{u^2}}$ (Unit; m/sec)

(2.54 x 2.54 cm diag.)

Z\X	-1.0m	0.0m	0.5m	1.0m	1.5m	2.0m	3.0m	4.0m	6.0m	8.0m
cm										
3.0	.780	1.050	.773	.430	.439	.545	.615	.678	.520	.587
5.0	.730	.900	.715	.536	.666	.735	.814	.811	.677	.785
7.0	.707	.758	.785	.765	.964	1.015	1.058	1.063	.870	.950
9.0	.699	.758	1.040	1.150	1.297	1.303	1.294	1.318	1.103	1.100
12.0	.692	.738	1.235	1.430	1.567	1.400	1.380	1.470	1.205	1.235
15.0	.690	.725	.882	1.738	1.610	1.523	1.485	1.462	1.298	1.272
20.0	.705	.720	.656	1.090	1.445	1.504	1.538	1.468	1.380	1.315
25.0	.703	.708	.646	.769	.975	1.265	1.505	1.435	1.363	1.330
30.0	.703	.723	.651	.698	.702	.940	1.285	1.363	1.365	1.355
35.0	.700	.703	.637	.698	.665	.790	1.125	1.235	1.355	1.340
40.0	.678	.687	.640	.712	.649	.700	.905	1.080	1.300	1.273
45.0	.628	.680	.638	.710	.648	.702	.745	.900	1.180	1.204
50.0	.585	.661	.625	.675	.653	.694	.689	.750	1.102	1.155
55.0	.493	.626	.598	.666	.628	.698	.964	.670	.970	1.072
60.0	.404	.586	.550	.633	.607	.677	.700	.616	.850	1.002

Z\X	9.0m	10.0m	11.0m
cm			
3.0	.523	.560	.514
5.0	.639	.680	.647
7.0	.851	.875	.836
9.0	1.066	1.088	1.110
12.0	1.210	1.154	1.255
15.0	1.270	1.200	1.190
20.0	1.278	1.220	1.180
25.0	1.283	1.247	1.195
30.0	1.320	1.214	1.225
35.0	1.306	1.220	1.218
40.0	1.250	1.210	1.235
45.0	1.224	1.192	1.200
50.0	1.155	1.148	1.147
55.0	1.150	1.110	1.088
60.0	1.092	1.082	1.050

TABLE 8. TURBULENT VELOCITY; $u' = \sqrt{\overline{u^2}}$ (Unit; m/sec)

(5.08 x 5.08 cm sq.)

Z\X	-1.0m	0.0m	0.5m	1.0m	1.5m	2.0m	3.0m	4.0m	6.0m	8.0m
cm										
1.0	.894	1.000	.694	.606	.532	.519	.652	.641	.601	.557
2.0	.869	.996	.715	.624	.556	.570	.667	.670	.628	.577
3.0	.862	.762	.740	.665	.584	.636	.710	.701	.678	.618
5.0	.797	.794	.816	.775	.662	.831	.908	.872	.817	.723
7.0	.754	.724	.903	.916	.816	.948	1.143	1.039	.980	.849
9.0	.726	.665	.775	1.101	1.067	1.131	1.314	1.242	1.150	.994
12.0	.702	.683	.657	1.106	1.219	1.308	1.434	1.366	1.259	1.122
15.0	.722	.678	.608	.953	1.217	1.345	1.500	1.434	1.327	1.217
20.0	.734	.661	.622	.618	.988	1.188	1.497	1.429	1.354	1.261
25.0	.760	.676	.644	.583	.694	.911	1.278	1.330	1.341	1.280
30.0	.770	.684	.651	.581	.588	.694	1.000	1.222	1.282	1.260
35.0	.772	.697	.659	.607	.576	.600	.731	1.023	1.211	1.200
40.0	.799	.710	.659	.602	.625	.607	.629	.870	1.119	1.142
45.0	.737	.716	.675	.630	.625	.602	.613	.727	.983	1.084
50.0	.710	.658	.648	.605	.605	.606	.601	.648	.879	1.052
55.0	.629	.642	.621	.633	.592	.601	.568	.633	.776	.982
60.0	.528	.608	.633	.633	.571	.627	.588	.649	.669	.915

Z\X	9.0m	10.0m	11.0m
cm			
1.0	.454	.502	.568
2.0	.490	.563	.627
3.0	.525	.609	.689
5.0	.615	.745	.817
7.0	.714	.844	.957
9.0	.863	.916	1.071
12.0	1.056	1.055	1.163
15.0	1.044	1.129	1.194
20.0	1.134	1.179	1.143
25.0	1.128	1.193	1.089
30.0	1.107	1.200	1.099
35.0	1.098	1.223	1.111
40.0	1.098	1.203	1.083
45.0	1.071	1.130	1.022
50.0	1.000	1.076	.937
55.0	.954	1.000	.851
60.0	.920	.933	.796

TABLE 9. TURBULENCE INTENSITY; $\frac{u'}{U_{local}} = \frac{\sqrt{\overline{u^2}}}{U_{local}}$

(1.27 x 1.27 cm diag.)

Z\X	-1.0m	0.5m	1.0m	2.0m	3.0m	4.0m	Z X	5.0m
cm							cm	
2.0	.095	--	--	--	--	--	8.0	.376
3.0	.093	--	--	--	--	--	13.0	.284
5.0	.087	--	--	.431	--	.432	19.0	.215
7.0	.083	--	.482	.427	.526	.443	24.5	.179
9.0	.082	.218	.445	.353	.417	.387	29.5	.156
12.0	.082	.180	.337	.285	.325	.298	35.0	.129
15.0	.084	.074	.251	.235	.273	.243	40.5	.107
20.0	.079	.059	.145	.185	.217	.189	46.0	.086
25.0	.076	.062	.081	.142	.180	.156	51.5	.080
30.0	.074	.061	.064	.103	.150	.134	56.5	.070
35.0	.069	.060	.062	.070	.127	.116	61.5	.057
40.0	.064	.057	.058	.053	.107	.101	65.0	.054
45.0	.056	.052	.058	.048	.081	.087	70.0	.046
50.0	.047	.046	.057	.045	.061	.073	75.0	.038
55.0	.033	.040	.053	.043	.052	.062	80.0	.029
60.0	.025	.033	.049	.039	.051	.053	85.0	.023
65.0					.042	.047	90.0	.017
70.0					.034	.041	95.0	.012
75.0					.027	.036		
80.0					.022	.031		
85.0					.016	.026		
90.0					.010	.021		
95.0					.007	.014		

TABLE 10. TURBULENCE INTENSITY; $\frac{u'}{U_{local}} = \frac{\sqrt{\overline{u^2}}}{U_{local}}$

(2.54 x 2.54 cm sq.)

Z\X	-0.5m	0.0m	0.5m	1.5m	4.0m	6.0m	8.5m	11.0m
cm								
1.0	--	.221	--	--	.411	.400	.452	--
2.0	--	.153	.182	--	.481	.423	.463	.353
3.0	.125	.127	.183	--	.462	.513	.460	.346
5.0	.115	.111	.198	.397	.479	.525	.420	.325
7.0	.107	.103	.221	.478	.498	.516	.420	.307
9.0	.101	.098	.232	.440	.468	.471	.428	.290
12.0	.095	.092	.209	.364	.385	.381	.384	.256
15.0	.092	.088	.150	.280	.296	.323	.315	.247
20.0	.092	.088	.078	.182	.241	.259	.256	.221
25.0	.090	.087	.061	.116	.206	.217	.214	.205
30.0	.088	.086	.060	.075	.175	.185	.188	.186
35.0	.085	.085	.058	.061	.144	.157	.165	.164
40.0	.078	.081	.055	.059	.123	.137	.146	.152
45.0	.070	.079	.053	.056	.097	.117	.132	.137
50.0	.061	.072	.049	.052	.076	.103	.122	.122
55.0	.050	.066	--	.050	.062	.084	.107	.111
60.0	.038	.060	--	.048	.053	.068	.096	.094

TABLE 11. TURBULENCE INTENSITY; $\frac{u'}{U_{local}} = \frac{\sqrt{\overline{u^2}}}{U_{local}}$

(2.54 x 2.54 cm diag.)

Z\X	-1.0m	0.0m	0.5m	1.0m	1.5m	2.0m	3.0m	4.0m	6.0m
cm									
3.0	.104	.161	.212	.264	.406	.395	410	.370	.351
5.0	.092	.122	.191	.268	.422	.383	417	.360	.366
7.0	.086	.096	.195	.298	.428	.409	446	.354	.378
9.0	.082	.092	.210	.323	.429	.403	.431	.363	.398
12.0	.079	.085	.171	.275	.355	.335	.337	.340	.352
15.0	.077	.082	.100	.250	.278	.285	.294	.291	.313
20.0	.076	.078	.069	.122	.177	.221	.240	.236	.270
25.0	.074	.075	.066	.081	.104	.154	.197	.203	.221
30.0	.072	.074	.066	.071	.072	.101	.151	.170	.201
35.0	.069	.070	.063	.070	.067	.081	.120	.140	.182
40.0	.065	.067	.063	.070	.065	.070	.092	.115	.157
45.0	.059	.065	.062	.069	.063	.070	.075	.091	.134
50.0	.054	.061	.059	.064	.062	.068	.067	.074	.117
55.0	.044	.057	.055	.062	.059	.067	.067	.064	.099
60.0	.036	.053	.050	.058	.056	.064	.066	.059	.084

Z\X	8.0m	9.0m	10.0m	11.0m
cm				
3.0	.360	.304	.303	.264
5.0	.365	.312	.302	.281
7.0	.377	.334	.331	.299
9.0	.375	.358	.357	.336
12.0	.343	.332	.319	.318
15.0	.309	.289	.289	.272
20.0	.276	.243	.243	.225
25.0	.240	.219	.218	.217
30.0	.214	.197	.193	.186
35.0	.193	.185	.176	.168
40.0	.171	.166	.162	.155
45.0	.154	.152	.148	.144
50.0	.135	.135	.134	.132
55.0	.119	.128	.124	.120
60.0	.106	.118	.115	.112

TABLE 12. TURBULENCE INTENSITY; $\frac{u'}{U_{local}} = \frac{\sqrt{\overline{u^2}}}{U_{local}}$

(5.08 x 5.08 cm sq.)

Z\X	-1.0m	0.0m	0.5m	1.0m	1.5m	2.0m	3.0m	4.0m
cm								
1.0	.127	.240	.190	.192	.203	.356	.281	.310
2.0	.119	.195	.189	.194	.206	.342	.284	.303
3.0	.106	.127	.192	.199	.211	.323	.289	.303
5.0	.093	.110	.197	.214	.223	.324	.311	.299
7.0	.085	.095	.190	.222	.244	.377	.311	.297
9.0	.082	.082	.133	.223	.262	.350	.297	.287
12.0	.078	.080	.088	.168	.222	.287	.273	.268
15.0	.079	.077	.073	.121	.173	.251	.248	.246
20.0	.078	.072	.071	.069	.115	.196	.212	.211
25.0	.077	.072	.069	.063	.074	.144	.146	.171
30.0	.076	.071	.069	.061	.061	.106	.108	.140
35.0	.075	.070	.068	.062	.058	.076	.077	.109
40.0	.074	.069	.067	.061	.060	.064	.064	.090
45.0	.067	.067	.066	.061	.060	.061	.060	.072
50.0	.063	.060	.063	.057	.057	.060	.057	.063
55.0	.055	.058	.058	.058	.054	.054	.053	.060
60.0	.046	.053	.054	.057	.051	.054	.054	.060

Z\X	6.0m	8.0m	9.0m	10.0m	11.0m
cm					
1.0	.236	.223	.236	.243	.207
2.0	.238	.218	.243	.245	.215
3.0	.247	.229	.246	.244	.221
5.0	.258	.241	.258	.244	.233
7.0	.275	.250	.264	.248	.243
9.0	.275	.256	.266	.251	.242
12.0	.257	.247	.252	.237	.229
15.0	.239	.228	.237	.223	.212
20.0	.215	.209	.206	.208	.183
25.0	.188	.187	.184	.183	.161
30.0	.166	.171	.166	.168	.151
35.0	.146	.150	.155	.155	.138
40.0	.123	.134	.138	.140	.127
45.0	.103	.122	.126	.124	.115
50.0	.088	.111	.104	.112	.102
55.0	0.76	.100	.101	.100	.087
60.0	.063	.091	.091	.093	.080

TABLE 13. TURBULENT VELOCITY; $w' = \sqrt{\overline{w^2}}$ (Unit; m/sec)

(1.27 x 1.27 cm diag.)

Z\X	-1.0m	0.5m	1.0m	2.0m	3.0m	4.0m	5.0m
cm							
3.0	.471	--	--	--	--	--	--
5.0	.596	--	--	.192	--	.152	--
7.0	.613	--	.274	.330	.324	.273	.332
9.0	.649	.183	.335	.479	.536	.440	.476
12.0	.679	.314	.640	.705	.732	.690	.636
15.0	.706	.345	.870	.849	.853	.836	.750
20.0	.740	.609	.932	1.020	1.018	.953	.889
25.0	.751	.695	.760	1.060	1.126	1.000	.965
30.0	.751	.722	.710	.973	1.149	1.041	1.012
35.0	.743	.716	.725	.775	1.104	1.051	1.039
40.0	.707	.704	.751	.706	1.143	1.010	1.035
45.0	.657	.672	.757	.652	1.031	1.025	1.052
50.0	.564	.636	.737	.633	.842	.902	.994
55.0	.484	.578	.716	.594	.737	.795	.890
60.0	.376	.514	.670	.557	.660	.727	.797
65.0					.602	.700	.741
70.0					.537	.631	.644
75.0					.465	.558	.553
80.0					.395	.481	.477
85.0					.297	.427	.411
90.0					.235	.364	.352
95.0					.207	.295	.305

TABLE 14. TURBULENT VELOCITY; $w' = \sqrt{\overline{w^2}}$ (Unit; m/sec)

(2.54 x 2.54 cm sq.)

Z\X	-0.5m	0.0m	0.5m	1.5m	4.0m	6.0m	8.5m	11.0m
cm								
2.0	--	--	.288	--	.119	--	--	--
3.0	.468	.567	.310	--	.145	.124	--	--
5.0	.483	.519	.389	.135	.245	.206	--	.235
7.0	.500	.517	.455	.268	.379	.330	.280	.343
9.0	.521	.528	.534	.432	.516	.463	.235	.404
12.0	.548	.555	.691	.691	.678	.602	--	.562
15.0	.577	.579	.686	.884	.833	.704	.466	.672
20.0	.600	.618	.523	1.028	.963	.815	.680	.823
25.0	.597	.638	.526	.868	.968	.874	.810	.896
30.0	.601	.655	.533	.677	.927	.900	.772	.818
35.0	.607	.645	.533	.526	.870	.899	.800	.800
40.0	.584	.620	.531	.507	.775	.894	.835	.721
45.0	.537	.602	.517	.500	.691	.813	.772	.693
50.0	.490	.538	.454	.483	.591	.752	.700	.667
55.0	.437	.476	--	.469	.517	.677	.561	.668
60.0	.370	.422	--	.430	.483	.608	.508	.672

TABLE 15. TURBULENT VELOCITY; $w' = \sqrt{\overline{w^2}}$ (Unit; m/sec)

(5.08 x 5.08 cm 격.)

Z\X	-1.0m	1.0m	2.0m	3.0m	4.0m	6.0m	8.0m	10.0m
cm								
3.0	.787	--	.749	.612	.360	.596	.604	573
5.0	.812	--	1.022	.643	.473	.634	.667	667
7.0	.825	.234	1.026	.727	.662	.727	.738	747
9.0	.820	.387	1.376	.793	.806	.813	.787	773
12.0	.772	.621	1.462	.783	.803	.795	.831	754
15.0	.700	.451	1.300	.734	.710	.811	.835	752
20.0	.663	.570	1.071	.703	.619	.743	.756	822
25.0	.647	.555	0.754	.830	.748	.728	.652	853
30.0	.550	.599	.659	.860	.812	.628	.728	860
35.0	.424	.575	.582	.801	.758	.712	.712	758
40.0	.235	.540	.511	.686	.741	.758	.703	615
45.0	.255	.523	.427	.602	.579	.747	.730	652
50.0	.105	.508	.368	.602	.528	.697	.555	648
55.0	.283	.391	.298	.569	.436	.659	.423	600
60.0	.248	.236	--	.527	.369	.587	.291	550

Z\X	10.0m	11.0m
cm		
3.0	.633	.762
5.0	.772	.862
7.0	.886	.975
9.0	.975	1.03
12.0	1.11	1.06
15.0	1.12	1.07
20.0	1.05	1.03
25.0	1.02	1.02
30.0	1.02	1.02
35.0	.990	1.00
40.0	.991	.959
45.0	.982	.932
50.0	.926	.899
55.0	.875	.875
60.0	.845	.826

TABLE 16. TURBULENT SHEAR STRESS $-\overline{uw}$ (Unit; m^2/sec^2)

(2.54 x 2.54 cm sq)

z \ x	0.0m	0.5m	4.0m	6.0m	8.5m	11.0m
cm						
3.0	.113	.006	.001	.014	.007	.005
5.0	.026	.007	.009	.026	.023	.009
7.0	.029	.027	.039	.067	.068	.022
9.0	.071	.091	.111	.131	.108	.055
12.0	.104	.333	.250	.144	.144	.093
15.0	.110	.339	.287	.145	.171	.129
20.0	.129	.059	.259	.240	.203	.176
25.0	.137	.072	.327	.239	.243	.232
30.0	.152	.112	.257	.267	.250	.191
35.0	.154	.118	.219	.276	.242	.177
40.0	.152	.131	.194	.298	.285	.140
45.0	.152	.138	.094	.247	.266	.140
50.0	.143	.068	.054	.206	.307	.130
55.0	.130	----	.039	.152	.211	.169
60.0	.098	----	.032	.127	.184	.137

TABLE 17. VALUES OF α IN EQ. (2-6); MEAN VELOCITY WITHIN CANOPY

(1.27 x 1.27 cm DIAG)

X	2.0m	3.0m	4.0m	7.0m	9.3m	10.3m
α	.252	.342	.272	.330	.182	.182

(2.54 x 2.54 cm SQ)

X	2.0m	4.0m	6.0m	7.45m	8.5m	9.5m	10.0m
α	.175	.162	.194	.194	.142	.151	.161

(2.54 x 2.54 cm DIAG)

X	1.0m	1.5m	2.0m	3.0m	4.0m	6.0m	8.0m	9.0m	10.0m
α	.124	.163	.141	.181	.181	.106	.0995	.106	.0877

(5.08 x 5.08 cm SQ)

X	2.0m	3.0m	4.0m	6.0m	8.0m	9.0m	10.0m
α	.0910	.0952	.0980	.0683	.0595	.0715	.0645

TABLE 18. SLOPES OF TURBULENCE INTENSITY PROFILES IN THE EXPONENTIAL FORM

	x(m)	6.0	8.5	11
Slopes	Below a kink	- 0.350	- 0.317	- 0.174
	Above a kink	- 0.663	- 0.588	- 0.485

(2.54 x 2.54 cm diag)

	x(m)	6.0	8.0	9.0	10.0
Slopes	Below a kink	- 0.276	- 0.268	- 0.267	- 0.276
	Above a kink	- 0.701	- 0.609	- 0.530	- 0.477

(5.08 x 5.08 cm sq)

	x(m)	6.0	8.0	9.0	10.0
Slopes	Below a kink	- 0.233	- 0.203	- 0.233	- 0.208
	Above a kink	- 0.682	- 0.566	- 0.588	- 0.536

Unclassified
Security Classification

DOCUMENT CONTROL DATA - R&D

(Security classification of title, body of abstract and indexing annotation must be entered when the overall report is classified)

1. ORIGINATING ACTIVITY *(Corporate author)*

Colorado State University
Fort Collins, Colorado 80521

2a. REPORT SECURITY CLASSIFICATION

Unclassified

2b. GROUP

3. REPORT TITLE

THE STRUCTURE OF CANOPY FLOW FIELD

4. DESCRIPTIVE NOTES *(Type of report and inclusive dates)*

5. AUTHOR(S) *(Last name, first name, initial)*

KAWATANI, Takeshi and Meroney, Robert N.

6. REPORT DATE	7a. TOTAL NO. OF PAGES	7b. NO. OF REFS
August 1968	122	30

8a. CONTRACT OR GRANT NO.
DA-AMC-28-043-65-G20

b. PROJECT NO.
2246

c.

d.

9a. ORIGINATOR'S REPORT NUMBER(S)

CER67-68RNM66

9b. OTHER REPORT NO(S) *(Any other numbers that may be assigned this report)*

10. AVAILABILITY/LIMITATION NOTICES

Distribution of this document is unlimited

11. SUPPLEMENTARY NOTES

12. SPONSORING MILITARY ACTIVITY

U.S. Army Materiel Command

13. ABSTRACT

A model study of canopy flow over high roughness elements was carried out in the Army Meteorological Wind Tunnel at Colorado State University using roughness consisting of pegs 9. cm high and 0.48 cm in diameter arranged in four patterns. The mean velocity and the turbulence intensity were measured within and above the roughness elements. Empirical expressions derived from field measurements for mean velocity profiles, turbulent velocity, and turbulence intensity were used to examine the data obtained in this model study. The logarithmic profile was adapted to analyze the data of mean velocity above the canopy. In this analysis, the friction velocity and the roughness parameter were calculated from the mean velocity profiles and related to the density of roughness elements to show the effects of roughness density on the flow field. The growth of the internal boundary layer was estimated from the mean velocity profiles and the turbulence intensity. The results of estimation were compared with semi-imperical equations. Although the coefficient of anisotropy above the canopy in this model study is larger than that in the field, the model study gave data about the turbulent flow field similar to the field data. Hence, this model was verified to be suitable for the study of diffusion.

DD FORM 1 JAN 64 1473

Unclassified
Security Classification

14. KEY WORDS	LINK A		LINK B		LINK C	
	ROLE	WT	ROLE	WT	ROLE	WT
Simulation Atmospheric Modeling Wind-Tunnel Laboratory Turbulent Flow Fluid Mechanics Micrometeorology Forest Meteorology Vegetative Canopies						

INSTRUCTIONS

1. ORIGINATING ACTIVITY: Enter the name and address of the contractor, subcontractor, grantee, Department of Defense activity or other organization *(corporate author)* issuing the report.

2*a*. REPORT SECURITY CLASSIFICATION: Enter the overall security classification of the report. Indicate whether "Restricted Data" is included. Marking is to be in accordance with appropriate security regulations.

2*b*. GROUP: Automatic downgrading is specified in DoD Directive 5200.10 and Armed Forces Industrial Manual. Enter the group number. Also, when applicable, show that optional markings have been used for Group 3 and Group 4 as authorized.

3. REPORT TITLE: Enter the complete report title in all capital letters. Titles in all cases should be unclassified. If a meaningful title cannot be selected without classification, show title classification in all capitals in parenthesis immediately following the title.

4. DESCRIPTIVE NOTES: If appropriate, enter the type of report, e.g., interim, progress, summary, annual, or final. Give the inclusive dates when a specific reporting period is covered.

5. AUTHOR(S): Enter the name(s) of author(s) as shown on or in the report. Enter last name, first name, middle initial. If military, show rank and branch of service. The name of the principal author is an absolute minimum requirement.

6. REPORT DATE: Enter the date of the report as day, month, year; or month, year. If more than one date appears on the report, use date of publication.

7*a*. TOTAL NUMBER OF PAGES: The total page count should follow normal pagination procedures, i.e., enter the number of pages containing information.

7*b*. NUMBER OF REFERENCES: Enter the total number of references cited in the report.

8*a*. CONTRACT OR GRANT NUMBER: If appropriate, enter the applicable number of the contract or grant under which the report was written.

8*b*, 8*c*, & 8*d*. PROJECT NUMBER: Enter the appropriate military department identification, such as project number, subproject number, system numbers, task number, etc.

9*a*. ORIGINATOR'S REPORT NUMBER(S): Enter the official report number by which the document will be identified and controlled by the originating activity. This number must be unique to this report.

9*b*. OTHER REPORT NUMBER(S): If the report has been assigned any other report numbers *(either by the originator or by the sponsor)*, also enter this number(s).

10. AVAILABILITY/LIMITATION NOTICES: Enter any limitations on further dissemination of the report, other than those imposed by security classification, using standard statements such as:

(1) "Qualified requesters may obtain copies of this report from DDC."

(2) "Foreign announcement and dissemination of this report by DDC is not authorized."

(3) "U. S. Government agencies may obtain copies of this report directly from DDC. Other qualified DDC users shall request through _____."

(4) "U. S. military agencies may obtain copies of this report directly from DDC. Other qualified users shall request through _____."

(5) "All distribution of this report is controlled. Qualified DDC users shall request through _____."

If the report has been furnished to the Office of Technical Services, Department of Commerce, for sale to the public, indicate this fact and enter the price, if known.

11. SUPPLEMENTARY NOTES: Use for additional explanatory notes.

12. SPONSORING MILITARY ACTIVITY: Enter the name of the departmental project office or laboratory sponsoring *(paying for)* the research and development. Include address.

13. ABSTRACT: Enter an abstract giving a brief and factual summary of the document indicative of the report, even though it may also appear elsewhere in the body of the technical report. If additional space is required, a continuation sheet shall be attached.

It is highly desirable that the abstract of classified reports be unclassified. Each paragraph of the abstract shall end with an indication of the military security classification of the information in the paragraph, represented as *(TS)*, *(S)*, *(C)*, *or (U)*.

There is no limitation on the length of the abstract. However, the suggested length is from 150 to 225 words.

14. KEY WORDS: Key words are technically meaningful terms or short phrases that characterize a report and may be used as index entries for cataloging the report. Key words must be selected so that no security classification is required. Identifiers, such as equipment model designation, trade name, military project code name, geographic location, may be used as key words but will be followed by an indication of technical context. The assignment of links, rules, and weights is optional.

MINIMUM BASIC DISTRIBUTION LIST FOR USAMC SCIENTIFIC AND TECHNICAL REPORTS IN METEOROLOGY AND ATMOSPHERIC SCIENCES

Commanding General (1)
U. S. Army Materiel Command
Attn: AMCRD-RV-A
Washington, D. C. 20315

Commanding General (1)
U. S. Army Electronics Command
Attn: AMSEL-EW
Fort Monmouth, New Jersey 07703

Commanding General (1)
U. S. Army Test and Evaluation Command
Attn: NBC Directorate
Aberdeen Proving Ground, Maryland 21005

Commanding Officer (1)
U. S. Army Ballistics Research Laboratories
Attn: AMXBR-IA
Aberdeen Proving Ground, Maryland 21005

Chief, Atmospheric Physics Division (2)
Atmospheric Sciences Laboratory
U. S. Army Electronics Command
Fort Monmouth, New Jersey 07703

U. S. Army Munitions Command (1)
Attn: Irving Solomon
Operations Research Group
Edgewood Arsenal, Maryland 21010

Commanding Officer (1)
U. S. Army Dugway Proving Ground
Attn: Meteorology Division
Dugway, Utah 84022

Commanding Officer (1)
U. S. Army CDC, CBR Agency
Attn: Mr. N. W. Bush
Fort McClellan, Alabama 36205

Commanding General (1)
U. S. Army Test and Evaluation Command
Attn: AMSTE-EL
Aberdeen Proving Ground, Maryland 21005

Commandant (1)
U. S. Army Signal School
Attn: Meteorological Department
Fort Monmouth, New Jersey 07703

Assistant Chief of Staff for Force Development (1)
CBR Nuclear Operations Directorate
Department of the Army
Washington, D. C. 20310

Director (1)
Atmospheric Sciences Programs
National Sciences Foundation
Washington, D. C. 20550

Assistant Secretary of Defense (1)
Research and Engineering
Attn: Technical Library
Washington, D. C. 20301

R. A. Taft Sanitary Engineering Center (1)
Public Health Service
4676 Columbia Parkway
Cincinnati, Ohio

Dr. Hans A. Panofsky (1)
Department of Meteorology
The Pennsylvania State University
University Park, Pennsylvania

Commanding General (1)
U. S. Continental Army Command
Attn: Reconnaissance Branch ODCS
for Intelligence
Fort Monroe, Virginia 23351

Commander (1)
Air Force Cambridge Research Laboratories
Attn: CRZW
1065 Main Street
Waltham, Massachusetts

President (1)
U. S. Army Artillery Board
Fort Sill, Oklahoma 73504

National Center for Atmospheric Research (1)
Attn: Library
Boulder, Colorado

Dr. J. E. Cermak, Head (15)
Fluid Mechanics Program
Colorado State University
Fort Collins, Colorado 80521

Author (1)

Chief of Research and Development (1)
Department of the Army
Attn: CRD/M
Washington, D. C. 20310

Commanding General (1)
U. S. Army Missile Command
Attn: AMSMI-RRA
Redstone Arsenal, Alabama 35809

Commanding General (1)
U. S. Army Natick Laboratories
Attn: Earth Sciences Division
Natick, Massachusetts 01762

Director, U. S. Army Engineer (1)
Waterways Experiment Station
Attn: WES-FV
Vicksburg, Mississippi 39181

Chief, Atmospheric Sciences Research Division (5)
Atmospheric Sciences Laboratory
U. S. Army Electronics Command
Fort Huachuca, Arizona 85613

Commanding Officer (1)
U. S. Army Frankford Arsenal
Attn: SMUFA-1140
Philadelphia, Pennsylvania 19137

Commandant (1)
U. S. Army Artillery and Missile School
Attn: Target Acquisition Department
Fort Sill, Oklahoma 73504

Commanding General (1)
U. S. Army Electronics Proving Ground
Attn: Field Test Department
Fort Huachuca, Arizona 85613

Commanding General (1)
U. S. Army Test and Evaluation Command
Attn: AMSTE-BAF
Aberdeen Proving Ground, Maryland 21005

Office of Chief Communications - Electronics (1)
Department of the Army
Attn: Electronics Systems Directorate
Washington, D. C. 20315

Chief of Naval Operations (1)
Department of the Navy
Attn: Code 427
Washington, D. C. 20350

Director (1)
Bureau of Research and Development
Federal Aviation Agency
Washington, D. C. 20553

Director of Meteorological Systems (1)
Office of Applications (FM)
National Aeronautics and Space Administration
Washington, D. C. 20546

Director (1)
Atmospheric Physics and Chemistry Laboratory
Environmental Science Services Administration
Boulder, Colorado

Andrew Morse (1)
Army Aeronautical Activity
Ames Research Center
Moffett Field, California 94035

Commanding Officer (2)
U. S. Army Cold Regions Research and
Engineering Laboratories
Attn: Environmental Research Branch
Hanover, New Hampshire 03755

Mr. Ned L. Kragness (1)
U. S. Army Aviation Materiel Command
SMOSM-E
12th and Spruce Streets
Saint Louis, Missouri 63166

Commanding Officer, U. S. Army (1)
Artillery Combat Development Agency
Fort Sill, Oklahoma 73504

Commander, USAR Air Weather Service (MATS) (1)
Attn: AWSSS/TIPD
Scott Air Force Base, Illinois

Dr. John Bogusky (1)
7310 Cedardale Drive
Alexandria, Virginia 22308

Commanding General (1)
U. S. Army Combat Development Command
Attn: CDCMR-E
Fort Belvoir, Virginia 22060

Commanding General (1)
U. S. Army Munitions Command
Attn: AMSMU-RE-R
Dover, New Jersey 07801

Commanding Officer (1)
U. S. Army Ballistics Research Laboratories
Attn: AMXBR-B
Aberdeen Proving Ground, Maryland 21005

Director (2)
Atmospheric Sciences Laboratory
U. S. Army Electronics Command
Fort Monmouth, New Jersey 07703

Chief, Atmospheric Sciences Office (2)
Atmospheric Sciences Laboratory
U. S. Army Electronics Command
White Sands Missile Range, New Mexico 88002

Commanding Officer (1)
U. S. Army Picatinny Arsenal
Attn: SMUPA-TV-3
Dover, New Jersey 07801

Commanding Officer (1)
U. S. Army Communications - Electronics
Combat Development Agency
Fort Monmouth, New Jersey 07703

Commanding General (1)
Deseret Test Center
Attn: Design and Analysis Division
Fort Douglas, Utah 84113

Commandant (1)
U. S. Army CBR School Micrometeorological
Section
Fort McClellan, Alabama 36205

Assistant Chief of Staff for Intelligence (1)
Department of the Army
Attn: ACSI-DERSI
Washington, D. C. 20310

Officer in Charge (1)
U. S. Naval Weather Research Facility
U. S. Naval Air Station, Building 4-28
Norfolk, Virginia 23500

Chief, Fallout Studies Branch (1)
Division of Biology and Medicine
Atomic Energy Commission
Washington, D. C. 20545

Director (1)
U. S. Weather Bureau
Attn: Librarian
Washington, D. C. 20235

Dr. Albert Miller (1)
Department of Meteorology
San Jose State College
San Jose, California 95114

Mrs. Francis L. Wheedon (1)
Army Research Office
3045 Columbia Pike
Arlington, Virginia 22201

Commander (1)
Air Force Cambridge Research Laboratories
Attn: CRXL
L. G. Hanscom Field
Bedford, Massachusetts

Harry Moses, Asso. Meteorologist (1)
Radiological Physics Division
Argonne National Laboratory
9700 S. Cass Avenue
Argonne, Illinois 60440

Defense Documentation Center (20)
Cameron Station
Alexandria, Virginia 22314

Office of U. S. Naval Weather Service (1)
U. S. Naval Air Station
Washington, D. C. 20390

Dr. Gerald Gill (1)
University of Michigan
Ann Arbor, Michigan 48103